

STATUS OF THESIS

Title of thesis

SHAPE FROM FOCUS USING
LULU OPERATORS AND DISCRETE PULSE TRANSFORM IN
THE PRESENCE OF NOISE

I, ROUSHANAK RAHMAT

hereby allow my thesis to be placed at the information Resource Center (IRC) of
Universiti Teknologi PETRONAS (UTP) with the following conditions:

1. The thesis becomes the property of UTP
2. The IRC of UTP may make copies of the thesis for academic purposes only.
3. This thesis is classified as

Confidential

Non-confidential

If the thesis is confidential, please state the reason:

The contents of the thesis will remain confidential for _____ years.

Remarks on disclosure:

Endorsed By:

Signature of Author
Permanent Address
No. 63, Kashfian Alley,
Sheikhbahayi Shomali Avenue,
Mollasadra Street,
Tehran,
Iran

Signature of Supervisor
Assoc. Prof. Dr. Nidal Kamel

Date: _____

Date: _____

UNIVERSITI TEKNOLOGI PETRONAS

SHAPE FROM FOCUS USING
LULU OPERATORS AND DISCRETE PULSE TRANSFORM
IN THE PRESENCE OF NOISE

By

ROUSHANAK RAHMAT

The undersigned certify that they have read, and recommend to the Postgraduate Studies Programme for acceptance this thesis for the fulfillment of the requirements for the degree stated.

Signature: _____

Main Supervisor: Assoc. Prof. Dr. Nidal Kamel

Signature: _____

Co-Supervisor: Dr. Aamir Saeed Malik

Signature: _____

Head of Department: Assoc. Prof. Dr. Nor Hisham Hamid

Date: _____

SHAPE FROM FOCUS USING
LULU OPERATORS AND DISCRETE PULSE TRANSFORM
IN THE PRESENCE OF NOISE

By

ROUSHANAK RAHMAT

A Thesis

Submitted to the Postgraduate Studies Programme
as a Requirement for the Degree of

MASTER OF SCIENCE

ELECTRICAL & ELECTRONICS ENGINEERING DEPARTMENT

UNIVERSITI TEKNOLOGI PETRONAS

BANDAR SRI ISKANDAR

PERAK

DECEMBER 2011

DECLARATION OF THESIS

Title of thesis

SHAPE FROM FOCUS USING
LULU OPERATORS AND DISCRETE PULSE TRANSFORM
IN THE PRESENCE OF NOISE

I, ROUSHANAK RAHMAT
hereby declare that the thesis is based on my original work except for quotations and citations which have been duly acknowledged. I also declare that it has not been previously or concurrently submitted for any other degree at UTP or other institutions.

Signature of Author

Permanent Address
No. 63, Kashfian Alley,
Sheikhbahayi Shomali Avenue,
Mollasadra Street,
Tehran,
Iran

Date: _____

Witnessed By:

Signature of Supervisor

Name of Supervisor:
Assoc. Prof. Dr. Nidal Kamel

Date: _____

ABSTRACT

A study of three dimension (3D) shape recovery is an interesting and challenging area of research. Recovering the depth information of an object from normal two dimensional (2D) images has been studied for a long time with different techniques. One technique for 3D shape recovery is known as Shape from Focus (SFF). SFF is a method that depends on different focused values in reconstructing the shape, surface, and depth of an object. The different focus values are captured by taking different images for the same object by varying the focus length or varying the distance between object and camera. This single view imaging makes the data gathering simpler in SFF compared to other shape recovery techniques. Calculating the shape of the object using different images with different focused values can be done by applying sharpness detection methods to maximize and detect the focused values. However, noise destroys many information in an image and the result of noise corruption can change the focus values in the images. This thesis presents a new 3D shape recovery technique based on focus values in the presence of noise. The proposed technique is based on LULU operators and Discrete Pulse Transform (DPT). LULU operators are nonlinear rank selector operators that hold consistent separation, total variation and shape preservation properties. The proposed techniques show better and more accurate performance in comparison with the existing SFF techniques in noisy environment.

ABSTRAK

Kajian pembentukan semula 3D adalah suatu kajian yang menarik dan mencabar. Pemulihan maklumat kedalaman objek untuk imej 2D telah lama dikaji dengan menggunakan pelbagai teknik yang berbeza. Salah satu teknik bagi pembentukan semula 3D ialah Shape From Focus (SFF). SFF adalah satu kaedah yang bergantung pada nilai-nilai focus yang berlainan untuk membina semula bentuk, permukaan dan kedalaman objek. Nilai-nilai focus yang berbeza untuk sesuatu objek perlulah direkodkan sama ada dengan cara mengubah nilai focus atau mengubah jarak di antara objek dan camera. Teknik pengimejan tunggal ini menjadikan kaedah menghimpun data untuk teknik SFF ini lebih ringkas dan murah berbanding dengan teknik-teknik pembentukan semula yang lain. Pengiraan bentuk objek daripada imej-imej yang berbeza fokus boleh dilakukan dengan menggunakan kaedah pengesanan ketajaman untuk memaksimumkan dan mengesan nilai-nilai fokus. Walau bagaimanapun, kehadiran hingar di dalam imej boleh memusnahkan maklumat asal imej dan mengubah nilai fokus. Tesis ini membentangkan mengenai teknik baru pembentukan semula 3D yang berdasarkan nilai-nilai fokus yang berbeza dalam kehadiran hingar. Teknik yang dicadangkan adalah berdasarkan operator LULU dan Discrete Pulse Transform (DPT). Operator LULU adalah operator pemilih taraf yang tidak linear yang mempunyai ciri-ciri pemisahan yang konsisten, variasi yang menyeluruh dan pemeliharaan bentuk. Teknik yang dicadangkan menunjukkan hasil pembentukan semula 3D dalam kehadiran hingar yang lebih baik dan lebih tepat berbanding dengan teknik SFF yang sedia ada.

In compliance with the terms of the Copyright Act 1987 and the IP Policy of the university, the copyright of this thesis has been reassigned by the author to the legal entity of the university,
Institute of Technology PETRONAS Sdn Bhd.

Due acknowledgement shall always be made of the use of any material contained in, or derived from, this thesis.

© ROUSHANAK RAHMAT, 2011
Institute of Technology PETRONAS Sdn Bhd
All rights reserved.

ACKNOWLEDGEMENTS

One of the greatest pleasures of writing a report is acknowledging the effort of many people whose names may not appear on the cover. But without their hard work, cooperation, friendship and understanding, producing this report would have been impossible.

First and foremost, I would like to thank Allah the Almighty for the innumerable gifts that He has granted me; for guiding me along in completing this work and for giving me an opportunity to undergo higher education.

Secondly, I wish to express my deep and sincere gratitude to my dear supervisor, A. P. Dr. Nidal Kamel, for his support, attention and time. I have very much benefited from his professional and personal advice. Without his help, this work would never have been possible. I am very grateful to him for his constant encouragement and many fruitful discussions. Also, I would like to thank my precious co-supervisor, Dr. Aamir Saeed Malik, who found time in a very busy schedule to teach me about concepts of my work, monitor my progress and answer my questions. I am also deeply indebted for his advice, encouragement and patience during my M.Sc.

Thirdly, my deepest appreciation and love go to my dear parents, Dr. Gholamreza Rahmat and Ms. Foroughifar, my dear brothers, as well as Ms. Mary Rahmat, Mr. Vience and Dr. Ali Rahmat. I thank them for their sacrifice and patience. I also would like to thank the terrific people that I met during my master program, particularly Dr. Humaira Nisar and Dr. Ibrahima Faye for their good company and constructive support. I also would like to thank all my friends for their help and friendship.

Finally, I would like to express my thanks to A. P. Dr. Vijanth Asirvadam and Dr. Lai Weng Kin for taking the time to evaluate this thesis.

DEDICATION

To My Beloved Parents and Brothers

TABLE OF CONTENTS

TABLE OF CONTENTS.....	x
LIST OF FIGURES	xiii
LIST OF TABLES	xxii
LIST OF ABBREVIATIONS.....	xxiii
CHAPTER 1 INTRODUCTION	1
1.1 Introduction.....	1
1.2 Motivation.....	2
1.3 Problem Statement	3
1.4 Research Objectives.....	3
1.5 Research Scope	4
1.6 Thesis Outline	4
Chapter 2 LITERATURE REVIEW.....	5
2.1 Introduction.....	5
2.2 Shape from Focus	8
2.2.1 The Sum Modified Laplacian (SML)	11
2.2.2 The Tenenbaum (TEN).....	12
2.2.3 The Gray Level Variance (GLV).....	13
2.3 Existing Methods in the Presence of Noise	14
2.3.1 Impulse Noise	16
2.3.2 Gaussian Noise.....	17
2.3.3 Speckle Noise.....	18
2.4 Chapter Summary	18
CHAPTER 3 LULU OPERATORS AND DISCRETE PULSE TRANSFORM.....	19
3.1 Introduction.....	19
3.2 LULU Operators	20

3.2.1 1-Dimensional LULU	21
3.2.2 2-Dimensional LULU	22
3.2.3 Properties of LULU Operators.....	25
3.3 The Discrete Pulse Transform (DPT)	26
3.3.1 1D DPT	26
3.3.2 2D DPT	32
3.4 Chapter Summary	36
CHAPTER 4 SFF USING LULU AND DPT.....	37
4.1 Introduction.....	37
4.2 The Modified LULU Focus Measure (MLULU).....	37
4.2.1 Step 1: MLULU Algorithm	38
4.2.2 Step 2: MLULU Algorithm	42
4.3 The Modified DPT Focus Measure (MDPT).....	44
4.4 MLULU Cascaded with Other Techniques	45
4.5 Chapter Summary	46
CHAPTER 5 RESULT AND DISCUSSION	47
5.1 Introduction.....	47
5.2 Test Images	47
5.3 Experimental Results	48
5.3.1 Metric Measures.....	48
5.3.2 Results.....	50
5.3.3 Cascading proposed method with other FMs.....	56
5.4 Chapter Summary	60
CHAPTER 6 CONCLUSION AND RECOMMENDATIONS	61
6.1 Conclusion	61
6.2 Future Work.....	63
REFERENCES	64

APPENDIX A.....	69
APPENDIX B.....	71
APPENDIX C.....	75
PUBLICATIONS.....	105

LIST OF FIGURES

Figure 2.1 Pattern of focused and defocused images [3]	6
Figure 2.2 Depth estimation methods	6
Figure 2.3 Test image with different focusing values.....	8
Figure 2.4 Sequence of images	9
Figure 2.5 Shape recovery using SML method for the cone image.....	12
Figure 2.6 Shape recovery using TEN method for the cone image.....	13
Figure 2.7 Shape recovery using GLV method for the cone image.....	13
Figure 2.8 Existing SFF Techniques.....	14
Figure 2.9 Effect of different noises on baboon and cameraman; (a) Original image of cameraman in absence of noise, (b) Original image of baboon in absence of noise, (c) Cameraman in presence of impulse noise with noise density of 0.2, (d) Baboon in presence of impulse noise with noise density of 0.2, (e) Cameraman in presence of Gaussian noise with mean value of 0 and variance of 0.2, (f) Baboon in presence of Gaussian noise with mean value of 0 and variance of 0.2, (g) Cameraman in presence of speckle noise with noise density of 0.2 and (h) Baboon in presence of speckle noise with noise density of 0.2.....	15
Figure 2.10 Existing methods in the presence of impulse noise; (a) Ground truth, (b) TEN focus measure in the present of impulse noise with noise density of 0.5, (c) GLV focus measure in the present of impulse noise with noise density of 0.05 and (d) SML focus measure in the present of impulse noise with noise density of 0.005.....	16
Figure 2.11 Existing methods in the presence of Gaussian noise; (a) Ground truth, (b) GLV focus measure in the present of Gaussian noise with noise density of 0.5, (c) TEN focus measure in the present of Gaussian noise with noise density of 0.05 and (d) SML focus measure in the present of Gaussian noise with noise density of 0.005.....	17
Figure 2.12 Existing methods in the presence of speckle noise; (a) Ground truth, (b) GLV focus measure in the present of speckle noise with noise density of 0.5, (c) SML focus measure in the present of speckle noise with noise density of 0.05 and (d) TEN focus measure in the present of speckle noise with noise density of 0.005.....	18

Figure 3.1 a) Original signal, b) Result of L smoother on the signal, and c) Result of U smoother on the signal	21
Figure 3.2 Four different neighboring regions of pixel (i,j): a) 4-neighborhood, b) 8-neighborhood c) 12-neighborhood, and d) 24-neighborhood.....	22
Figure 3.3 Illustration of neighbors for Equations 3.3 to 3.6,.....	23
Figure 3.4 (a) Original binary image, (b) Resulted image after applying L smoother on it, and (c) Resulted image after applying U smoother on the original image	24
Figure 3.5 (a) Corrupted images of cameraman and baboon with impulse noise, (b) Resulted images after applying L smoother on it, and (c) Resulted image after applying U smoother on the original image.....	25
Figure 3.6 1D sequence (ξ) for DPT decomposition	27
Figure 3.7 Result of $D1$ on the 1D sequence of ξ	28
Figure 3.8 Result of $D2$ on the 1D sequence of ξ	30
Figure 3.9 Result of $D3$ on the 1D sequence of ξ	31
Figure 3.10 DPT decomposition for 2D	34
Figure 3.11 2D DPT for 4-Connectivity	35
Figure 3.12 2D DPT for 8-connectivity	36
Figure 4.1 2D neighborhood for L3U3L8U8.....	39
Figure 4.2 3D neighborhood of window size 3×3 for pixel "X".....	40
Figure 4.3 3D neighborhood for pixel "X"	41
Figure 4.4 Choosing the maximum value along all frames	43
Figure 5.1 Simulated Cone in the presence of impulse noise with noise density of 0.5; (a) Ground truth, (b) SML focus measure, (c) TEN focus measure, (d) GLV focus measure and (d) MLULU focus measure	50
Figure 5.2 Real LCD in the presence of impulse noise with noise density of 0.05; (a) Ground truth, (b) SML focus measure, (c) TEN focus measure, (d) GLV focus measure and (d) MLULU focus measure.....	51
Figure 5.3 RMSE comparison between different methods for simulated cone object in the presence of impulse noise	52
Figure 5.4 PSNR comparison between different methods for simulated cone object in the presence of impulse noise	53

Figure 5.5 Coin in the presence of Gaussian noise with mean value of 0 and variance of 0.5; (a) Ground truth, (b) SML focus measure, (c) TEN focus measure, (d) GLV focus measure and (d) MLULU focus measure.....	54
Figure 5.6 LCD in the presence of speckle noise with noise density of 0.5; (a) Ground truth, (b) SML focus measure, (c) TEN focus measure, (d) GLV focus measure and (d) MLULU focus measure	55
Figure 5.7 (a) Ground truth of Simulated Cone, (b) TEN focus measure result in the presence of impulse noise with noise density of 0.5, (c) MLULU+TEN focus measure result in the presence of impulse noise with noise density of 0.5, (d) GLV focus measure result in the presence of impulse noise with noise density of 0.05, (e) MLULU+GLV focus measure result in the presence of impulse noise with noise density of 0.05, (f) SML focus measure result in the presence of impulse noise with noise density of 0.005 and (g) MLULU+SML focus measure result in the presence of impulse noise with noise density of 0.005.....	56
Figure B.1 Test object: simulated cone; (a) focused on the based section of the cone, (b) focused on the middle part of the cone and (c) focused on the apex part	71
Figure B.2 Test object: simulated slope; (a) focused on a narrow column on the left side, (b) focused on a narrow column in the middle of the image and (c) focused on a narrow column on the right side.....	71
Figure B.3 Test object: simulated cosine; (a) focused on a large circular portion, (b) focused on a medium circular part and (c) focused on a small circular region in the middle	72
Figure B.4 Test object: real cone; (a) focused on the based section of the cone, (b) focused on the middle part of the cone and (c) focused on the apex part.....	72
Figure B.5 Test object: real coin; (a) far sectioned is focused, (b) focused on head section and (c) focused on the very far points	73
Figure B.6 Test object: real LCD; (a) focused on the back part, (b) focused on the middle part and (c) focused on the corner parts.....	73
Figure B.7 Test object: real plane(a) far sectioned is focused, (b) focused on the middle section and (c) focused on the front points	74
Figure C.1 Simulated cosine in the presence of speckle noise with noise density of 0.005; (a) Ground truth, (b) GLV focus measure and (d) MLULU+GLV focus measure	75

Figure C.2 Real plane in the presence of speckle noise with noise density of 0.005; (a) Ground truth, (b) SML focus measure and (d) MLULU+SML focus measure...76

Figure C.3 Simulated slope in the presence of speckle noise with noise density of 0.005; (a) Ground truth, (b) TEN focus measure and (d) MLULU+TEN focus measure76

Figure C.4 Real cone in the presence of speckle noise with noise density of 0.005; (a) Ground truth, (b) SML focus measure and (d) MLULU+SML focus measure...77

Figure C.5 Simulated cosine in the presence of speckle noise with noise density of 0.05; (a) Ground truth, (b) TEN focus measure and (d) MLULU+TEN focus measure77

Figure C.6 Simulated slope in the presence of speckle noise with noise density of 0.05; (a) Ground truth, (b) GLV focus measure and (d) MLULU+GLV focus measure78

Figure C.7 Simulated Cone in the presence of speckle noise with noise density of 0.05; (a) Ground truth, (b) SML focus measure and (d) MLULU+SML focus measure78

Figure C.8 Simulated slope in the presence of speckle noise with noise density of 0.05; (a) Ground truth, (b) TEN focus measure and (d) MLULU+TEN focus measure79

Figure C.9 Real Plane in the presence of speckle noise with noise density of 0.05; (a) Ground truth, (b) GLV focus measure and (d) MLULU+GLV focus measure...79

Figure C.10 Simulated cosine in the presence of speckle noise with noise density of 0.5; (a) Ground truth, (b) GLV focus measure and (d) MLULU+GLV focus measure80

Figure C.11 Simulated cone in the presence of speckle noise with noise density of 0.5; (a) Ground truth, (b) SML focus measure and (d) MLULU+SML focus measure80

Figure C.12 Simulated cosine in the presence of speckle noise with noise density of 0.5; (a) Ground truth, (b) TEN focus measure and (d) MLULU+TEN focus measure81

Figure C.13 Simulated slope in the presence of impulse noise with noise density of 0.005; (a) Ground truth, (b) GLV focus measure and (d) MLULU+GLV focus measure81

Figure C.14 Simulated cone in the presence of impulse noise with noise density of 0.005; (a) Ground truth, (b) SML focus measure and (d) MLULU+SML focus measure	82
Figure C.15 Simulated slope in the presence of impulse noise with noise density of 0.005; (a) Ground truth, (b) TEN focus measure and (d) MLULU+TEN focus measure	82
Figure C.16 Simulated cone in the presence of impulse noise with noise density of 0.005; (a) Ground truth, (b) GLV focus measure and (d) MLULU+GLV focus measure	83
Figure C.17 Real plane in the presence of impulse noise with noise density of 0.005; (a) Ground truth, (b) SML focus measure and (d) MLULU+SML focus measure	83
Figure C.18 Real cone in the presence of impulse noise with noise density of 0.005; (a) Ground truth, (b) GLV focus measure and (d) MLULU+GLV focus measure	84
Figure C.19 Real plane in the presence of impulse noise with noise density of 0.005; (a) Ground truth, (b) GLV focus measure and (d) MLULU+GLV focus measure	84
Figure C.20 Real LCD in the presence of impulse noise with noise density of 0.005; (a) Ground truth, (b) GLV focus measure and (d) MLULU+GLV focus measure	85
Figure C.21 Simulated cosine in the presence of impulse noise with noise density of 0.005; (a) Ground truth, (b) GLV focus measure and (d) MLULU+GLV focus measure	85
Figure C.22 Real cone in the presence of impulse noise with noise density of 0.005; (a) Ground truth, (b) SML focus measure and (d) MLULU+SML focus measure	86
Figure C.23 Real LCD in the presence of impulse noise with noise density of 0.005; (a) Ground truth, (b) SML focus measure and (d) MLULU+SML focus measure	86
Figure C.24 Real coin in the presence of impulse noise with noise density of 0.005; (a) Ground truth, (b) SML focus measure and (d) MLULU+SML focus measure	87

Figure C.25 Simulated cone in the presence of impulse noise with noise density of 0.005; (a) Ground truth, (b) TEN focus measure and (d) MLULU+TEN focus measure87

Figure C.26 Real cone in the presence of impulse noise with noise density of 0.005; (a) Ground truth, (b) TEN focus measure and (d) MLULU+TEN focus measure88

Figure C.27 Real LCD in the presence of impulse noise with noise density of 0.005; (a) Ground truth, (b) TEN focus measure and (d) MLULU+TEN focus measure88

Figure C.28 Real coin in the presence of impulse noise with noise density of 0.005; (a) Ground truth, (b) TEN focus measure and (d) MLULU+TEN focus measure89

Figure C.29 Simulated slope in the presence of impulse noise with noise density of 0.05; (a) Ground truth, (b) GLV focus measure and (d) MLULU+GLV focus measure89

Figure C.30 Real cone in the presence of impulse noise with noise density of 0.05; (a) Ground truth, (b) GLV focus measure and (d) MLULU+GLV focus measure...90

Figure C.31 Real plane in the presence of impulse noise with noise density of 0.05; (a) Ground truth, (b) GLV focus measure and (d) MLULU+GLV focus measure90

Figure C.32 Simulated cone in the presence of impulse noise with noise density of 0.05; (a) Ground truth, (b) GLV focus measure and (d) MLULU+GLV focus measure91

Figure C.33 Simulated slope in the presence of impulse noise with noise density of 0.05; (a) Ground truth, (b) GLV focus measure and (d) MLULU+GLV focus measure91

Figure C.34 Simulated cosine in the presence of impulse noise with noise density of 0.05; (a) Ground truth, (b) GLV focus measure and (d) MLULU+GLV focus measure92

Figure C.35 Real cone in the presence of impulse noise with noise density of 0.05; (a) Ground truth, (b) SML focus measure and (d) MLULU+SML focus measure...92

Figure C.36 Real plane in the presence of impulse noise with noise density of 0.05; (a) Ground truth, (b) SML focus measure and (d) MLULU+SML focus measure	93
Figure C.37 Simulated cone in the presence of impulse noise with noise density of 0.05; (a) Ground truth, (b) SML focus measure and (d) MLULU+SML focus measure	93
Figure C.38 Real LCD in the presence of impulse noise with noise density of 0.05; (a) Ground truth, (b) SML focus measure and (d) MLULU+SML focus measure...	94
Figure C.39 Real coin in the presence of impulse noise with noise density of 0.05; (a) Ground truth, (b) SML focus measure and (d) MLULU+SML focus measure...	94
Figure C.40 Simulated slope in the presence of impulse noise with noise density of 0.05; (a) Ground truth, (b) TEN focus measure and (d) MLULU+TEN focus measure	95
Figure C.41 Real cone in the presence of impulse noise with noise density of 0.05; (a) Ground truth, (b) TEN focus measure and (d) MLULU+TEN focus measure....	95
Figure C.42 Real plane in the presence of impulse noise with noise density of 0.05; (a) Ground truth, (b) TEN focus measure and (d) MLULU+TEN focus measure	96
Figure C.43 Simulated cone in the presence of impulse noise with noise density of 0.05; (a) Ground truth, (b) TEN focus measure and (d) MLULU+TEN focus measure	96
Figure C.44 Real LCD in the presence of impulse noise with noise density of 0.05; (a) Ground truth, (b) TEN focus measure and (d) MLULU+TEN focus measure....	97
Figure C.45 Simulated cosine in the presence of impulse noise with noise density of 0.05; (a) Ground truth, (b) TEN focus measure and (d) MLULU+TEN focus measure	97
Figure C.46 Simulated cone in the presence of impulse noise with noise density of 0.5; (a) Ground truth, (b) TEN focus measure and (d) MLULU+TEN focus measure	98
Figure C.47 Real plane in the presence of impulse noise with noise density of 0.5; (a) Ground truth, (b) TEN focus measure and (d) MLULU+TEN focus measure....	98

Figure C.48 Simulated slope in the presence of Gaussian noise with noise density of 0.005; (a) Ground truth, (b) GLV focus measure and (d) MLULU+GLV focus measure	99
Figure C.49 Simulated cone in the presence of Gaussian noise with noise density of 0.005; (a) Ground truth, (b) GLV focus measure and (d) MLULU+GLV focus measure	99
Figure C.50 Real plane in the presence of Gaussian noise with noise density of 0.005; (a) Ground truth, (b) GLV focus measure and (d) MLULU+GLV focus measure	100
Figure C.51 Simulated slope in the presence of Gaussian noise with noise density of 0.005; (a) Ground truth, (b) TEN focus measure and (d) MLULU+TEN focus measure	100
Figure C.52 Simulated cosine in the presence of Gaussian noise with noise density of 0.005; (a) Ground truth, (b) TEN focus measure and (d) MLULU+TEN focus measure	101
Figure C.53 Simulated slope in the presence of Gaussian noise with noise density of 0.05; (a) Ground truth, (b) GLV focus measure and (d) MLULU+GLV focus measure	101
Figure C.54 Simulated cosine in the presence of Gaussian noise with noise density of 0.05; (a) Ground truth, (b) GLV focus measure and (d) MLULU+GLV focus measure	102
Figure C.54 Simulated cone in the presence of Gaussian noise with noise density of 0.05; (a) Ground truth, (b) SML focus measure and (d) MLULU+SML focus measure	102
Figure C.55 Real plane in the presence of Gaussian noise with noise density of 0.05; (a) Ground truth, (b) SML focus measure and (d) MLULU+SML focus measure	103
Figure C.56 Real coin in the presence of Gaussian noise with noise density of 0.05; (a) Ground truth, (b) SML focus measure and (d) MLULU+SML focus measure	103
Figure C.57 Simulated slope in the presence of Gaussian noise with noise density of 0.05; (a) Ground truth, (b) TEN focus measure and (d) MLULU+TEN focus measure	104

LIST OF TABLES

Table 2.1 SFF-based techniques	10
Table 4.1 DPT operators for SFF.....	44
Table 5.1 MLULU and DPT performance in the presence of impulse noise for simulated cone object.....	52
Table 5.2 Cascaded methods performance in the presence of impulse	57
Table 5.3 Cascaded methods performance in the presence of Gaussian	58
Table 5.4 Cascaded methods performance in the presence of speckle	59
Table A.1 Some of the properties of LULU operator	69

LIST OF ABBREVIATIONS

DPT	Discrete Pulse Transform
FM	Focus Measure
GLV	Gray Level Variance
ND	Noise Density
SFF	Shape from Focus
SML	Sum Modified Laplacian
TEN	Tenenbaum
V	Variance

CHAPTER 1

INTRODUCTION

1.1 Introduction

Recovering the 3D shape of an object based on 2D image information is a challenging area of research. It is an emerging area of research aimed at improving the human's understanding of the shape and size of objects in images. This area of research is finding its implementation in many applications, such as virtual games, product modelling, facial representation, biomedical imaging, microscopic imaging, vehicle navigation, astronomy, distance measuring for CCTV (automatic surveillance systems), etc. 2D image information from same view seems to carry less information about the object's shape but since it is simpler compared to other multi-view methods, numerous research has been reported for 3D shape recovery using single view images. Single-view 2D image information can convey information of object's depth using different techniques. Focusing techniques are promising ones due to the 3D information that they detect. Image focusing is one of the principal schemes of 3D shape reconstruction. The shape from focus (SFF) is one of the best 3D shape recovery methods which reconstructs the 3D shape from a sequence of 2D images taken from same angle. The SFF images of an object are defined as a sequence of frames which carry different focused values of an object's surface. Each frame carries different focusing information about different sections of the 3D object.

Reconstructing the 3D shape based on the focused values requires a sharpness extraction technique which can detect the focused parts in each frame. There are different sharpness measures for detecting the focus of image pixels along all the frames of SFF sequence.

Tenenbaum (TEN), Gray Level Variance (GLV), Mean, Laplacian, Modified Laplacian (ML), Sum of the Modified Laplacian (SML), Curvature and M_2 , are known to be some of the best methods in detecting the best focus value in noiseless situation. However the behaviour of these existing SFF methods significantly worsens in noisy environments.

In this thesis, a new focus measure for shape from focus estimation is proposed for noisy environments. The proposed method is based on LULU operators which has the inherent property of filtering out the noise as well as performing initial estimation of the depth map by computing best focused pixels. LULU operators are nonlinear rank selector operators that hold consistent separation, total variation and shape preservation properties. The implementation of LULU is followed with Discrete Pulse Transform for optimized detection of the focused pixels in each frame. Furthermore, different combinations between LULU and the existing SFF methods, like Tenenbaum (TEN), sum modified Laplacian (SML) and Gray Level Variance (GLV), are considered as potential solution to depth map problem. The experimental results show good potential for the proposed LULU combined with DPT or with other existing SFF techniques in solving the depth map problem, especially in noisy environments.

1.2 Motivation

In practice, the acquired images are frequently corrupted with noise. There are many different types of noises from various sources which corrupt the image such as Gaussian, speckle and impulse noise. The presence of noise in the image limits the processing and subsequent analysis of images.

Although the existing focus measures for 3D shape recovery using SFF perform well in noiseless environments but their performance deteriorates considerably in noisy environments. This deterioration is due to the fact that the existing focus measures are based on derivatives and variance information. As a result, their performance is poor for Gaussian noise as well as randomly distributed impulse noise.

This results of depth maps are far from the ground truth data and hence cannot be used for 3D shape recovery. Therefore, developing a reliable method for calculating depth map for 3D shape recovery using SFF in noisy environment is the major motivation of this research.

1.3 Problem Statement

The existing focus measures perform well in noiseless environments but their performance deteriorate in noisy environments. During image acquisition process, additive white Gaussian noise (AWGN) is present. In addition, based on the environment condition and the camera, speckle noise and impulse noise may also be present. Presence of these types of noise in the image destroys the focus information, especially sharpest pixel values. Hence, the algorithms computing the best focus values fail in such a situation. Therefore, a SFF method is required that be able to present acceptable results in the existence of noise.

The main problems with the current SFF techniques are:

- Noise removal is not inherently present in existing focus measures.
- Existing methods depend on derivatives and statistics which does not perform well in the presence of noise.

1.4 Research Objectives

The main objectives of this research can be summarized in the following points:

- To develop a 3D shape recovery method based on LULU and DPT.
- To come up with new SFF based technique capable of extracting 3D in noisy environments.
- To verify the performance of the developed SFF technique with real and simulated images.
- To study the impact of different types of noise; Gaussian, impulse and speckle on the performance of the proposed techniques.

1.5 Research Scope

This research introduces LULU and DPT and modify them to be used as focus measures for 3D shape recovery based on SFF. LULU based focus measure is proposed to be used in combination with other existing SFF methods like SML, TEN and GLV. The capability of LULU combined with DPT or with other SFF methods is tested in noisy environments and compared with existing methods.

1.6 Thesis Outline

Chapter 1, describes the problem statement, motivation of the work, research objectives, scope and study milestone.

Chapter 2 begins with a brief description of 3D shape recovery and Shape From Focus (SFF). Then, it explains some of the different SFF techniques, like SML, GLV and TEN which are used and compared in this work.

Chapter 3 describes LULU operators and DPT, and discuss the properties and applications of them. This chapter also shows the inherent capability of LULU in removing noise from images.

Chapter 4 introduces modified versions of LULU and DPT for 3D shape recovery applications. Combinations between LULU and other existing SFF techniques are considered and outlined.

In Chapter 5, the proposed techniques based on LULU operators and DPT are applied on seven different SFF test objects. All the experiments are considered in the presence of impulse, Gaussian and speckle noise. The experiments are run several times and the results are analyzed quantitatively and qualitatively. Also, all the obtained results are compared with other techniques.

Chapter 6 concludes this thesis and sheds light on possible future work.

CHAPTER 2

LITERATURE REVIEW

2.1 Introduction

Reconstructing the 3D shape of an object is a primary step in 3D technology. The information of a scene can be captured by different optical systems and presented in different ways. Different images with different camera lens settings can capture photometric and geometric information differently. Different objects in an image can be defined with different information such as luminous intensity, colours, radiance, size, depth and distance. This information can be used in many data acquisitions applications from 2D images, such as 3D shape recovery. Shape recovery or shape reconstruction is widely used where the shape of the object is not easy to be estimated, such as astronomy and biomedical fields [1].

Figure 2.1, illustrates the fundamental geometry formation of an image, where u refers to the distance of the object from the lens, v shows the distance of the image from the lens and f indicated the focal length of the lens. This figure illustrates well that when there is an object at point P , it will be well focused at the point P' and if the object point is not focused in image plane, there will be a blur image around P'' point [2]. In thin lens law, the connection between the focal length, object and image distance, is given:

$$\frac{1}{f} = \frac{1}{u} + \frac{1}{v} \quad (2.1)$$

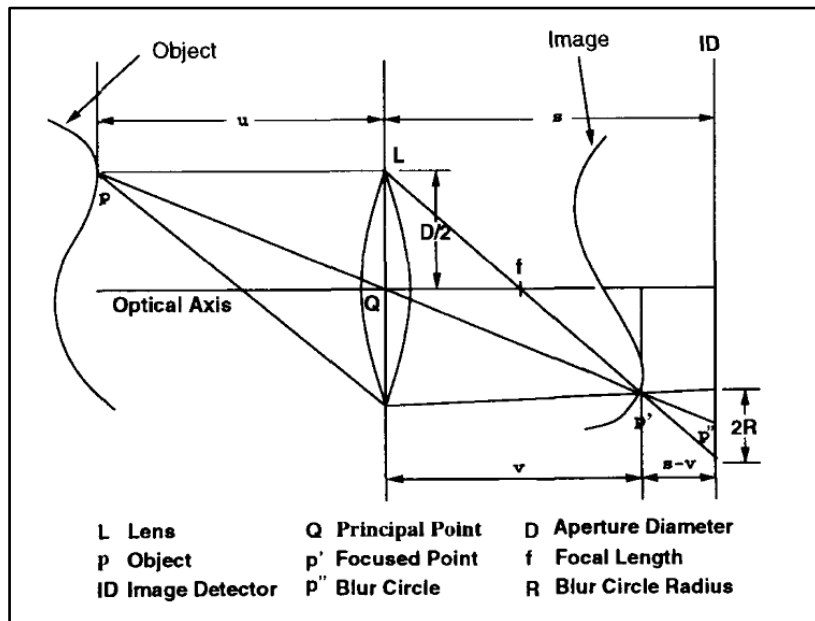


Figure 2.1 Pattern of focused and defocused images [3]

In general, 3D shape recovery can be performed by using three different techniques as shown in Figure 2.2. The first technique is a contact one which depends on the mechanical and inertial objects in order to estimate the shape. The second technique is transmissive, like CTR/MRI which is based on X ray or EM radiation. The third technique is reflective which can be optical or non-optical (e.g. radar, sonar, etc).

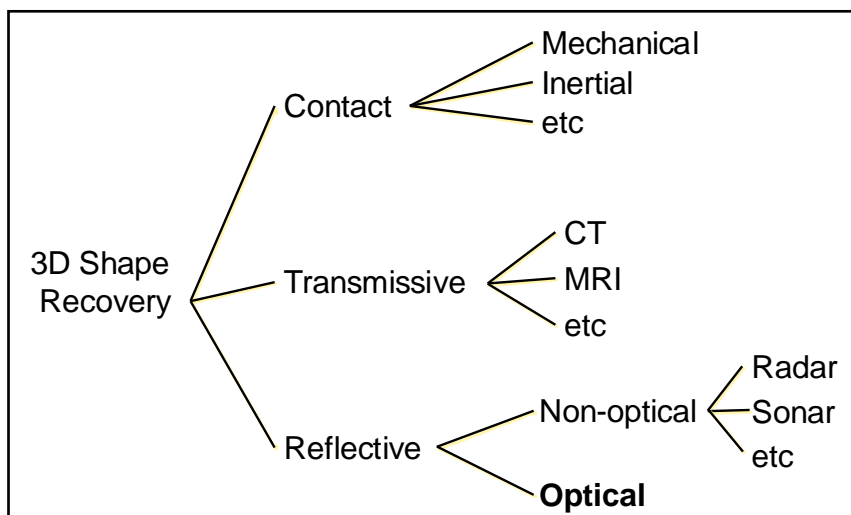


Figure 2.2 Depth estimation methods

In this research we concentrate on the optical method because it is inexpensive and non-contact (with the object) which prevents damaging the object; though it has some disadvantages such as sensitivity to illumination, noise and confusion by secularity and inter reflections.

Many optical techniques have been proposed over the last few years for 3D shape recovery. These techniques are mainly based on shape extraction as described here:

- stereo

The method of recovering the 3D depth from two or more intensity based images taken from different angles. The stereo method verifies which point in one image matches which point in another image [4].

- texture

Shape from texture determines the depth of object from texture information in an image [5].

- focus

This method is based on focus/sharpness detection of a particular object in different images for estimating the depth between different focused points [1].

- defocus

Estimating shape from defocus is based on retrieving the depth information of a scene using the blurring variation of a number of images captured at different focus settings [2].

- motion

Shape from motion recovers the 3D shape and motion from a small set of points matched in two images from single camera [4].

- shading

This technique recovers the 3D shape of an object from the variations caused by shading in the image [6].

This thesis proposed new focus measurement technique in shape from focus (SFF). The developed technique uses SFF since focused image conveys more information about the shape of an object than normal image.

2.2 Shape from Focus

SFF method requires capturing many different image frames for the same object from a specific angle. In general, there are two methods of capturing different sequences; the first is by changing the focus value of the lens and keeping the object and camera's positions fixed, whereas the second is achieved by keeping the camera's focus value fixed and change the distance between object and camera gently for different shots.

In Figure 2.3, the test image shows different focused images of a cone object. This database is constructed from 97 different images with different focus values from the cone object. Figure 2.4, shows this concept clearer. It shows a sequence of frames that indicate to changed degrees of object focus achieved through a single camera.

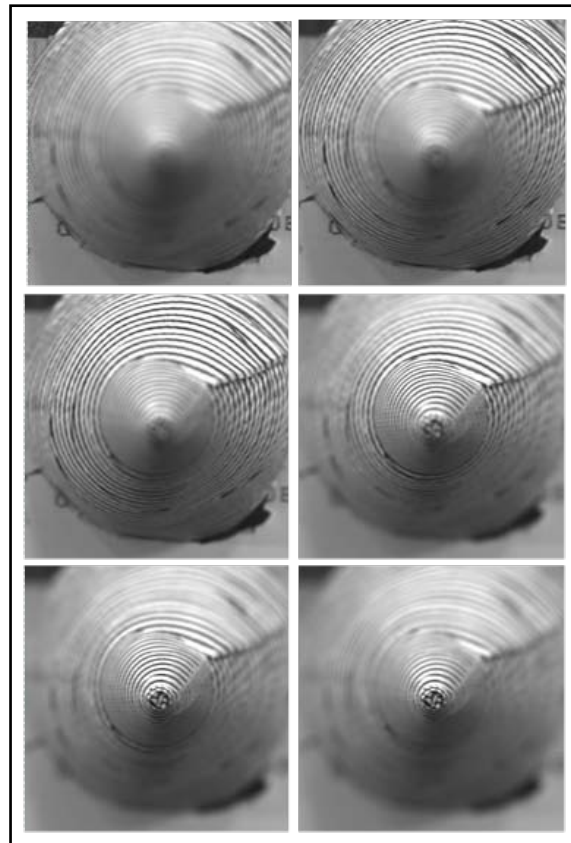


Figure 2.3 Test image with different focusing values

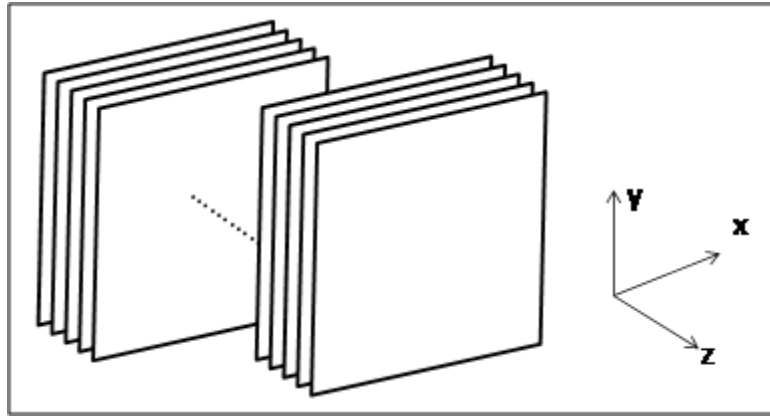


Figure 2.4 Sequence of images

After collecting the data, we needed to determine the exact frame where the depth of the object is in focus or has the maximum sharpness. A sharpness measure or focus measure for each image in the sequence is computed at each pixel location using a small window around the pixel. The success of any focus measure depends on how accurate is the sharpness in image pixels. By applying different well known mathematical techniques for SFF such as Laplacian [7], modified Laplacian (ML), sum of the modified Laplacian (SML), Tenenbaum(TEN) [8], Gray Level Variance (GLV), mean, curvature and M_2 , the best depth value for each single point of the object from the lens of camera can be obtained. This information shows the highest amount of sharpness or best focusing values among the different captures. By selecting the pixel with highest focus value among all frames, the 3D shape of the object from a single view can be reconstructed. Besides these methods, other approximation methods can be used in order to obtain better results such as are the Gaussian interpolation [1] and Neural Networks [9] and [10].

Many techniques for shape recovery out of focus have been proposed over the last three decades with different degrees of success. Among the best known SFF-based techniques are the followings:

Table 2.1 SFF-based techniques

Scientist	Year	Proposed Technique
Horn	1968	a technique based on Fourier transform [11]
Tenenbaum	1970	built up the gradient magnitude maximization technique which is based on sharpness of edges to optimize focus quality [12]
Buffington	1974	introduced aperture-plane distortion [13]
Erteza	1976	obtained an index value for sharpness by considering the intensity distribution of the image [14]
Jarvis	1976	established a new technique based on the sum-modulus-difference [15]
Pentland	1985	assessment of image blur [13]
Krotkov	1986	discussed about the distance calculation of the sharply focused point [16]
Grossmann	1987	suggested the evaluation of depth of edge points by considering the blur of the edges [17]
Darrell and Wohn	1988	applied Laplacian and Gaussian pyramids for depth estimation [18]
Nayar	1990	built the first SFF system, he introduced Gaussian interpolation in 3D microscope [1]. He also in 1994 introduced sum modified Laplacian in shape recovery [7]
Dillion	1992	combined shape from focus and stereo to get better results [19]
Asada	1998	described eliminating windowing [20]
Zhang	2000	proposed 2nd/4th order central moment as a sharpness detector [21]
Helmi	2002	introduced new techniques based on mean, curviture and point focus methods [8]
Yap	2004	suggested Chebyshev moments for focus detection [19]

All these focusing techniques help in detecting the sharpness of the image. Calculating the sharpness in the image helps in finding the focused points which leads

to reconstructing the 3D shape of the object. Some of these SFF methods are used in this work and compared to DPT like the SML, TEN and GLV. In the subsequent section, these methods are outlined. More information about other SFF methods, can be found in [10].

2.2.1 The Sum Modified Laplacian (SML)

Laplacian operators are differential operators. We can also define them as the divergence of the gradient. Overall, these operators are symmetric and suitable for exact shape reconstruction. For an image, with the function of $f(x, y)$, the Laplacian can be defined as its second derivatives across x and y coordinates.

$$\text{Laplacian} = \frac{\partial^2 f(x, y)}{\partial x^2} + \frac{\partial^2 f(x, y)}{\partial y^2} \quad (2.2)$$

Modified Laplacian operator is summing the squared value of each derivative in Laplacian method.

$$\text{ML} = \left(\frac{\partial^2 f(x, y)}{\partial x^2} \right)^2 + \left(\frac{\partial^2 f(x, y)}{\partial y^2} \right)^2 \quad (2.3)$$

Sum modified Laplacian is the completed shape of Laplacian operators which detects the focus value for each single pixel. It is proper to be used at each pixel where $p(x, y)$ is a pixel in the neighborhood $U(x_0, y_0)$ of pixel (x_0, y_0) [10].

$$\text{SML}(x_0, y_0) = \sum_{p(x, y) \in U(x_0, y_0)} \left(\frac{\partial^2 f(x, y)}{\partial x^2} \right)^2 + \left(\frac{\partial^2 f(x, y)}{\partial y^2} \right)^2 \quad (2.4)$$

Figure 2.5, shows the 3D shape recovery using SML operator for cone image with 97 frames with different focus values.

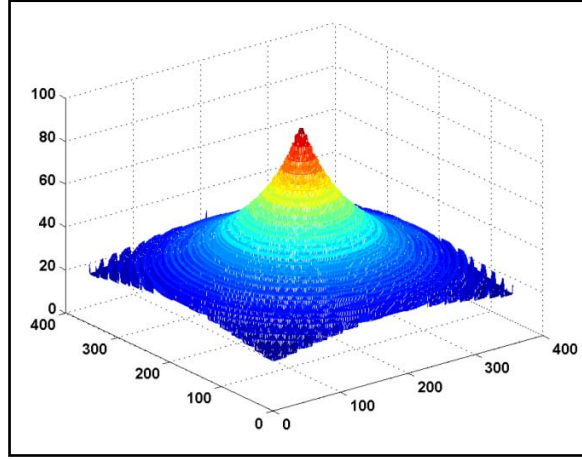


Figure 2.5 Shape recovery using SML method for the cone image

2.2.2 The Tenenbaum (TEN)

Tenenbaum operator maximizes the gradient magnitude. It is defined as the summation of the Sobel operators along x axis and y axis.

$$FM_T(x_0, y_0) = \sum_{p(x,y) \in U(x_0, y_0)} (f_x(x, y)^2 + f_y(x, y)^2) \quad (2.5)$$

Where $f(x, y)$ is the image function and $p(x, y)$ is a pixel in the neighborhood $U(x_0, y_0)$ of pixel (x_0, y_0) [10].

The 3D reconstructed shape of a cone image using TEN operator is shown in Figure 2.6.

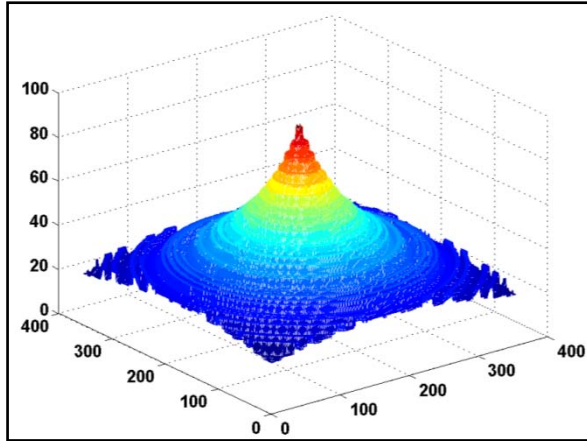


Figure 2.6 Shape recovery using TEN method for the cone image

2.2.3 The Gray Level Variance (GLV)

GLV operator, which is a statistical based method so far, is being widely used to get sharp images. Equation 2.6 shows the concept of GLV, where $f(x,y)$ is the image function and $\mu_U(x_0,y_0)$ is the gray values' mean in the neighborhood $U(x_0,y_0)$ of pixel (x_0,y_0) [10]. Figure 2.7, illustrates the 3D shape recovery using GLV operator.

$$GLV(x_0, y_0) = \frac{1}{N - 1} \sum_{p(x,y) \in U(x_0,y_0)} (f(x,y) - \mu_U(x_0, y_0))^2 \quad (2.6)$$

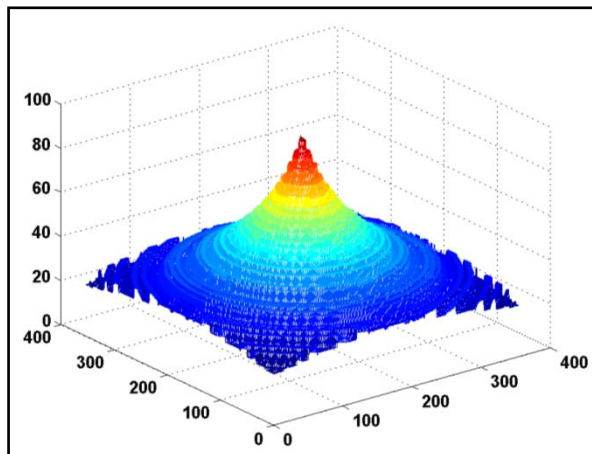


Figure 2.7 Shape recovery using GLV method for the cone image

In general, we can illustrate the concept for shape from focus as shown in Figure 2.8.

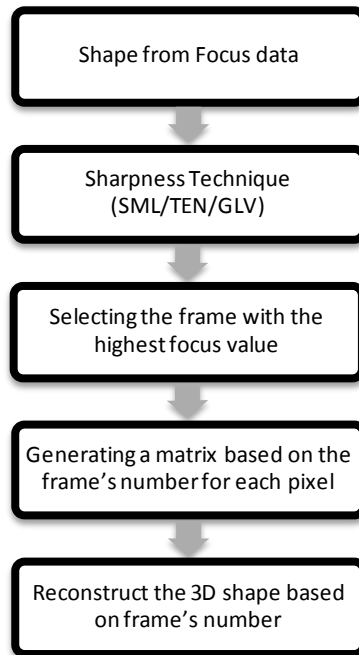


Figure 2.8 Existing SFF Techniques

As it is shown in Figure 2.8, SML, GLV and TEN techniques with their different characteristics have the same flow of operation in SFF. The first step is the data which should carry different focused values of the object. After collecting the data we need to determine the exact frame where the depth of the object is in focus or where the sharpness is at its maximum. A sharpness measure or focus measure for each image in the sequence is computed at each pixel location. As a result, the output of SFF is 2D data/matrices; one matrix encloses the resultant frame number that the pixel is best focused, and the other matrix holds the best focus value for each of the pixels. We choose the matrix based on frame numbers and simply reconstruct the 3D based on this matrix.

2.3 Existing Methods in the Presence of Noise

The success of any focus measuring method is based on the estimation of sharpness calculation in image pixels even in the presence of noise. Applying the existing sharpness detection methods on a noisy SFF data show the failure of focus detection techniques in the presence of noise.

In this section, the result of applying SML, GLV and TEN is shown in the presence of impulse, Gaussian and speckle noise. Figure 2.9 shows the effect of these three noises on baboon and cameraman pictures.

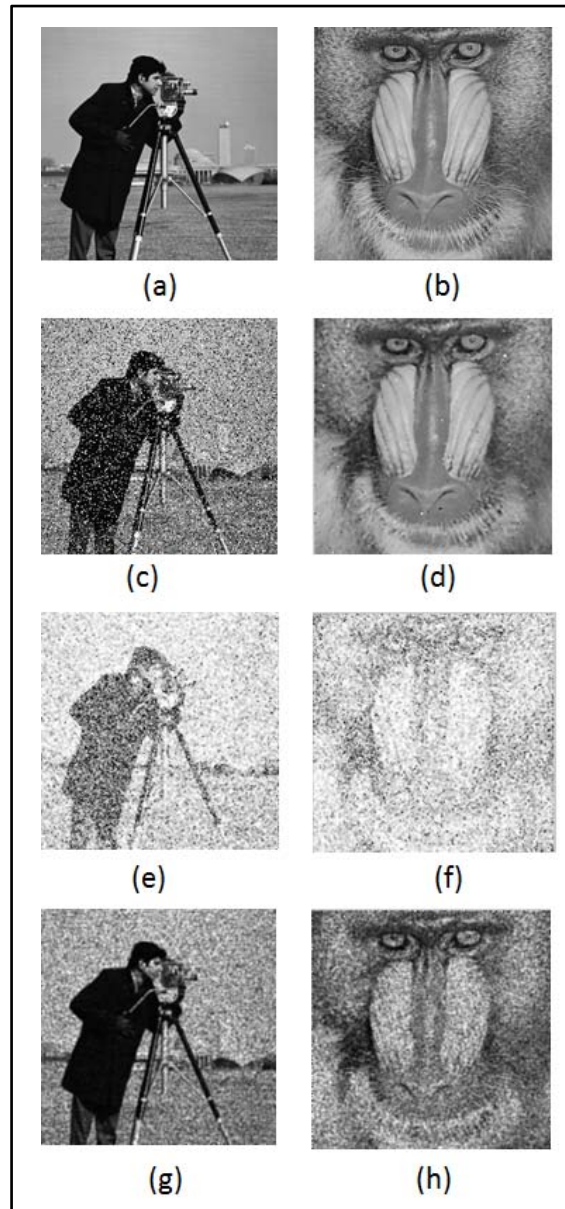


Figure 2.9 Effect of different noises on baboon and cameraman; (a) Original image of cameraman in absence of noise, (b) Original image of baboon in absence of noise, (c) Cameraman in presence of impulse noise with noise density of 0.2, (d) Baboon in presence of impulse noise with noise density of 0.2, (e) Cameraman in presence of Gaussian noise with mean value of 0 and variance of 0.2, (f) Baboon in presence of Gaussian noise with mean value of 0 and variance of 0.2, (g) Cameraman in presence of speckle noise with noise density of 0.2 and (h) Baboon in presence of speckle noise with noise density of 0.2

2.3.1 Impulse Noise

Impulse noise is a result of image sensors and transmission channels malfunction. It has a considerable bad affect on the image and decreases its quality. Even with low noise density this noise can corrupt the image due to the large difference of intensity of each pixel than neighborhood pixels [22]. The amplitude of the corruption is the maximum or the minimum intensity of the original image.

Figure 2.10, shows the performance of SML, GLV and TEN Focus Measures (FM) in the presence of impulse noise with different noise densities.

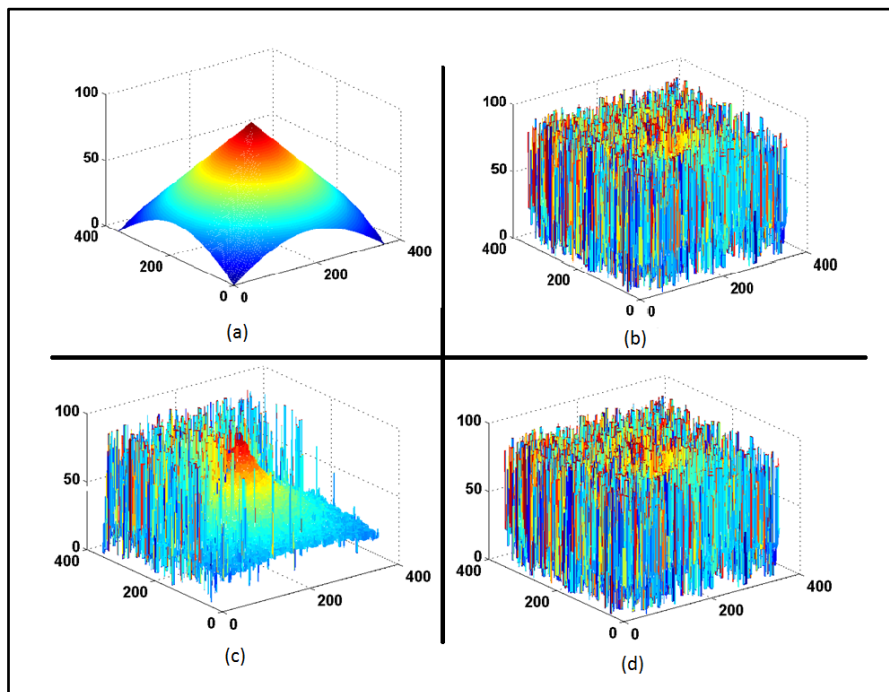


Figure 2.10 Existing methods in the presence of impulse noise; (a) Ground thruth, (b) TEN focus measure in the present of impulse noise with noise density of 0.5, (c) GLV focus measure in the present of impulse noise with noise density of 0.05 and (d) SML focus measure in the present of impulse noise with noise density of 0.005

2.3.2 Gaussian Noise

Gaussian noise is a random distribution which does not depend on the image original values. Gaussian noise is an additive and statistical noise which is generated by arbitrary interference generated by thermal friction of the atoms in conductors or photo-electronic sensors. The most significant feature of the Gaussian noise is that no matter how much the variance and histogram of the original image is, the histogram of contaminated image will always follow the Gaussian distribution [23]. Since noise has small range of amplitude, the noise performs poorly on the edge and for texture data, and it results in a large corruption on the smooth parts of the image [23].

The result of SML, GLV and TEN FMs in the presence of Gaussian noise with different noise variances is shown in Figure 2.11.

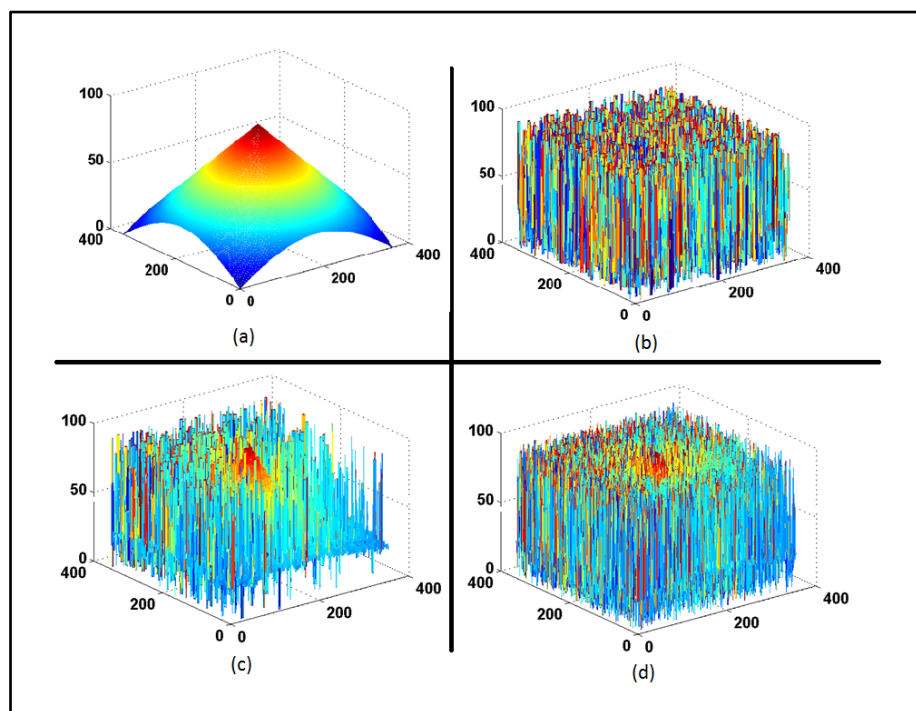


Figure 2.11 Existing methods in the presence of Gaussian noise; (a) Ground truth, (b) GLV focus measure in the present of Gaussian noise with noise density of 0.5, (c) TEN focus measure in the present of Gaussian noise with noise density of 0.05 and (d) SML focus measure in the present of Gaussian noise with noise density of 0.005

2.3.3 Speckle Noise

Speckle noise is also known as multiplicative noise which is caused by oscillations in the received signal from an object [24]. Figure 2.12 is showing the 3D shapes recovered with SML, GLV and TEN when the SFF data is corrupted by speckle noise.

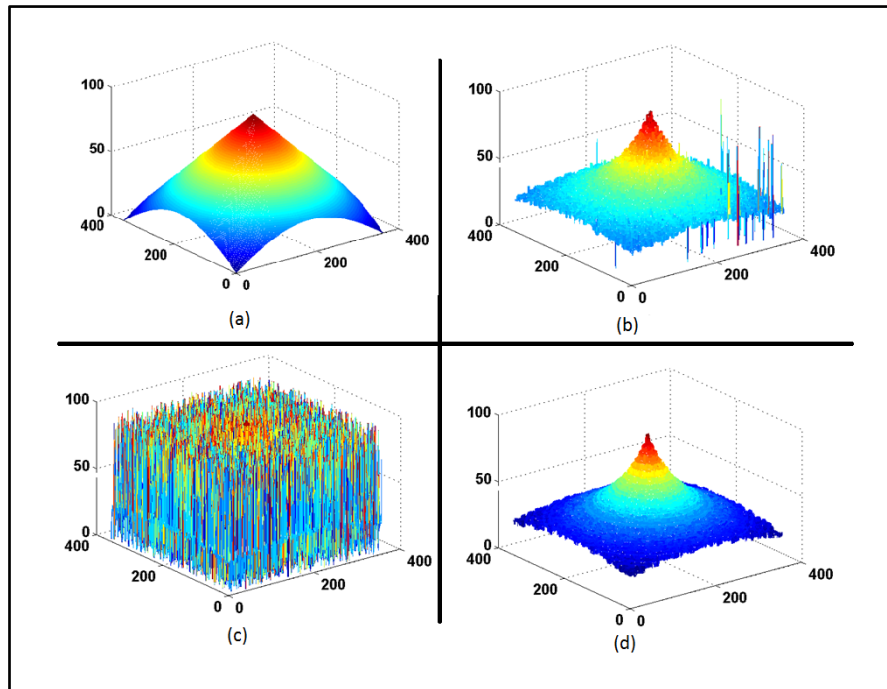


Figure 2.12 Existing methods in the presence of speckle noise; (a) Ground truth, (b) GLV focus measure in the present of speckle noise with noise density of 0.5, (c) SML focus measure in the present of speckle noise with noise density of 0.05 and (d) TEN focus measure in the present of speckle noise with noise density of 0.005

2.4 Chapter Summary

A brief description of the problem of 3D shape recovery is presented. Three well-known and widely used techniques in SFF are described and analysed. These techniques are the Sum Modified Laplacian, the Gray Level Variance and Tenenbaum which are three of the best SFF techniques. Some of the results of performance of these existing methods in the presence of impulse, Gaussian and speckle noise which are almost present in all images, is shown in this chapter. The considered techniques in this chapter will be compared with the developed technique in Chapter 4 and Chapter 5.

CHAPTER 3

LULU OPERATORS AND DISCRETE PULSE TRANSFORM

3.1 Introduction

In signal and image processing techniques, many challenges are faced when attempting to recover the original data from the noisy one. This sort of processing is usually performed using different methods, including both linear and nonlinear smoothers. Linear smoothers or filters perform well in case of additive Gaussian noise. However, their performance degrades with data corrupted with impulse noise. Meanwhile, nonlinear methods deal with discontinuities or large impulses, which relatively, provide better results. In this work, we focus on LULU, which is one of the nonlinear methods.

Rohwer and Toerien in the late 1980s introduced LULU operators based on extreme order statistics [25]. LULU operators reduce impulse noise content in the signal prior to information extraction. LULU operators are computationally convenient and simple in comparison to the median smoothers. LULU operators have the properties of trend and total variation preserving that make them essential tool for multi-resolution analysis of sequences. They have a critical role in the analysis and comparison of nonlinear smoothers (an operator A can be defined as a smoother if it has the property of $AE=EA$ where $E x_i = x_{i+1}$; also $A(x+b)=Ax+b$ for all constant sequences b ; and it should be suited in $A(cx)=c(Ax)$ for all scalars for $c \geq 0$) [26].

LULU operators are also used in two dimensional analysis, i.e., image analysis, for smoothing or filtering the image and also for object detection and extraction (by using DPT) with composition of different L and U operators.

The other application of LULU smoothers is in applying Discrete Pulse Transform (DPT) to images. DPT is a new and powerful method for the analysis of signals and can be extended to images by using LULU operators.

Since, DPT decomposes the image into different pulses, it can be used to extract the specific objects in the image by selecting the appropriate pulses. Furthermore, DPT is being used in the estimation of standard deviation of a random distribution [27].

A multi-resolution analysis of a space consists of a sequence of nested subspaces that satisfies certain self-similarity relations in time/space and scale/frequency, as well as completeness and regularity relations. DPT and Wavelet are two of the most important multi-resolution analysis methods. The properties of multi-resolution analysis is described in more detail in [28] and [29].

In this chapter, we first explain LULU operators and discuss their properties. Next, we discuss the main concept of DPT and the different applications of a combined LULU and DPT in the areas of signal and image processing.

3.2 LULU Operators

LULU operators are called MaxMin and MinMax filters due to their characteristics. They are local and nonlinear operators used for impulse noise removal. LULU operators consist of the sub-operators L (low) and U (upper) with different orders for different filters.

For one dimensional analysis of the sequences of the signal, noise removal can be done via LU or UL operators. These operators remove the positive and negative peaks which have small widths similar to impulse noise. The resulted sequence after filtering with LU and UL operators is a local and monotone sequence without any detectable noise (the sequence ξ is n-monotone if it is either $\xi_i \leq \xi_{i+1} \leq \dots \leq \xi_{i+n} \leq \xi_{i+n+1}$ or $\xi_i \geq \xi_{i+1} \geq \dots \geq \xi_{i+n} \geq \xi_{i+n+1}$, it should fulfil for all values of i such that both of ξ_i and ξ_{i+n+1} are members of the sequence [26]).

Also, the one dimensional LULU operators fulfil the idempotent condition (A is idempotent if it meets the condition of: $A^2 = A$ and co-idempotent if $I - A$ is idempotent [26]).

3.2.1 1-Dimensional LULU

When LULU is being used for signals by simply removing the locally peaks and valleys. Figure 3.1, illustrates the power of L and U operators in filtering/smoothing the signal. In this figure, the top one is the original signal while the middle and the bottom one show the smoothed signals after applying L and U operators respectively. For a given bi-infinite sequence, $\xi = (\xi_i), i \in Z$, the 1D LULU operators are defined by Equation 3.1 and Equation 3.2, as follows [30]:

$$(L_n \xi)_i = \max \{ \min \{ \xi_{i-n}, \dots, \xi_i \}, \min \{ \xi_i, \dots, \xi_{i+n} \} \}, i \in Z \quad (3.1)$$

$$(U_n \xi)_i = \min \{ \max \{ \xi_{i-n}, \dots, \xi_i \}, \max \{ \xi_i, \dots, \xi_{i+n} \} \}, i \in Z \quad (3.2)$$

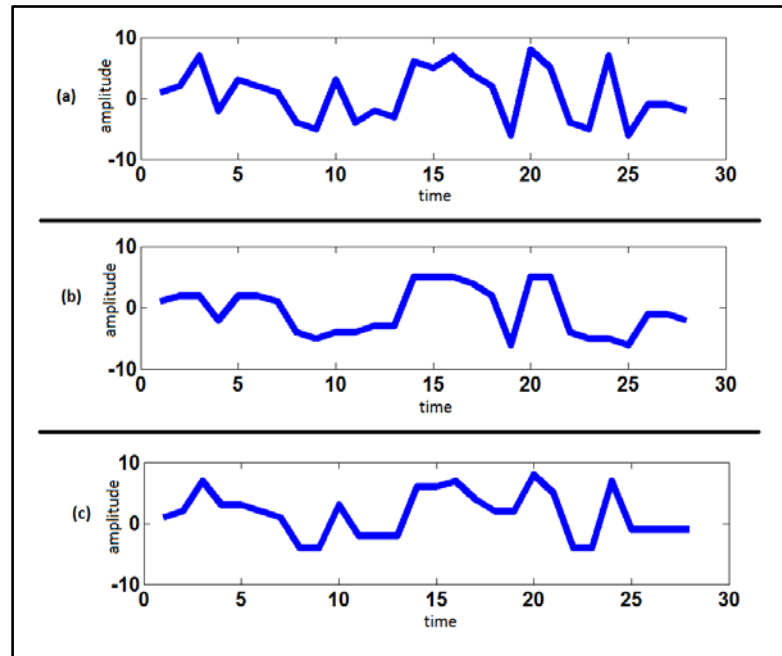


Figure 3.1 a) Original signal, b) Result of L smoother on the signal, and c) Result of U smoother on the signal

3.2.2 2-Dimensional LULU

When LULU smoothers are applied on a two dimensional array, they simply compare the elements with all their neighbors. The neighborhood of a pixel can be defined in different ways as shown in the Figure 3.2.

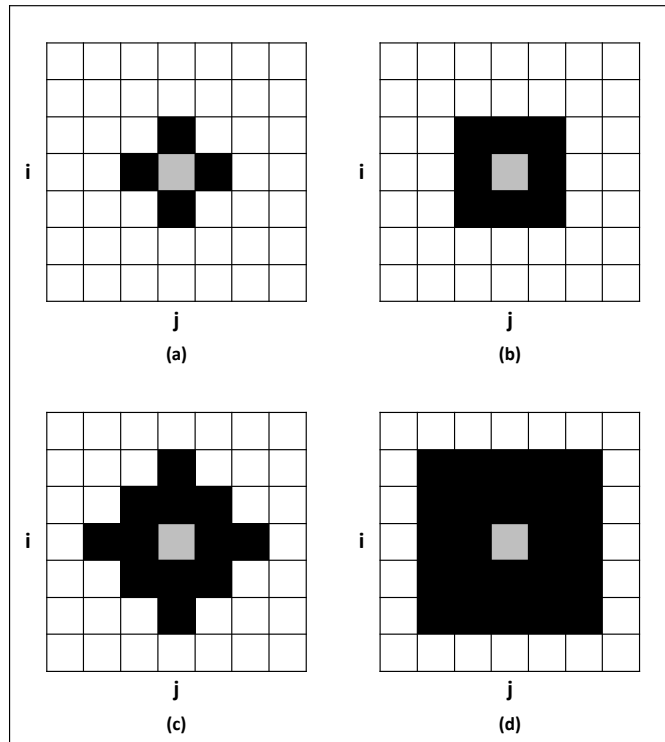


Figure 3.2 Four different neighboring regions of pixel (i,j) : a) 4-neighborhood, b) 8-neighborhood c) 12-neighborhood, and d) 24-neighborhood

To further clarify the concept of 2D processing using LULU operators, an example is provided. This example illustrates one of the many different possible neighborhood and sub-neighborhoods for a pixel. LULU in 2D, similar to 1D, can be extended to neighborhoods by considering more pixels surrounding each pixel.

In this example, the neighbors of the pixel $I(i,j)$ are divided to four different regions as shown in Equation 3.3 to Equation 3.6.

$$I_1 = [I(i, j - 1), I(i, j), I(i + 1, j - 1), I(i + 1, j)]; \quad (3.3)$$

$$I_2 = [I(i - 1, j - 1), I(i - 1, j), I(i, j), I(i, j - 1)]; \quad (3.4)$$

$$I_3 = [I(i, j + 1), I(i, j), I(i + 1, j), I(i + 1, j + 1)]; \quad (3.5)$$

$$I_4 = [I(i - 1, j + 1), I(i - 1, j), I(i, j), I(i, j + 1)]; \quad (3.6)$$

Others possible neighbors are not considered here. Figure 3.3 illustrates the Equation 3.3 to Equation 3.6, where O represents the corresponding pixel and X refers to the neighboring pixels.

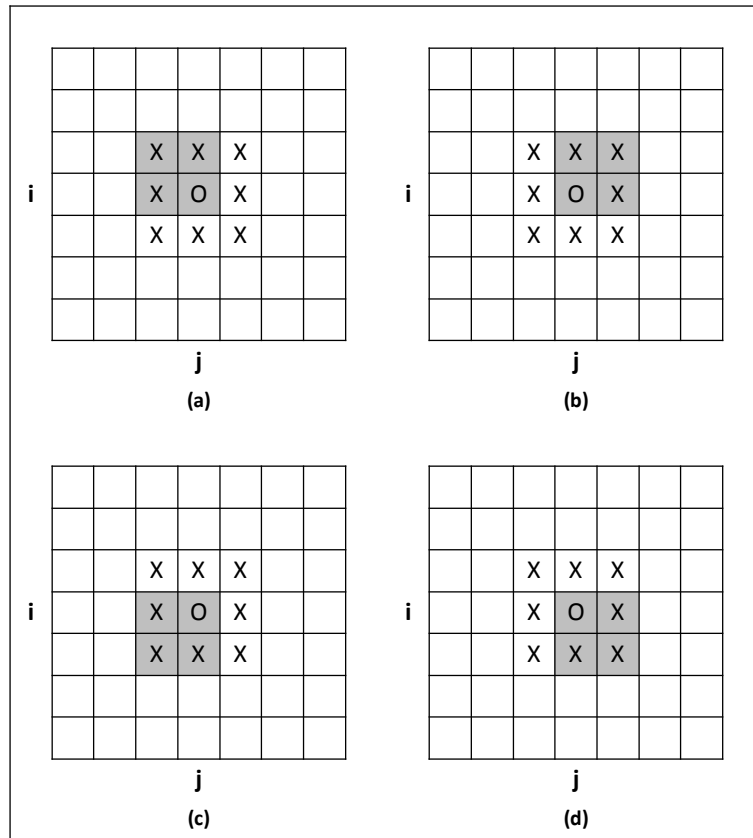


Figure 3.3 Illustration of neighbors for Equations 3.3 to 3.6, (a) I_1 , (b) I_2 , (c) I_3 , and (d) I_4

Then the L and U operators were applied as follow:

$$L(i, j) = \max(\min(I_1), \min(I_2), \min(I_3), \min(I_4)); \quad (3.7)$$

$$U(i, j) = \min(\max(I_1), \max(I_2), \max(I_3), \max(I_4)); \quad (3.8)$$

The Figure 3.4(a) shows a randomly generated binary image and Figure 3.4(b) and Figure 3.4(c) shows the smoothed images after applying L and U smoothers. The L and U in Equation 3.7 and Equation 3.8 are actually L_3 and U_3 because of considering a neighborhood of four pixels in each region. In this example, the binary image has balanced numbers of black and white parts. After applying L smoother on the image, the black parts increased. That can be described according to Equation 3.7. L operators maximize the local minima of the neighborhood (this is the reason that Figure 3.4(b) has more black spots than the original image). U smoothers are opposite of L smoothers. Therefore Figure 3.4(c) is whiter compared to the original image. Other examples are given in Figure 3.5, to illustrate the concept of L and U filters on corrupted cameraman and baboon images with impulse noise.

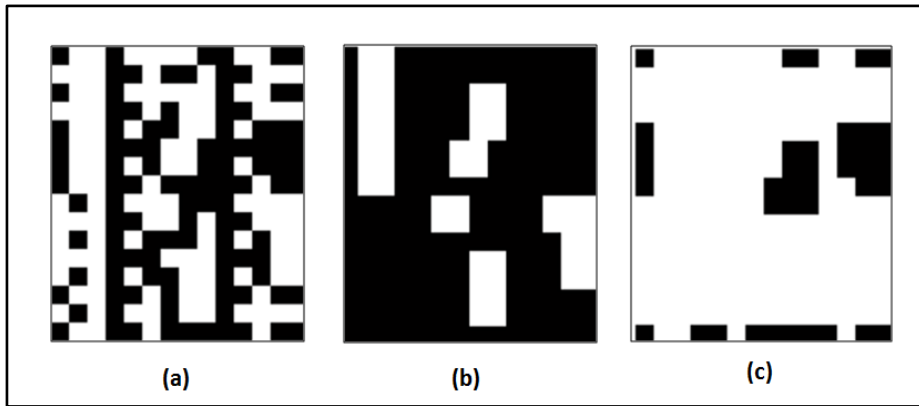


Figure 3.4 (a) Original binary image, (b) Resulted image after applying L smoother on it, and (c) Resulted image after applying U smoother on the original image

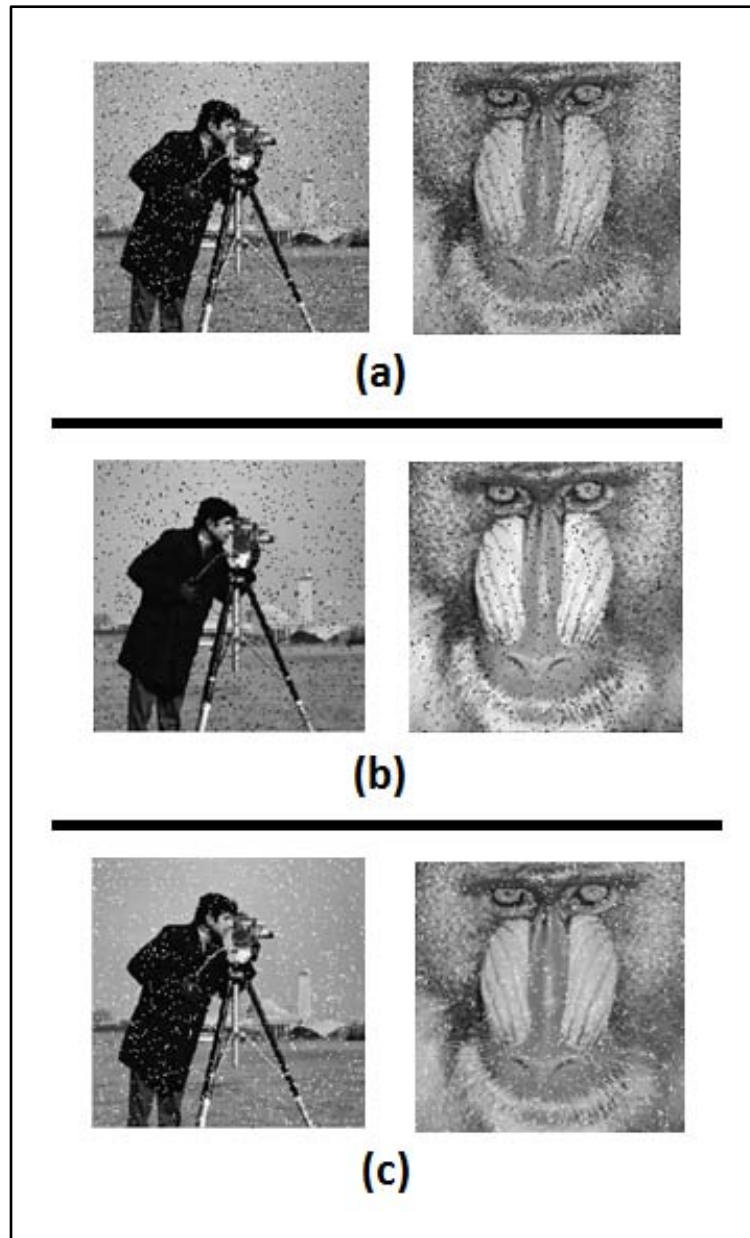


Figure 3.5 (a) Corrupted images of cameraman and baboon with impulse noise, (b) Resulted images after applying L smoother on it, and (c) Resulted image after applying U smoother on the original image

3.2.3 Properties of LULU Operators

Some of the properties of LULU operators, as introduced by Rohwer et.al., [26] are listed in APPENDIX A. However, detailed discussion of properties as well as their proofs, can be found in [26] and [31].

3.3 The Discrete Pulse Transform (DPT)

DPT is a composition of different pulses, it is discrete like Discrete Fourier and Wavelet transforms. DPT is very similar to Discrete Fourier Transform (DFT), except that DPT separates the signal to positive and negative parts (pulses) but DFT divides the signal to even and odd parts.

In image processing, DPT is used to separate the objects in the image by identifying the pulses corresponding to different objects in the image. For processing images with DPT, we need to use the LULU operators on multidimensional arrays. Sub-images are constructed based on the disparity of neighboring pixels and DPT is based on capturing the contrast in the original image on the boundary of their supports. Detailed comparison of DFT and DPT is provided by Rohwer in [26].

3.3.1 1D DPT

In general, DPT can map the bi-infinite sequences such as $\xi = (\dots, \xi_{-1}, \xi_0, \xi_1, \xi_2, \dots)$ onto an infinite vector

$$DPT(\xi) = (D_1(\xi), D_2(\xi), \dots) \quad (3.9)$$

where $D_n(\xi)$ is a sequence composed of well detached, discrete block pulses with support n (the set of non-zero values of a function is called the function's support) [32].

As shown in Equation 3.9, DPT of a sequence is a composition of DPT of different orders (pulses), and we shall calculate D_1, D_2, \dots, D_n , one by one to be able to reconstruct the signal. D_n is a sequence made up of block pulses with the support n ; for instance, it only compares the values of any position with n before and n after, and removes the pulses with width size n .

As an example for 1D DPT, consider a sequence of $\xi = \{1, 2, 7\}$, which is shown in Figure 3.6. The following is a step by step explanation for processing this sequence with 1D-DPT. In this example, the calculation for all DPT decomposition for this sequence, which is D_1 , D_2 and D_3 has been shown. This signal has only three elements, therefore its DPT can be calculated only up to three decompositions.

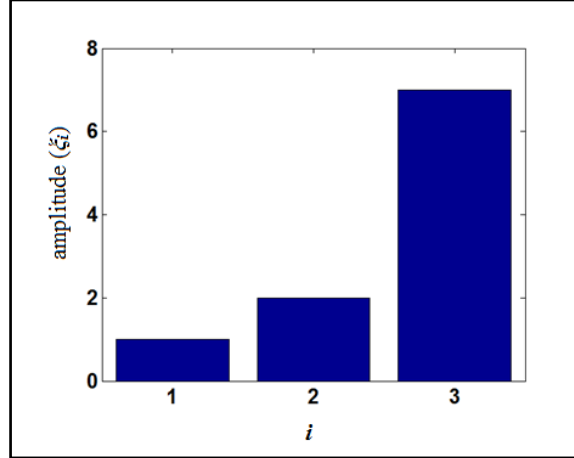


Figure 3.6 1D sequence (ξ) for DPT decomposition

Step 1: First, we have to filter the signal with $L_1 U_1$ operator. For calculating L_1 , we shall filter the signal with L_1 and remove all the signal's peaks with width of size one. Then we apply U_1 on the result to remove all the valleys with width of size one. $L_1 U_1$ smoothes the signal by removing all the local maximum and minimum pulses with width 1.

Please note that for processing boundary elements and also maintaining the size of the signal, we add zeros to the sequence. For example, for calculating L_1 , because it considers the neighborhood with only one element before and one after. We shall add one zero to the beginning of ξ and one at the end.

$$L_1 = \{1, 2, 2\} \quad (3.10)$$

The first element of L_1 is 1 which is obtained by using Equation 3.1, i.e., $\min\{\xi_{i-1}, \xi_i\}=0$ (since $\xi_{i-1}=0$ and $\xi_i=1$), and $\min\{\xi_i, \xi_{i+1}\}=1$ (since $\xi_i=1$ and $\xi_{i+1}=2$), and then $\max\{\min\{\xi_{i-1}, \xi_i\}, \min\{\xi_i, \xi_{i+1}\}\}_i = 1$. This process is repeated for all elements of ξ . Next, U_1 operator is applied on the result of L_1 and the following result is obtained.

$$L_1 U_1 = \{1, 2, 2\} \quad (3.11)$$

The first element of $L_1 U_1$ is 1 which is obtained by using Equation 3.2 on the result of L_1 , (here we represent the elements of $L_1 U_1$ by “ x ”), i.e., $\max\{x_{i-1}, x_i\}=1$, also $\max\{x_i, x_{i+1}\}=2$ and then $\min\{\max\{x_{i-1}, x_i\}, \max\{x_i, x_{i+1}\}\}_i = 1$ where $x_i = 1$ in sequence L_1 .

Step 2: For calculating D_1 , we subtract the smoothed signal $L_1 U_1$ from the original signal to get all peaks and valleys of size one as shown in Figure 3.7.

$$D_1 = \xi - L_1 U_1 = \{0, 0, 5\} \quad (3.12)$$

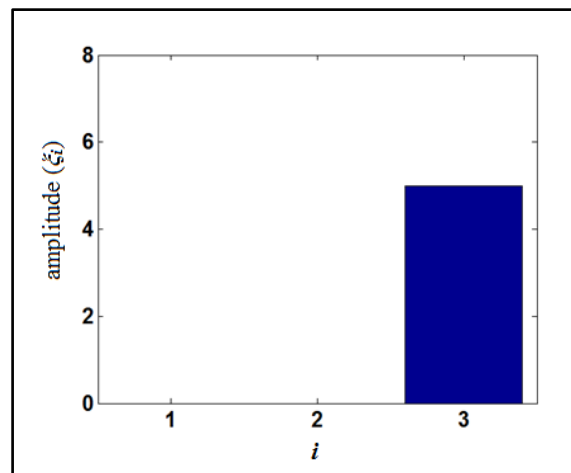


Figure 3.7 Result of D_1 on the 1D sequence of ξ

Step 3: For calculating D_2 , we shall find the pulses of width two, and for this reason we need to apply L_2U_2 operator on the result of step one. It means that we applied $L_1U_1L_2U_2$ operator on the signal according to their orders and we remove all the peaks and valleys of the signal with width one and two. Please note that we shall increase the previous sequence's size by adding two zeros at the beginning and two at the end of it to consider the L_2 and U_2 neighborhood of size two.

$$L_1U_1L_2 = \{1, 0, 1\} \quad (3.13)$$

The first element of $L_1U_1L_2$ is 1 which is obtained by using Equation 3.1 on the result of L_1U_1 , (here we represent the elements of $L_1U_1L_2$ by “z”), i.e., $\min\{z_{i-2}, z_{i-1}, z_i\}=0$, $\min\{z_i, z_{i+1}, z_{i+2}\}=1$ and then $\max\{\min\{z_{i-2}, z_{i-1}, z_i\}, \min\{z_i, z_{i+1}, z_{i+2}\}\}_i=1$ where $\xi_i=1$ in sequence L_1U_1 . In a same way we calculate $L_1U_1L_2U_2$.

$$L_1U_1L_2U_2 = \{1, 1, 1\} \quad (3.14)$$

Step 4: Here we need to subtract the result of step 3 from the original signal to get all the pulses with width of one and two.

$$\xi - L_1U_1L_2U_2 = \{0, 1, 6\} \quad (3.15)$$

Step 5: The result of step 4 gives us the peaks and the valleys with width one and two, but for calculating D_2 , our concern is only to find pulses with width two. Therefore we shall remove the width one pulses from the result of last step by applying L_1U_1 filter on that.

$$(\xi - L_1U_1L_2U_2) L_1 = \{0, 1, 1\} \quad (3.16)$$

$$D_2 = (\xi - L_1U_1L_2U_2) L_1U_1 = \{0, 1, 1\} \quad (3.17)$$

The result of D_2 is shown in Figure 3.8.

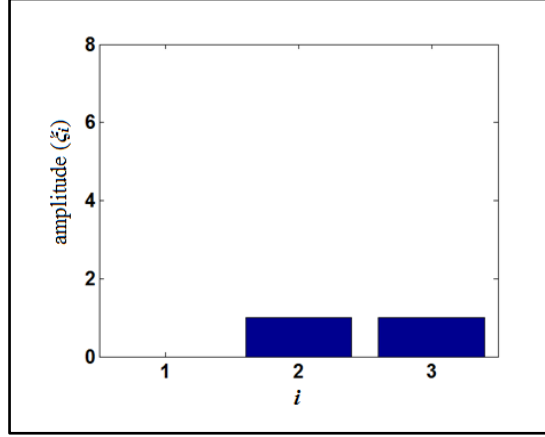


Figure 3.8 Result of D_2 on the 1D sequence of ξ

Step 6: For calculating D_3 we need to apply L_3U_3 and keep the pulses with width three. Please note that this time, for calculating L_3U_3 , we shall increase the previous sequence's size by adding three zeros at the beginning and three at the end of it to consider the L_3 and U_3 neighborhood of size three.

$$L_1U_1L_2U_2L_3 = \{0, 0, 0\} \quad (3.18)$$

The first element of $L_1U_1L_2U_2L_3$ is 0 which is obtained by using Equation 3.1 on the result of $L_1U_1L_2U_2$ (here we represent the elements of $L_1U_1L_2$ by “w”), i.e., $\min\{w_{i-3}, w_{i-2}, w_{i-1}, w_i\}=0$, also $\min\{w_i, w_{i+1}, w_{i+2}, w_{i+3}\}=0$ and then $\max\{\min\{w_{i-3}, w_{i-2}, w_{i-1}, w_i\}, \min\{w_i, w_{i+1}, w_{i+2}, w_{i+3}\}\}_i=0$ where $w_i=1$ in sequence $L_1U_1L_2U_2$. In the same way we calculate $L_1U_1L_2U_2L_3U_3$.

$$L_1U_1L_2U_2L_3U_3 = \{0, 0, 0\} \quad (3.19)$$

Step 7: By reducing the filtered sequence with $L_1U_1L_2U_2L_3U_3$ from the original one, we can sift all the peaks and valleys remaining from the $L_1U_1L_2U_2L_3U_3$ filter.

$$\xi - L_1U_1L_2U_2L_3U_3 = \{1, 2, 7\} \quad (3.20)$$

Step 8: This step is similar to step 5. The difference is we need to filter with L_2U_2 L_1U_1 to take all the pulses with width less than three out.

$$(\xi - L_1U_1L_2U_2L_3U_3) L_2 = \{1, 0, 1\} \quad (3.21)$$

$$(\xi - L_1U_1L_2U_2L_3U_3) L_2U_2 = \{1, 1, 1\} \quad (3.22)$$

$$(\xi - L_1U_1L_2U_2L_3U_3) L_2U_2L_1 = \{1, 1, 1\} \quad (3.23)$$

$$D_3 = (\xi - L_1U_1L_2U_2L_3U_3) L_2U_2L_1U_1 = \{1, 1, 1\} \quad (3.24)$$

The result of D_3 is shown in Figure 3.9.

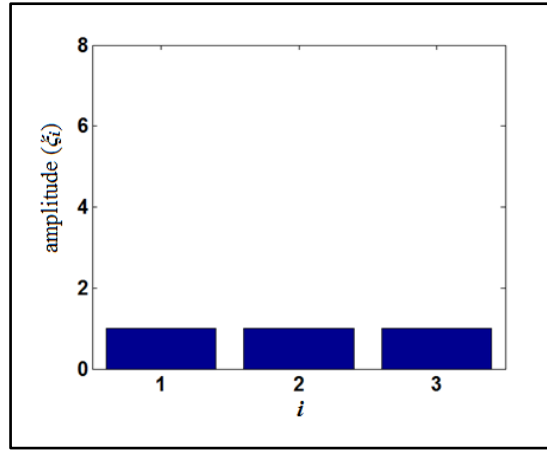


Figure 3.9 Result of D_3 on the 1D sequence of ξ

Step 9: In this step, we want to show that after summing all the DPT decompositions for different pulses, we can get the sequence ξ again.

$$D_1 + D_2 + D_3 = \{1, 2, 7\} \quad (3.25)$$

We can extend the work from 1D sequences to the multi-dimensional arrays, that is to say, functions on Z^d , $d > 1$. The notation Z^d refers to an n-dimensional space with integer coordinates. For example, a value of Z^3 consists of three integer numbers and specifies a location in 3-dimensional space [33].

3.3.2 2D DPT

$A(Z^2)$ refers to the set of all functions defined on Z^2 . Assume having a gray scale image $f \in A(Z^2)$ such that the support of the image is a finite rectangular subset Ω of Z^2 . Then the discrete pulse transform of the image $f \in A(Z^2)$ is given as [34]:

$$DPT(f) = (D_1(f), D_2(f), \dots, D_N(f)) \quad (3.26)$$

The $DPT(f)$ is finite because f has a finite support. In the equation above, N is the number of pixels in the image f . $D_N(f)$ is given as $D_n(f) = \sum_{s=1}^{\gamma(n)} \varphi_{ns}$ where φ_{ns} represents the pulses. The functions $\varphi_{ns}, s = 1, 2, \dots, \gamma(n)$ affects the number of pulses of each pixel where $\gamma(n)$ is a function of n . These functions are discrete pulses with support of size $n, n = 1, 2, \dots, \gamma(n)$. A discrete pulse is a function $\varphi \in A(Z^2)$ which is constant magnitude on a connected set W and zero elsewhere. The set W is called the support of the pulse, $w = \text{supp}(\varphi)$. The value of φ on W is the value of the pulse. If the value of φ is positive then φ is an up-pulse; if it is negative, φ is a down-pulse. Using DPT, we represent a function $f \in A(Z^2)$ as a sum of pulses [35].

$$f = \sum_{n=1}^N D_n(f) = \sum_{n=1}^N \sum_{s=1}^{\gamma(n)} \varphi_{ns} \quad (3.27)$$

Furthermore, similar to 1D discrete pulse transform, 2D DPT as in Equation 3.11 preserves the total variation (TV) of the data as formulated in Equation 3.12. The total variation (TV) is an important characteristic of an image and it is used in noise removal as in [35] and [36].

$$TV(f) = \sum_{n=1}^N TV(D_n(f)) = \sum_{n=1}^N \sum_{s=1}^{\gamma(n)} TV(\varphi_{ns}) \quad (3.28)$$

The DPT of $f \in A(Z^2)$ is obtained via iterative application of the operators L_n and U_n with n increasing from 1 to N . The order of applying the L_n and the U_n operators does not change the properties of the function DPT because both operators add a bias upward or downward only. Let P_n denote either the composition $L_n \circ U_n$ or the composition $U_n \circ L_n$. For combining L and U , we apply opening operators. In mathematical morphology, opening is the dilation of the erosion of a set A by a structuring element B : $A \circ B = ((A \ominus B) \oplus B)$ [37]. Now let the function $Q_n = P_n \circ P_{n-1} \circ \dots \circ P_2 \circ P_1$ which is iteratively applying the opening operation multiple times [38].

On the other hand, the filtered parts by P_n , $n = 1, 2, \dots, \gamma(n)$ are very important. These portions indicate the information about f which are peeled off [35]. More precisely,

$$\begin{aligned}
 f = & (id - P_1)(f) + ((id - P_2) \circ Q_1)(f) + ((id - P_3) \circ Q_2)(f) + \dots \\
 & + ((id - P_{N-1}) \circ Q_{N-2})(f) + ((id - P_N) \circ Q_{N-1})(f) + Q_N(f)
 \end{aligned}
 \tag{3.29}$$

where id denotes the identity operator. Similarly to this application of area opening and area closing, in [39], Acton and Mukherjee used these operators for image classification. In this application, filtering is done for specific values of n and instead of the layers of peeled off portions, the authors keep a record of filtered images at every scale. For more information, please refer to [34], [40] and [41].

DPT for 2D considers a wider neighborhood for each pixel compared to 1D. Besides, the size of support can vary up to the matrix's size. An example for 2D DPT is provided here, which shows the affects of different pulses on the image. The following steps show the DPT decomposition for the image with the pixel values illustrated in Figure 3.10.

1	0	1	1	1
1	0	1	1	0
0	0	1	1	1
0	1	1	1	0
1	0	1	0	1

Figure 3.10 DPT decomposition for 2D

Please note that we can consider a different neighborhood, but here we just illustrated the result of the 4-connectivity and 8-connectivity neighborhoods as shown in Figure 3.11 and Figure 3.12 respectively. 2D DPT is concerned about connectivity. Therefore for calculating different decompositions, we shall follow the steps below. The properties of connectivity and segmentation are described in more detail in [42] and [43].

Step 1: First step is finding the local maximum sets. For this, we shall find the connected sets. For example, to calculate D_1 , we can consider all the pixels one by one because each one makes a set of size one. For any D_n , any n pixels with the same value that are connected can be considered as one set of size n. Any set which has a higher value than its neighbors will be highlighted and its value will be changed to its neighbor values.

Step 2: This step is the same as the first step; the difference is that we are looking for local minimum sets on the result of the previous step. After finding the local minimum sets, we convert the whole set's value to its neighbors' values and continue with the next decomposition (D_{n+1}), which shall repeat step 1 followed by step 2 for the result of D_n .

Step 3: The last step is when all values of the image become the same. This will be the point when we shall stop.

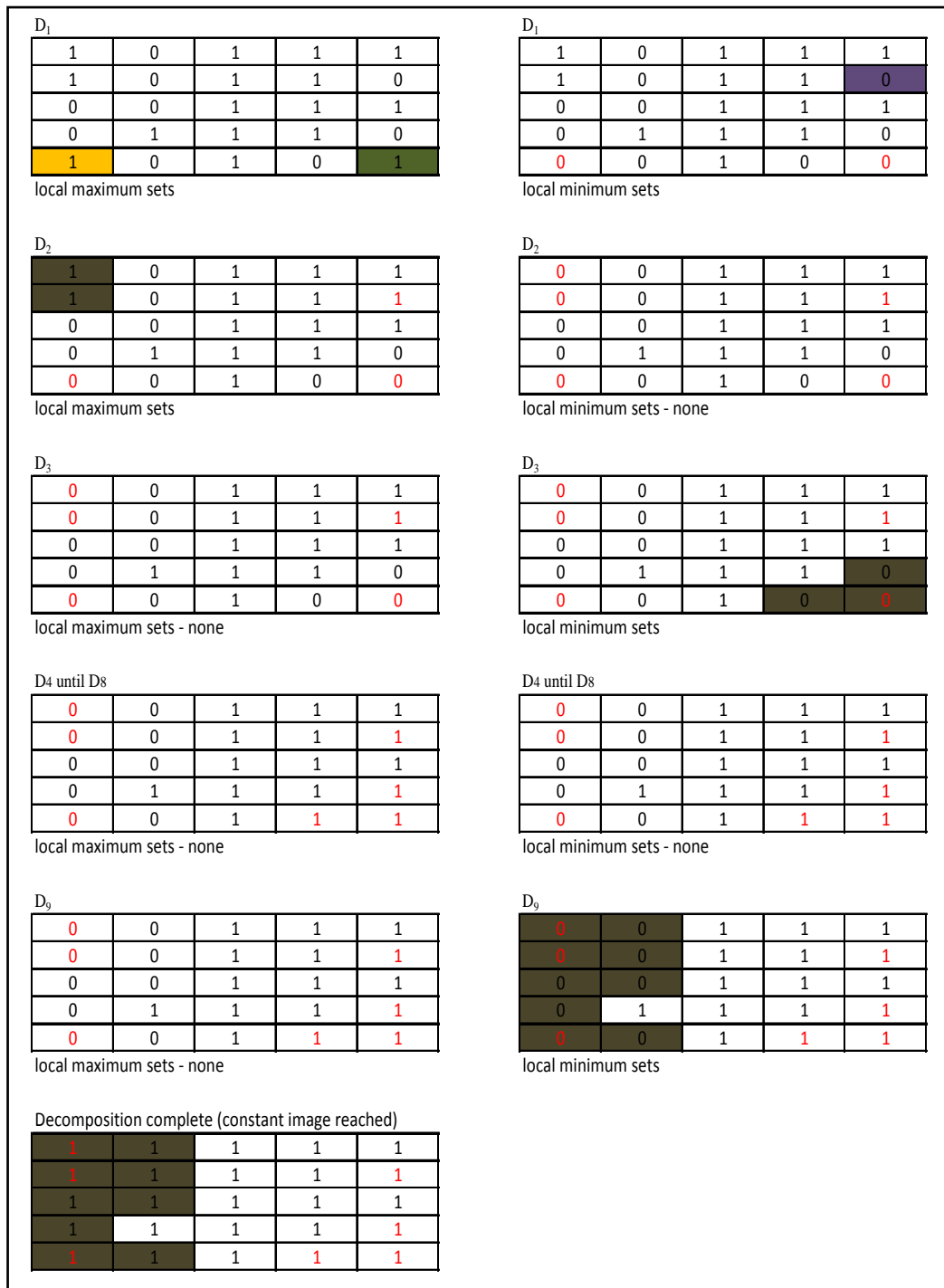


Figure 3.11 2D DPT for 4-Connectivity

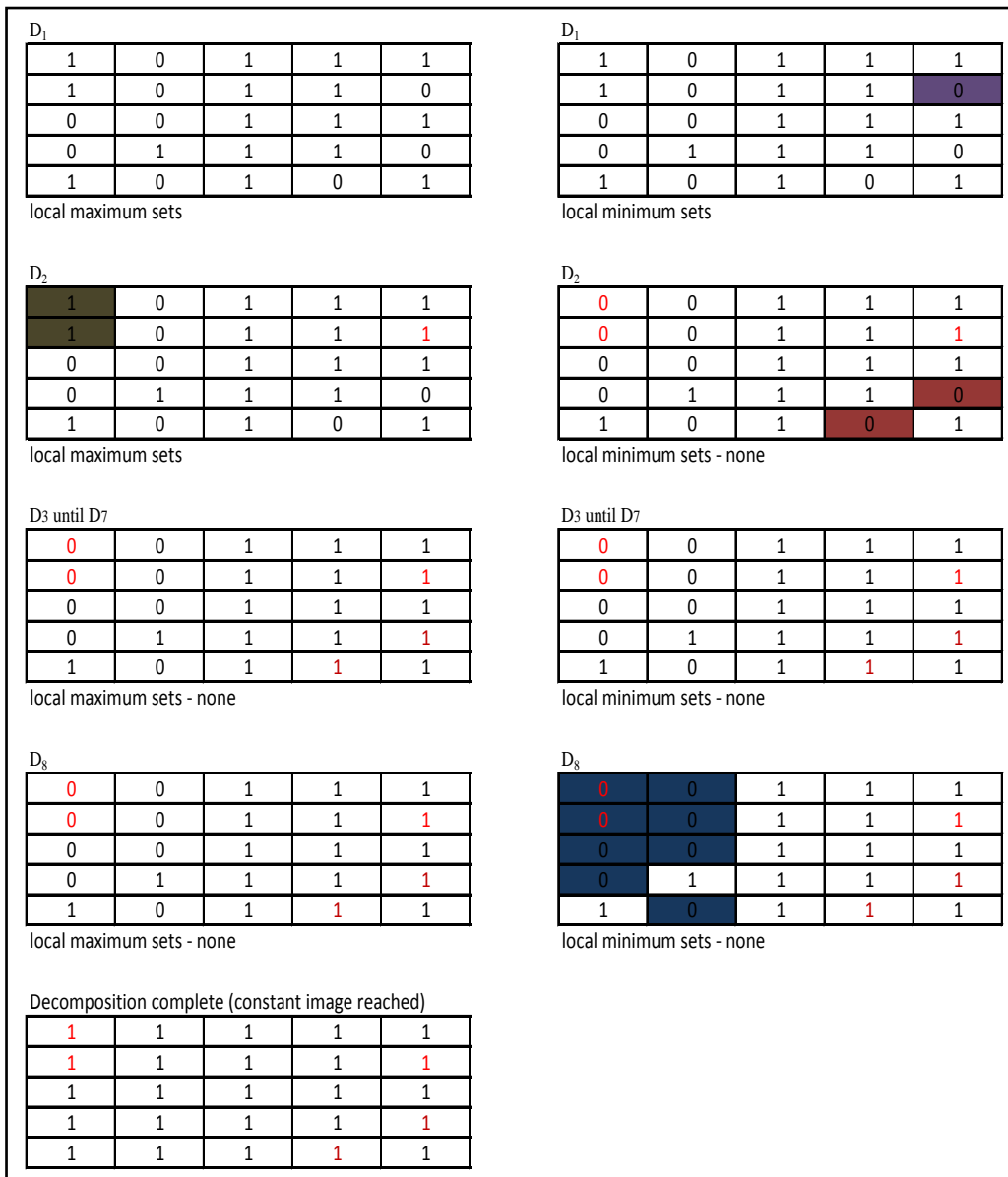


Figure 3.12 2D DPT for 8-connectivity

3.4 Chapter Summary

In this chapter, LULU operators and DPT's are explained and thoroughly analyzed and their properties are described. LULU operators are the nonlinear operators which have been applied recently in image processing for different applications and one of their well known applications is DPT. Different examples in 1D and 2D are given in order to clarify their implementation in signal and image processing.

CHAPTER 4

SFF USING LULU AND DPT

4.1 Introduction

In this thesis, we propose a new shape from focus method. The method is based on LULU filters and Discrete Pulse Transform in determining the frame number with the best focus with respect to particular pixel in the image. Up to date, the best frame number is selected according to the best maximum focus value for each pixel along all the frames. This is due to the characteristic of SFF which calculates the depth based on focused values.

The proposed technique is also implemented as a combination between LULU operators and the existing SFF methods including Sum Modified Laplacian (SML), Tenenbaum and Gray Level Variance (GLV). These methods are selected because they are the most widely used SFF methods. The performances of these combinations are tested with images corrupted with impulse, Gaussian and speckle noise. The reconstructed depth map is compared with the original data by using different image quality matrices, like Peak Signal to Noise Ratio (PSNR) and Root Mean Square Error (RMSE).

4.2 The Modified LULU Focus Measure (MLULU)

This algorithm is an extension of 2D LULU operators applied in 2D or 3D neighborhood.

The algorithm can be described as follow:

4.2.1 Step 1: MLULU Algorithm

Apply LULU operators in 2D or 3D neighborhood on each frame. The neighboring area can be defined in different ways, as it is explained below.

2D neighborhood means to apply LULU operators on each frame separately, regardless of the frames before and after. This is shown in Equation 3.3 to Equation 3.8 and Figure 3.3.

Derived from Equation 3.7 and Equation 3.8, we can apply L and U operators on each frame, which are actually L_3 and U_3 due to considering only four pixels in each sub-neighborhood. Hence, for applying LU, we shall first apply L_3 and then apply U_3 on the obtained result of L_3 , and vice versa for UL. But if we need to apply LUL, ULU, LULU or ULUL, we need to expand the window size because they are actually referring to $L_3U_3L_8$, $U_3L_3U_8$, $L_3U_3L_8U_8$ and $U_3L_3U_8L_8$. For example, for applying LULU filter on a single image, firstly we apply L_3 , followed by U_3 and next we apply L_8 and then U_8 as illustrated in Figure 4.1. As it is shown in Figure 4.1, the sub-window size will increase to;

$$A' = \begin{bmatrix} X(i-1, j-1), X(i-1, j), X(i, j), X(i, j-1), X(i-2, j), \\ X(i-2, j-1), X(i-2, j-2), X(i-1, j-2), X(i, j-2) \end{bmatrix}; \quad (4.1)$$

$$B' = \begin{bmatrix} X(i-1, j+1), X(i-1, j), X(i, j), X(i, j+1), X(i-2, j), \\ X(i-2, j+1), X(i-2, j+2), X(i-1, j+2), X(i, j+2) \end{bmatrix}; \quad (4.2)$$

$$C' = \begin{bmatrix} X(i, j+1), X(i, j), X(i+1, j), X(i+1, j+1), X(i, j+2), \\ X(i+1, j+2), X(i+2, j+2), X(i+2, j+1), X(i+2, j) \end{bmatrix}; \quad (4.3)$$

$$D' = \begin{bmatrix} X(i, j-1), X(i, j), X(i+1, j-1), X(i+1, j), X(i+2, j), \\ X(i+2, j-1), X(i+2, j-2), X(i+1, j-2), X(i, j-2) \end{bmatrix}; \quad (4.4)$$

Subsequently, the L and U formula becomes:

$$L(i, j) = \max(\min(A'), \min(B'), \min(C'), \min(D')); \quad (4.5)$$

$$U(i, j) = \min(\max(A'), \max(B'), \max(C'), \max(D')); \quad (4.6)$$

It is necessary to mention that higher orders of LULU operators can be performed by increasing the sub-neighbors window size. However, to avoid blurring the image, we applied until $L_3U_3L_8U_8$ and $U_3L_3U_8L_8$.

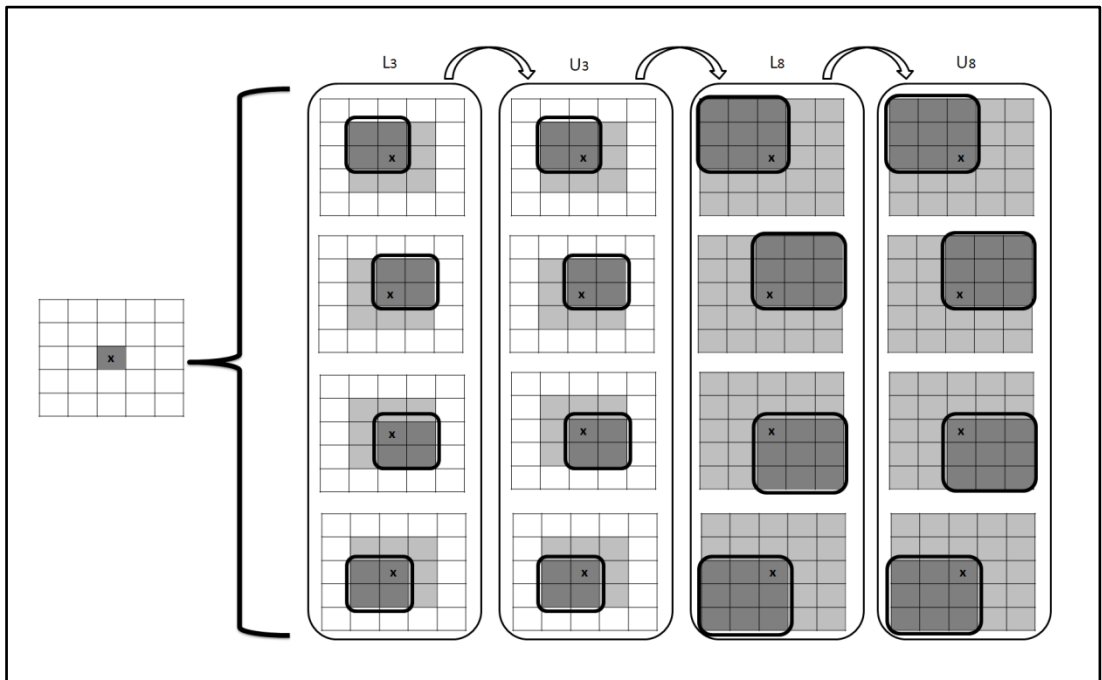


Figure 4.1 2D neighborhood for $L_3U_3L_8U_8$

For **3D neighborhood** the neighborhood's window around each pixel is different. It means that LULU value for each pixel does not only depend on its neighbors of the same frame but also on the neighbors of the frames before and after. Therefore the neighborhood is a 3D one as it is shown in Figure 4.2.

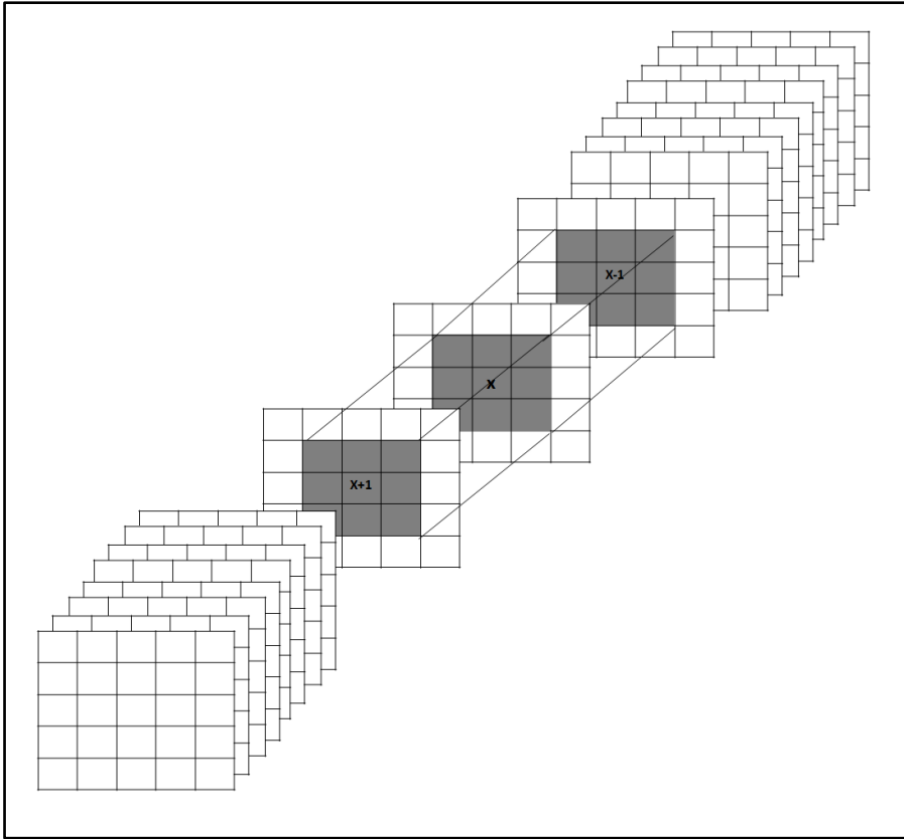


Figure 4.2 3D neighborhood of window size 3×3 for pixel "X"

With the new 3D neighborhood defined around a pixel "X" as shown in Figure 4.2, the sub-windows are defined as in Figure 4.3.

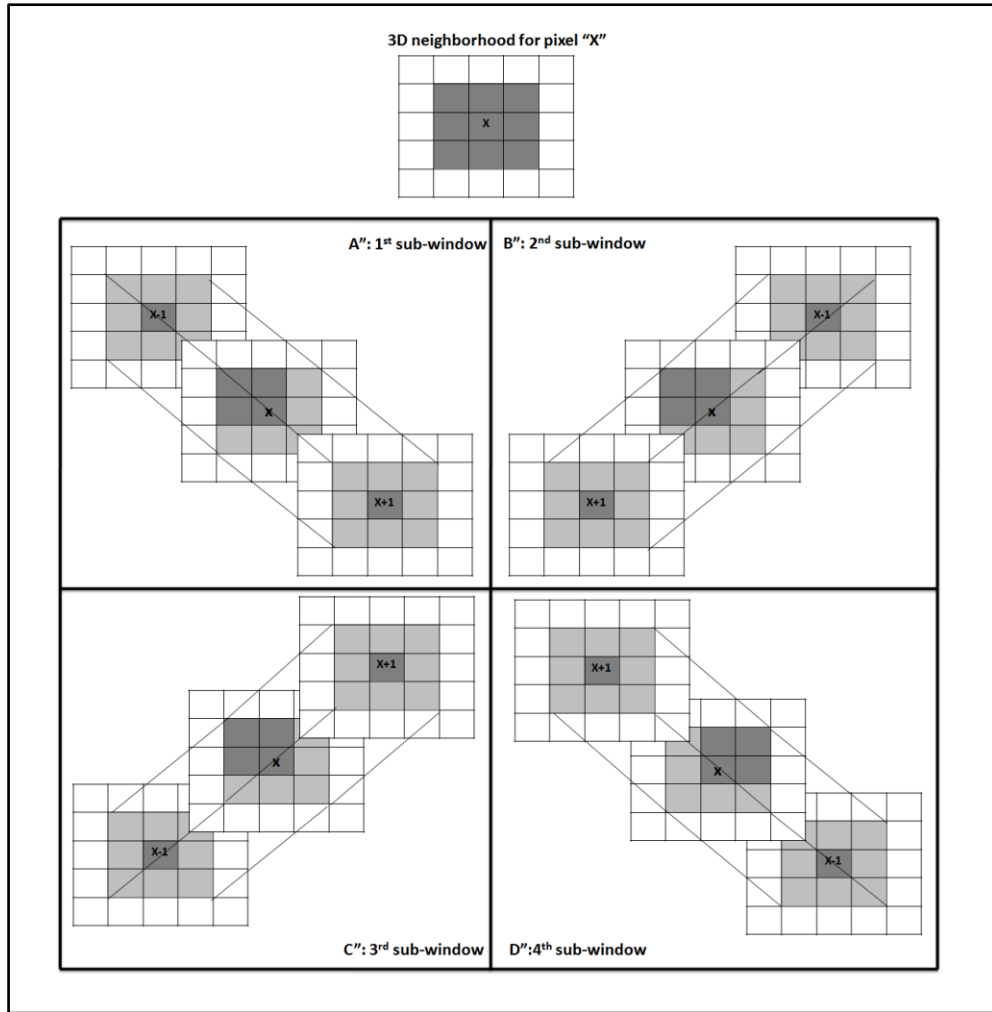


Figure 4.3 3D neighborhood for pixel "X"

Based on Figure 4.3, the sub-windows equations are as follow:

$$A'' = [X(i-1, j-1), X(i-1, j), X(i, j), X(i, j-1), X_{-1}(i, j), X_{+1}(i, j)]; \quad (4.7)$$

$$B'' = [X(i-1, j+1), X(i-1, j), X(i, j), X(i, j+1), X_{-1}(i, j), X_{+1}(i, j)]; \quad (4.8)$$

$$C'' = [X(i, j+1), X(i, j), X(i+1, j), X(i+1, j+1), X_{-1}(i, j), X_{+1}(i, j)]; \quad (4.9)$$

$$D'' = [X(i, j-1), X(i, j), X(i+1, j-1), X(i+1, j), X_{-1}(i, j), X_{+1}(i, j)]; \quad (4.10)$$

The formulas for L and U are the same as Equation 4.5 and Equation 4.6. Instead of A, B, C and D, we substitute A'' , B'' , C'' and D'' .

In the Equations 3.3-3.6, Equations 4.1-4.4 and Equations 4.7-4.10, it is obvious that the LULU operators detect the peaks and valleys in each sub-window. These operations illustrate that when we apply L or U based on Equation 4.5 to Equation 4.6, they minimize noise in each region by eliminating the very high or very low intensities and ensure a smooth focus measure in the presence of noise.

Smoothing characteristic of LULU operators plays a very important role in focus measurement. For images corrupted with noise, the noise value is wrongly interpreted as focused value. However, the focus value should be at least similar to few neighboring pixels, because in each frame, the focusing part is not a point. Rather it refers to a small part, tiny group of pixels, near each other. Based on the concept of focusing, it is obvious that high frequencies may be chosen as the focused values which are in fact the noise values.

4.2.2 Step 2: MLULU Algorithm

After applying LULU operators in step 1, substitute each pixel's intensity by its LULU value. For reconstructing the 3D shape, select the maximum value for each pixel along all frames as shown in Figure 4.4.

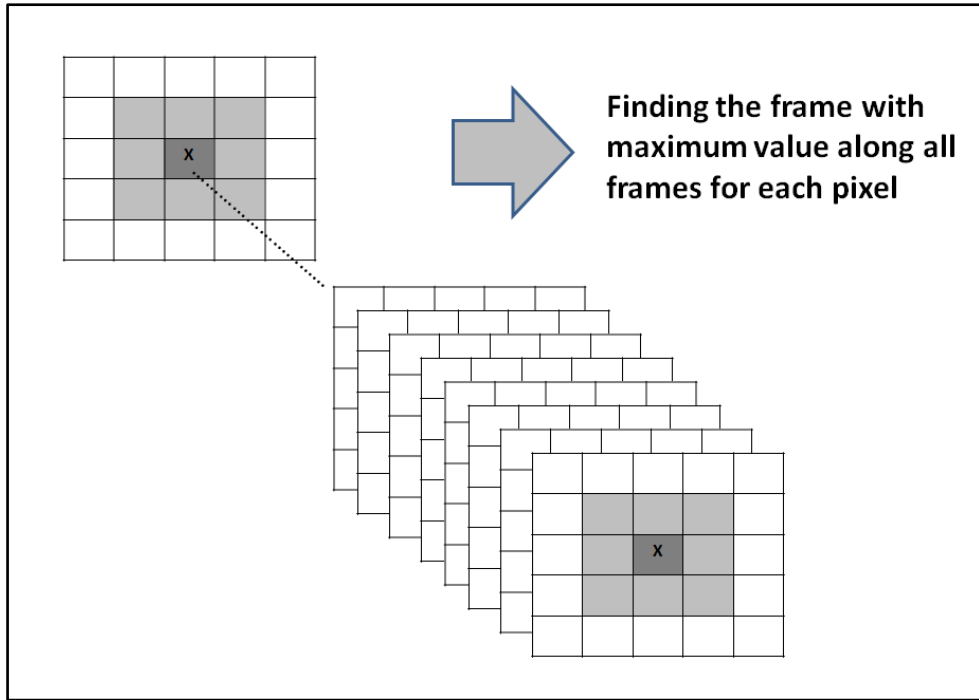


Figure 4.4 Choosing the maximum value along all frames

Figure 4.4, illustrates the sequence of frames for calculating the focused frame for pixel X among all the frames for pixel (i, j) . As a result, the output of SFF is two 2D matrices; maximum intensity and corresponding frame index. Maximum intensity holds the best focus value for each one of the pixels, and corresponding frame index holds the resultant frame number where the pixel is best focused [4].

$$[Max\ Index(i, j), Max\ Intensity(i, j)] = \max[k\ LULU(i, j)] \quad (4.11)$$

Where k refers to the frame number, which varies from 1 to last frame number. These two matrices provide the depth map of the object.

After implementing LULU and getting an initial estimation of the best focusing frame for each pixel in the image, we propose the use of a modified version of DPT for further improvement on depth map.

4.3 The Modified DPT Focus Measure (MDPT)

The main concept behind this algorithm is to reconstruct the 3D shape based on the very high frequencies of the image which are the focused pixels. DPT decomposes the image into many pulses and each object in the image can have a specific number of pulses. For detecting the object, we shall find out the range of pulses and eliminate other pulses from the image. We use this concept of pulses in SFF. The focused parts of the images can be selected by choosing the correct pulses.

In this proposed Focus Measure (FM), we apply DPT on each frame based on Equation 3.11. Since LULU operators are only applied up to L_3 , U_3 , L_3U_3 , U_3L_3 , $L_3U_3L_8$, $U_3L_3U_8$, $L_3U_3L_8U_8$ and $U_3L_3U_8L_8$, therefore the DPT operators are also limited as it is shown in Table 4.1.

Table 4.1 DPT operators for SFF

LULU Operator	DPT Operator
L_3	$f = (id - L_3)(f)$
U_3	$f = (id - U_3)(f)$
L_3U_3	$f = (id - L_3U_3)(f)$
U_3L_3	$f = (id - U_3L_3)(f)$
$L_3U_3L_8$	$f = (id - L_3U_3)(f) + ((id - L_3U_3L_8) \circ Q_3)(f)$
$U_3L_3U_8$	$f = (id - U_3L_3)(f) + ((id - U_3L_3U_8) \circ Q_3)(f)$
$L_3U_3L_8U_8$	$f = (id - L_3U_3)(f) + ((id - L_3U_3L_8U_8) \circ Q_3)(f)$
$U_3L_3U_8L_8$	$f = (id - U_3L_3)(f) + ((id - U_3L_3U_8L_8) \circ Q_3)(f)$

Where f refers to DPT values, id is the original pixel value and Q_3 refers to the DPT value of the third order operators, which are $(id - L_3)(f)$, $(id - U_3)(f)$, $(id - L_3U_3)(f)$ or $(id - U_3L_3)(f)$ in this work.

In this work, we considered the first two pulses in images which are D_3 and D_8 to detect the focused values.

4.4 MLULU Cascaded with Other Techniques

In addition to the original form of the MLULU, this method can be used in cascade with other methods such as SML, Tenenbaum (TEN) or GLV for further improvement on depth map estimation. The procedure is same as with MLULU alone, and the only difference is to replace each frame with its LULU values and then implement it with the second operator (SML, TEN or GLV). This combination produces accurate sharpness detection estimation in the presence of noise.

This algorithm is implemented as follow:

Step 1) Apply LULU operators in 2D or 3D neighborhood on each frame.

Step 2) Process the output of step 1 with SML/GLV/TEN FM in 2D neighborhood.

Step 3) Calculate the maximum index for each pixel along all the frames.

Step 4) Build up the 3D shape out of step 3 output.

Other combinations, like swapping step 1 and step 2 or adding more LULU stages may improve the accuracy but at the expense of higher computational load.

4.5 Chapter Summary

In this Chapter LULU and DPT for a 3D shape recovery application, are described. Furthermore, LULU operators are combined with the existing techniques to increase the 3D shape recovery accuracy. In the combination of LULU with other techniques, LULU is considered as a pre-processing that helps in removing part of the noise and giving initial estimation of depth map, whereas the combined technique helps in refining the obtained results.

CHAPTER 5

RESULT AND DISCUSSION

5.1 Introduction

Different objects have been chosen to be studied in this work. Simulation has been performed using two different quality measures; RMSE and PSNR to compare proposed methods with SML, GLV and TEN for different types of noises. For the purpose of comparison seven test sequences are used, including both the simulated and real objects, i.e. simulated cone, simulated slope, simulated cosine, real cone, real coin, real LCD and real plane, as shown in APPENDIX B. In total, seven objects are evaluated; three simulated objects and four real objects.

5.2 Test Images

The test objects are chosen from different textures with different level of details. Coin and cosine carry good amount of details. These high textured images are good SFF images which help to test the outcomes of focusing. Slope and plane have poor uniformed texture. Cone is a dense textured object and it is considered as medium level of details, but Liquid Crystal Display (LCD) image has low level of details and variance and it is a microscopic image. The resolution is $360 \times 360 \times 97$ for simulated and real data Cone, $320 \times 320 \times 60$ for Slope and Cosine objects, $300 \times 300 \times 68$ for Coin, $300 \times 300 \times 60$ for LCD and $200 \times 200 \times 87$ for Plane. More explanation about the test images are given in APPENDIX B.

5.3 Experimental Results

The seven different test objects are considered in the presence of impulse noise, Gaussian noise and speckle noise. Each noise is evaluated with three different noise density/variance values, which are; 0.005, 0.05 and 0.5. The results of the proposed methods are compared with SML, GLV and TEN techniques. These techniques were explained in Chapter 2.

In general, all the results obtained for each object are compared qualitatively and quantitatively with SML, the GLV and TEN. This comparison is done qualitatively and quantitatively.

5.3.1 Metric Measures

The subjective image quality assessment is ideal for assessing the quality of images and videos. It reflects subjective analysis of the quality of an image or video as most of the people commonly perceive. However, it has some critical constraints, i.e. a large number of images and tests are required. Therefore, the objective image quality assessment is preferred in practical situations and thus has been widely investigated [44]. Different image quality measures have been proposed for assessment of the methods. Among the widely used metrics are the root mean square error (RMSE), peak signal to noise ratio (PSNR), mean absolute error (MAE), correlation and some newly introduced methods like structural similarity (SSIM), phase quantization code (PQC) [45], contourlet structural similarity (CSSIM) [46] and singular value decomposition (SVD) [47]. For their simplicity and less computational complexity, the RMSE and PSNR are used in this research to assess the performances of the different techniques.

A. *RMSE*

RMSE is one the most famous quality assessment methods. It is easy to compute, has understandable physical meaning and enjoys mathematical convenience in the context of optimization [48]. The MSE is the second moment of the error. It simply measures the average of the squares of the errors. The error indicates the intensity variation

between two images which needs to be compared. It estimates the total difference between the ground truth and the studied image. Equation (5.1) shows the formula for RMSE.

$$\text{RMSE} = \sqrt{\frac{1}{XY} \sum_{x=0}^{X-1} \sum_{y=0}^{Y-1} |f(x, y) - g(x, y)|^2} \quad (5.1)$$

B. PSNR

PSNR is commonly used in image quality measures. It is defined in logarithmic scale, therefore provides a large dynamic scale. PSNR is easy to calculate and has low computational complexity. PSNR is a ratio of the highest intensity of a signal to the RMSE. The PSNR tends to move to infinity as the RMSE moves toward zero, and consequently a higher PSNR value presents a higher image quality but a small value of the PSNR means that there is a high numerical differences between images [49]. PSNR value presents a good assessment of the image quality when the features of image, like its signal variations, tend to get lost in a sea of random variations when the noise variance increases [50]. Equation (5.2) shows the formula for PSNR, where MAX_I refers to the maximum possible pixel value in the image and MSE is square value of the Equation (5.1) [51].

$$\text{PSNR} = 10 \cdot \log_{10} \left(\frac{\text{MAX}_I^2}{\text{MSE}} \right) \quad (5.2)$$

5.3.2 Results

This section shows the result for the proposed methods which are described in Chapter 4 and comparison is provided both qualitatively and quantitatively with SML, GLV and TEN. The 3D recovered shapes for the seven objects in the presence of various types of noise are shown in this section.

Three noise levels are used for experiments, i.e., high (noise density/variance=0.5), medium (noise density/variance=0.05) and low (noise density/variance=0.005). Figure 5.1 illustrates the performance of SML, TEN, GLV, MDPT and MLULU Focus Measures (FM's) for simulated cone object in the presence of impulse noise with the noise density (ND) of 0.5.

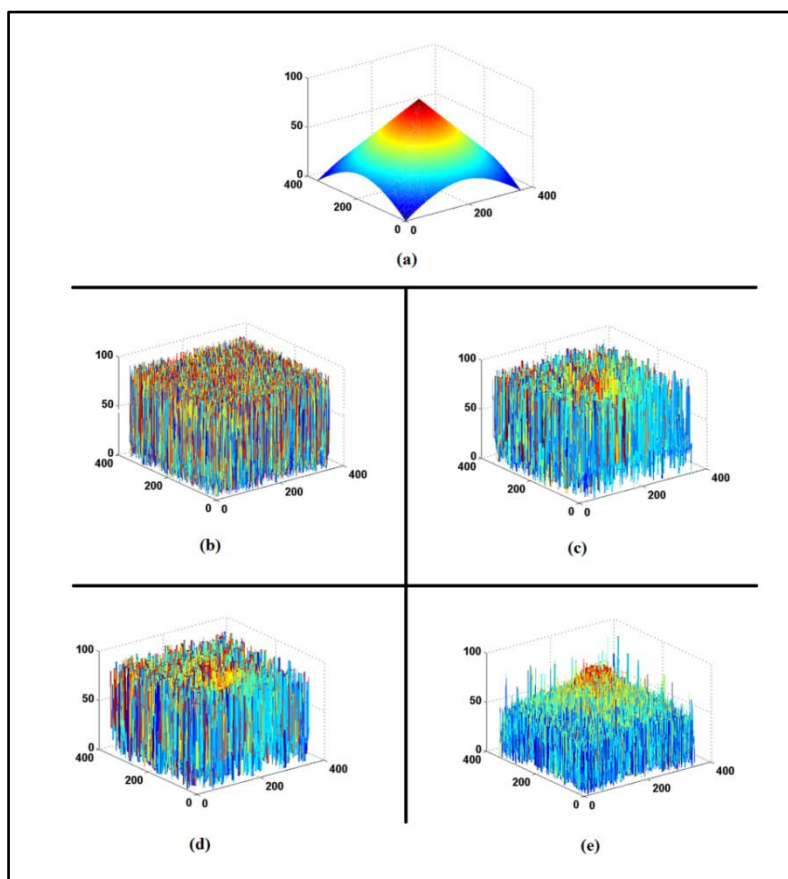


Figure 5.1 Simulated Cone in the presence of impulse noise with noise density of 0.5; (a) Ground truth, (b) SML focus measure, (c) TEN focus measure, (d) GLV focus measure and (e) MLULU focus measure

In Figure 5.2, the performance of MLULU is compared with other three methods in the presence of impulse noise with noise density of 0.05 for real LCD.

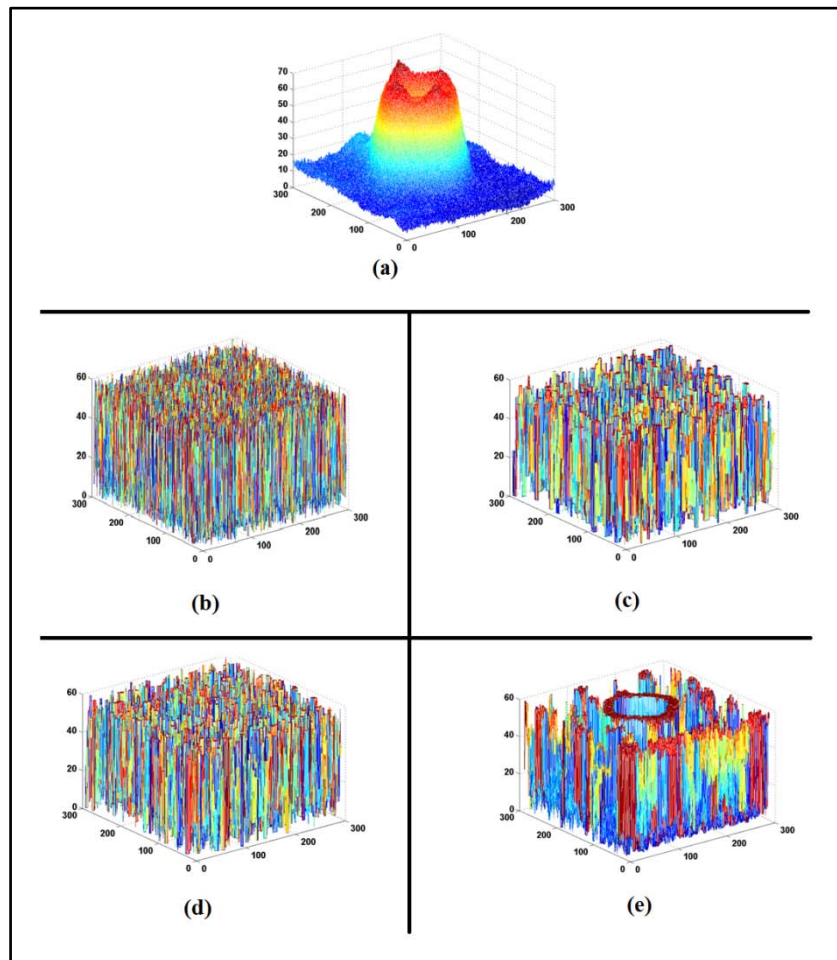


Figure 5.2 Real LCD in the presence of impulse noise with noise density of 0.05; (a) Ground truth, (b) SML focus measure, (c) TEN focus measure, (d) GLV focus measure and (e) MLULU focus measure

In general, proposed focus measure performs well in the presence of impulse noise as is evident from Figure 5.1 and Figure 5.2. MLULU FM removes the locally occurring hills and valleys of signals and images. It is clear that in the presence of impulse noise, the other focus measures (FMs) are not performing well and the 3D shape reconstructed based on them is not clear at all. Their result is a set of noisy data which does not show anything similar to the object. This is true for high noise density (0.5) as well as medium noise density (0.05) levels. But the 3D shape reconstructed based on MLULU FM is clear and shows the shape at three noise levels. The quantitative result for simulated cone is provided in Table 5.1 and Figure 5.3 and Figure 5.4.

Table 5.1 MLULU and DPT performance in the presence of impulse noise for simulated cone object

Noise Density	Focus measure (FM)	RMSE	PSNR
0.5	MLULU	15.69	24.21
	MDPT	28.74	18.99
	SML	32.01	18.02
	GLV	22.37	21.13
	TEN	25.24	20.09
0.05	MLULU	12.12	26.46
	MDPT	17.09	23.47
	SML	29.34	19.49
	GLV	14.8	24.72
	TEN	12.13	26.46
0.005	MLULU	15.01	24.55
	MDPT	17.32	23.47
	SML	27.04	19.49
	GLV	9.71	28.38
	TEN	8.55	29.49

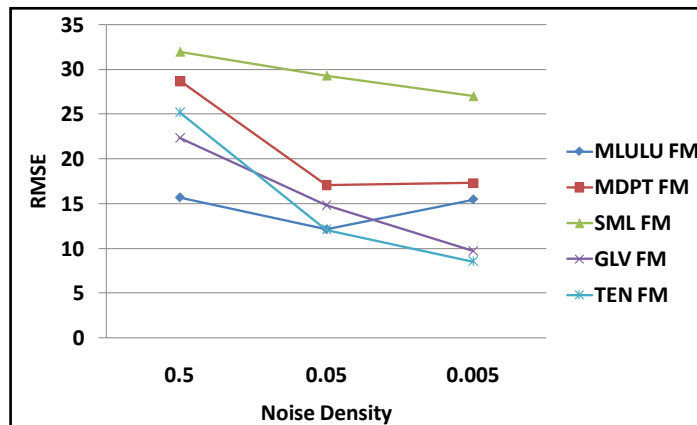


Figure 5.3 RMSE comparison between different methods for simulated cone object in the presence of impulse noise

It is clear in Figure 5.3 that MLULU is performing better than SML and MDPT in general and at high and medium impulse noise levels, its performance is better than all focus measures. This is also evident from Figure 5.4.

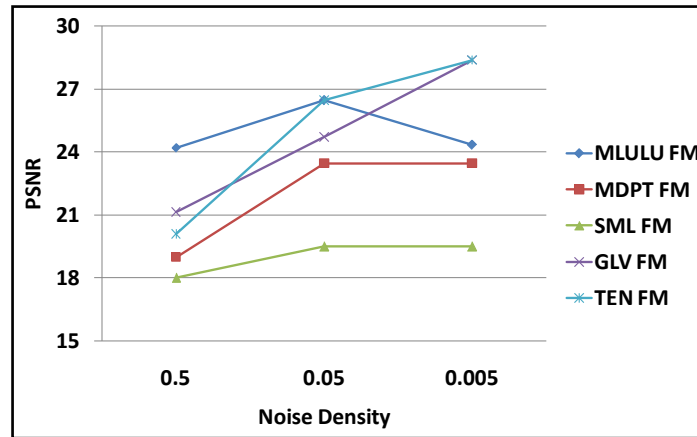


Figure 5.4 PSNR comparison between different methods for simulated cone object in the presence of impulse noise

In Figure 5.5 and Figure 5.6, we show the comparison between MLULU, SML, GLV and TEN for Gaussian and speckle noises. We illustrate that MLULU is not only a good focus measure in the presence of impulse noise, but its performance is comparable in the presence of other types of noise like speckle and Gaussian. In Figure 5.5, MLULU method is performing better than other methods in the presence of Gaussian noise with variance (V)=0.5.

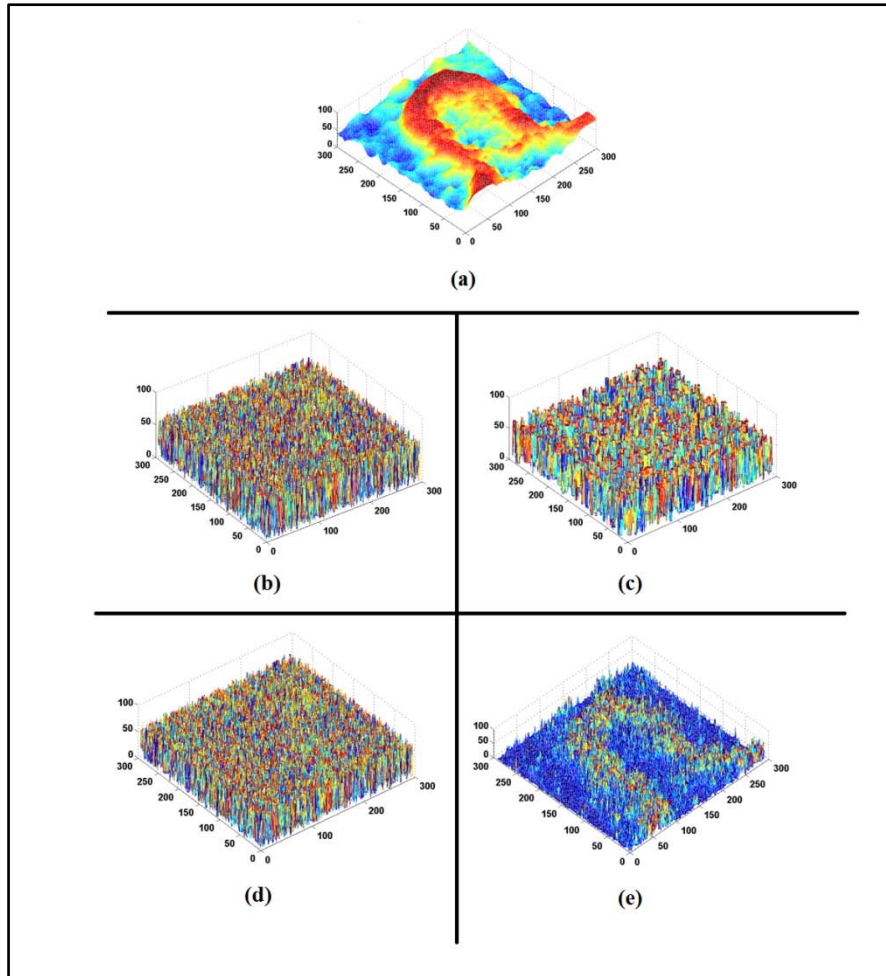


Figure 5.5 Coin in the presence of Gaussian noise with mean value of 0 and variance of 0.5; (a) Ground truth, (b) SML focus measure, (c) TEN focus measure, (d) GLV focus measure and (e) MLULU focus measure

Figure 5.5 shows that SML, GLV and TEN focus measurement techniques failed totally in recovering the 3D shape of coin object, their result show nothing similar to the ground truth but MLULU can recover a shape similar to the ground truth. Similarly in Figure 5.6, the good performance of MLULU can be seen. In Figure 5.6. the other methods show noisy result and the 3D shape is not clearly recovered but MLULU managed to reconstruct it well.

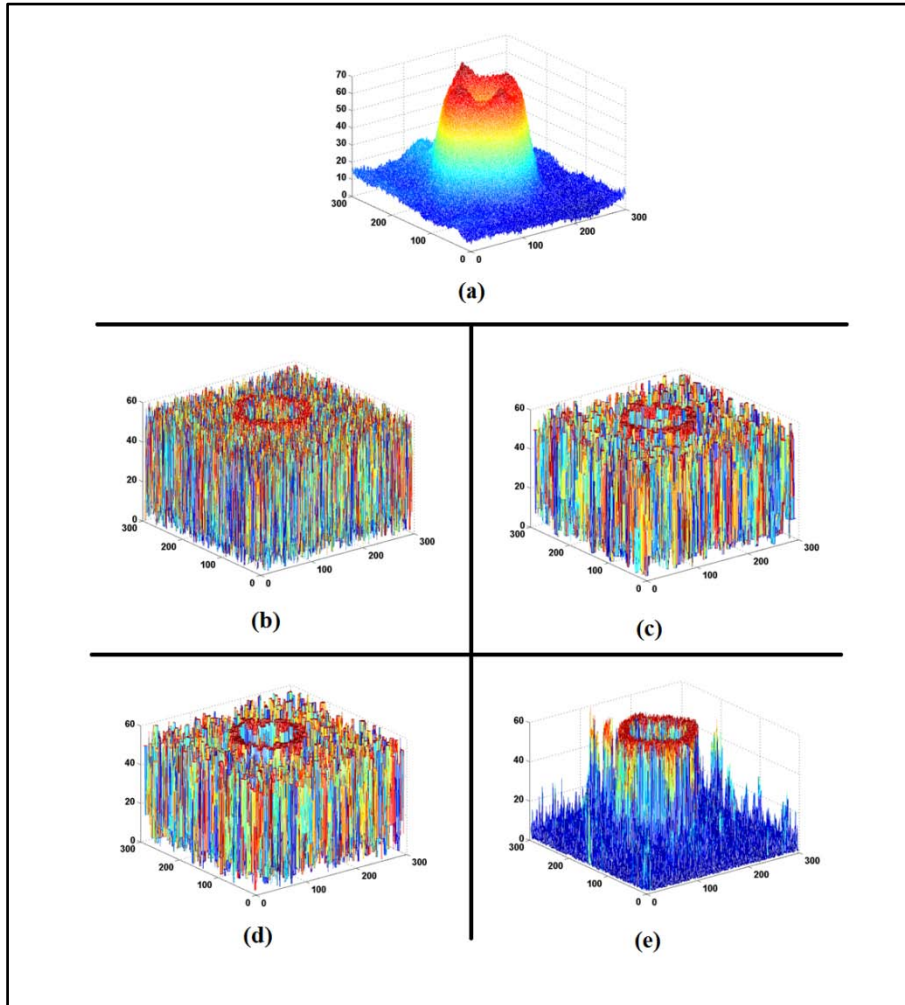


Figure 5.6 LCD in the presence of speckle noise with noise density of 0.5; (a) Ground truth, (b) SML focus measure, (c) TEN focus measure, (d) GLV focus measure and (e) MLULU focus measure

From Figure 5.6, it is obvious that MLULU performance is comparable with other focus measures in the presence of speckle noise.

5.3.3 Cascading proposed method with other FMs

In this section, we cascade the proposed focus measure based on MLULU with existing focus measures, i.e., MLULU+SML, MLULU+GLV and MLULU+TEN. Figure 5.7 demonstrates the result of combining MLULU with other focus measuring techniques. Figure 5.7 is showing the simulated cone object with three levels of impulse noise and each cascading option is compared with the existing focus measure, i.e., SML, GLV and TEN. The improvement in the 3D shape recovery is due to dual performance of MLULU, i.e., noise reduction and focused points extraction.

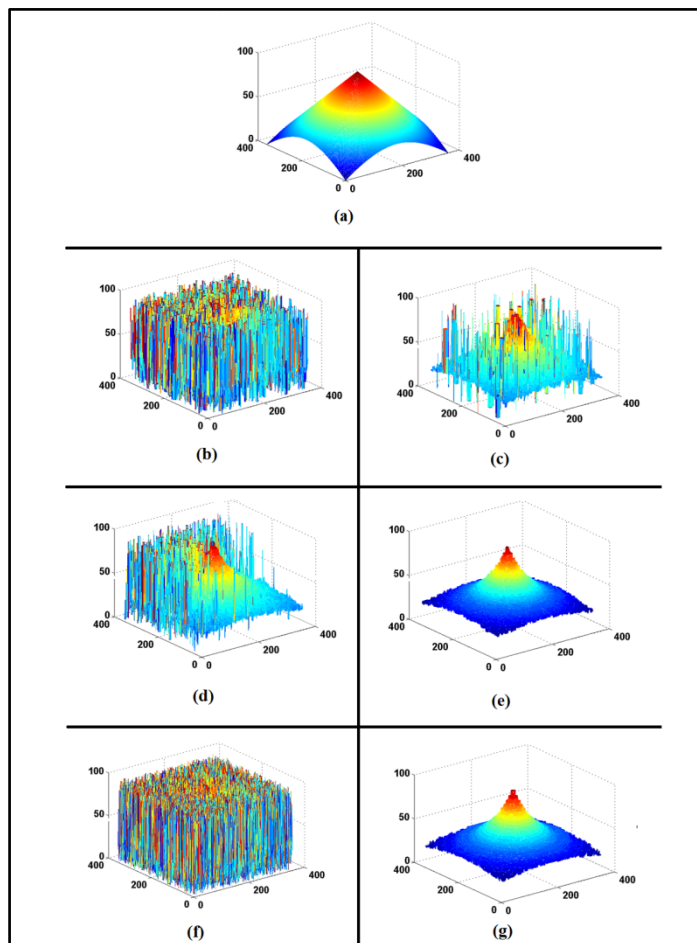


Figure 5.7 (a) Ground truth of Simulated Cone, (b) TEN focus measure result in the presence of impulse noise with noise density of 0.5, (c) MLULU+TEN focus measure result in the presence of impulse noise with noise density of 0.5, (d) GLV focus measure result in the presence of impulse noise with noise density of 0.05, (e) MLULU+GLV focus measure result in the presence of impulse noise with noise density of 0.05, (f) SML focus measure result in the presence of impulse noise with noise density of 0.005 and (g) MLULU+SML focus measure result in the presence of impulse noise with noise density of 0.005

The quantitative comparison for cascaded option is shown in Table 5.2 which clearly illustrates that cascading proposed Focus Measure with existing ones gives good results.

Table 5.2 Cascaded methods performance in the presence of impulse noise for simulated cone object

Noise density	Focus measure (FM)	RMSE	PSNR
0.5	SML	35.02	18.02
	MLULU+SML	38.22	16.48
	GLV	22.38	21.13
	MLULU+GLV	17.62	23.21
	TEN	25.24	20.09
	MLULU+TEN	10.9	27.38
0.05	SML	29.33	18.78
	MLULU+SML	7.89	30.18
	GLV	14.80	24.72
	MLULU+GLV	7.75	30.35
	TEN	12.13	26.46
	MLULU+TEN	7.75	30.34
0.005	SML	27.04	19.49
	MLULU+SML	7.89	30.19
	GLV	9.71	28.39
	MLULU+GLV	7.75	30.33
	TEN	8.55	29.49
	MLULU+TEN	7.68	30.42

The results in Table 5.2 show the improvement for each focus measure technique after cascading it with MLULU. The only failure of the cascading methods is at high level of noise (ND=0.5) for SML technique because second derivative is very sensitive to noise. APPENDIX C shows qualitative results for various objects and different noise levels.

Some of the results for each one of the seven different objects which are experimented with proposed focus measure are shown in APPENDIX C. The cascaded methods show better result as it is shown for all the objects in the figure. For example for plane object, TEN is not performing well in the low density speckle noise, but when it is cascaded with MLULU, the result is very clear. Cosine object in the presence of Gaussian noise (variance=0.005) can be well reconstructed if GLV is cascaded with MLULU, otherwise the GLV result is not similar to the cosine object at all. LCD object which is a microscopic image can be nicely reconstructed and similar to the original ground truth with MLULU+GLV even when there is impulse noise with medium level of noise. The cascaded options give good results for Gaussian and speckle noise too as shown in Table 5.3 and Table 5.4.

Table 5.3 Cascaded methods performance in the presence of Gaussian noise for simulated cone object

Variance	Focus measure (FM)	RMSE	PSNR
0.5	SML	34.46	17.52
	MLULU+SML	29.93	18.61
	GLV	34.33	17.42
	MLULU+GLV	27.44	19.36
	TEN	31.73	18.10
	MLULU+TEN	28.52	19.03
0.05	SML	33.94	17.52
	MLULU+SML	13.50	25.53
	GLV	16.87	23.59
	MLULU+GLV	8.10	29.96
	TEN	9.61	28.48
	MLULU+TEN	8.44	29.60
0.005	SML	23.00	20.90
	MLULU+SML	7.97	30.10
	GLV	8.32	29.73
	MLULU+GLV	7.73	30.36
	TEN	8.21	29.84
	MLULU+TEN	7.68	30.41

Table 5.4 Cascaded methods performance in the presence of speckle noise for simulated cone object

Noise density	Focus measure (FM)	RMSE	PSNR
0.5	SML	27.48	19.35
	MLULU+SML	13.01	25.79
	GLV	8.23	29.82
	MLULU+GLV	7.77	30.36
	TEN	8.22	29.84
	MLULU+TEN	7.91	30.07
0.05	SML	20.57	21.86
	MLULU+SML	7.96	30.11
	GLV	8.26	30.12
	MLULU+GLV	7.75	30.33
	TEN	8.18	30.21
	MLULU+TEN	7.70	30.41
0.005	SML	8.28	29.77
	MLULU+SML	7.89	30.19
	GLV	8.34	30.35
	MLULU+GLV	7.75	30.34
	TEN	8.26	30.44
	MLULU+TEN	7.65	30.45

5.4 Chapter Summary

In this chapter, the proposed 3D shape recovery techniques are applied on eight different SFF test objects individually and in combination with SML, GLV and TEN. The test objects are chosen from different textures in real and simulated data. The experiments are repeated in the presence of three different image noises which are impulse, Gaussian and speckle noises. Each noise experiment is considered ten times to provide a more accurate result. Achieved results are analyzed quantitatively and qualitatively with the original ground truth of each object to prove the accuracy of them. Although, the proposed techniques perform well in the presence of noise, however, the improvement comes at the cost of higher computational complexity.

CHAPTER 6

CONCLUSION AND RECOMMENDATIONS

6.1 Conclusion

In this thesis, we discussed the LULU operators and the concept of DPT based on LULU operators. LULU operators are nonlinear rank selector operators that are efficient with low complexity. They hold consistent separation, total variation and shape preservation properties. DPT is a transform that decomposes image into pulses. These two methods are implemented for 1D sequences as well as 2D arrays (images) for different applications. LULU is already being used widely in filtering and smoothing operations especially in econometrical and statistical literatures. Now, many researchers are employing LULU and DPT for image analysis too. DPT is a very efficient operator for multi-dimensional arrays unlike median operator. It is one of the best filtering methods for removing impulse noise from images as well as 1D sequences. Now, it is also being used for edge detection and contour tracing for object detection and object extraction applications. We have proposed to use LULU and DPT for 3D applications, i.e., depth map estimation, 3D shape extraction etc.

The most challenging concern in 3D shape extraction is the roughness of the surfaces. Image focusing is one of the principal schemes of 3D shape reconstruction. The shape from focus (SFF) is one of the best shape recovery methods which reconstructs the 3D shape from sequence of 2D images taken from same angle. The existing focus measures perform well in noiseless environments but their performance deteriorates in noisy environments. During image acquisition process, Gaussian noise is present. In addition, based on the environment condition and the camera, speckle noise and impulse noise may also be present. Presence of these types of noise in the image destroys the focus information, especially sharpest pixel values. Hence, the algorithms computing the best focus values fail in such a situation. This problem can be explained due to the reason that noise removal does not inherently exist in them

and because the existing techniques are based on variance and derivatives. Therefore, disability of the existing methods calls for a new technique which can perform well even in noisy environments.

In this thesis, new focus measures are proposed and tested for 3D shape recovery based on LULU operators and DPT. The proposed techniques are implemented on seven simulated and real data objects. The test objects are chosen from different textures with different level of details to verify the proposed techniques for different conditions. The proposed techniques are also cascaded with the existing SFF methods, i.e., Sum Modified Laplacian (SML), Tenenbaum (TEN) and Gray Level Variance (GLV). The experiments are repeated in the presence of impulse, Gaussian and speckle noise for 3D shape recovery. Each noise is evaluated in three different noise levels, which are; low noise density/variance (0.005), medium noise density/variance (0.05) and high noise density /variance (0.5).

In general, all the results obtained for each object are compared qualitatively and quantitatively with SML, the GLV and TEN. The reconstructed depth maps have been compared with the ground truth by using two different image quality metrics, which are; RMSE and PSNR.

Based on the quantitative and qualitative experimental results, the proposed techniques are more accurate in focused value extraction and shape recovery in the presence of various types of noise. MLULU focus measure performs better than existing methods when the SFF data is noisy. The performance of the cascaded MLULU and existing methods show a good improvement in shape recovery. However, the performance of MDPT method can be improved by combining it with other approximation methods, like Gaussian interpolation and choosing proper range of pulses.

6.2 Future Work

LULU is being used widely in filtering and smoothing operations, especially in econometrical and statistical applications. Recently many researchers are implementing LULU and DPT for image analysis as well. In the future, the proposed techniques based on LULU operators and DPT can be tested in various applications like 3D shape extraction, microscopic applications [52], communication [53], medical imaging [54] and [55], etc.

REFERENCES

- [1] S.K. Nayar, "Shape from Focus," *IEEE Transactions on Pattern Analysis and Machine Intelligence*, vol. 16, 1994, pp. 824-83.
- [2] P. Favaro and S. Soatto, "Learning Shape from Defocus," *Proceedings of the 7th European Conference on Computer Vision-Part II*, 2002, pp. 735-745.
- [3] M. Subbarao and T. Choi, "Accurate Recovery of Three-Dimensional Shape from Image Focus," *IEEE transaction on Pattern Analysis and Machine In*, vol. 17, 1995, pp. 226-274.
- [4] R. Szeliski and S.B. Kang, "Shape Ambiguities in Structure from Motion," *Pattern Analysis and Machine Intelligence, IEEE Transactions on*, vol. 19, 1997, pp. 506-512.
- [5] D.A. Forsyth, "Shape from texture and integrability," *Eighth IEEE International Conference on Computer Vision, 2001(ICC'V 2001) Proceedings.*, vol. 2, 2001, pp. 447-452.
- [6] R. Zhang, P.-sing Tsai, J.E. Cryer, and M. Shah, "Shape from Shading : A Survey," *Pattern Analysis and Machine Intelligence, IEEE Transactions on*, vol. 21, 1999, pp. 690-706.
- [7] S.K. Nayar and Y. Nakagawa, "Shape from Focus : An Effective Approach for Rough Surfaces," *IEEE International Conference on Robotics and Automation, 1990. Proceedings.*, 1990, pp. 218-225.
- [8] F.S. Helmlí and S. Scherer, "Adaptive Shape from Focus with an Error Estimation in Light Microscopy," *Proceedings of the 2nd International Symposium on Image and Signal Processing and Analysis*, 2001, pp. 188-193.
- [9] M. Asif and T.-sun Choi, "Shape from focus using multilayer feedforward neural networks," *IEEE Transactions on Image Processing*, vol. 10, 2001, pp. 1670-1675.
- [10] A.S. Malik and T.-sun Choi, "A Novel Algorithm for Estimation of Depth Map using Image Focus for 3D Shape Recovery in the Presence of Noise," *Pattern Recognition*, vol. 41, 2008, pp. 2200 - 2225.
- [11] B.K.P. Horn, "Focussing," *M.I.T., Project MAC, AI Memo*, 1968.
- [12] J.M. Tenenbaum, "Accommodation in Computer Vision," *Ph.D. Thesis, Stanford University*, 1970.
- [13] A.P. Pentland, R. Ave, and M. Park, "A New Sense for Depth of Field," *IEEE Transactions on Pattern Analysis and Machine Intelligence*, vol. PAMI-9, 1985, pp. 988-994.

- [14] A. Erteza, "Sharpness index and its application to focus control," *Applied Optics*, vol. 15, 1976, pp. 877-881.
- [15] R.A. Jarvis, "Focus optimisation criteria for computer image processing," *Microscope*, vol. 24, 1976, pp. 163-180.
- [16] E. Krotkov and J.P. Martin, "Range from Focus," *IEEE International Conference on Robotics and Automation. Proceedings.*, vol. 3, 1986, pp. 1093-1098.
- [17] P. Grossmann, "Depth from Focus," *Pattern Recognition Letters*, vol. 5, 1987, pp. 63-69.
- [18] T. Darrell and K. Wohn, "Pyramid Based Depth from Focus," *Computer Society Conference on Computer Vision and Pattern Recognition, 1988. Proceedings CVPR '88.*, 1988, pp. 504-509.
- [19] P.T. Yap and P. Raveendran, "Image focus measure based on Chebyshev moments," *IEE Proceedings -Vision, Image and Signal Processing*, vol. 151, 2004, pp. 128-136.
- [20] N. Asada, H. Fujiwara, and T. Matsuyama, "Edge and Depth from Focus," *International Journal of Computer Vision*, vol. 26, 1998, pp. 153-163.
- [21] Y. Zhang, Y. Zhang, and C. Wen, "A new focus measure method using moments," *Image and Vision Computing*, vol. 18, 2000, pp. 959-965.
- [22] J.-H. Wang and L.-D. Lin, "Improved Median Filter using MinMax Algorithm for Image Processing," *Electronics Letters*, vol. 33, 1997, pp. 1362-1363.
- [23] K. He, X.-cheng Luan, C.-hua Li, and R. Liu, "Gaussian Noise Removal of Image on the Local Feature," *Second International Symposium on Intelligent Information Technology Application, IITA '08*, vol. 3, 2008, pp. 867-871.
- [24] A.K. Fazlul Haque, M. Hanif Ali, and M. Adnan Kiber, "Biomedical Image Analysis using Wavelet Tools for Emergency Medical Applications," *ARPVN Journal of Engineering and Applied Sciences*, vol. 5, 2010, pp. 15-20.
- [25] W.J. Conradie, T.D. Wet, and M. Jankowitz, "Exact and asymptotic distributions of LULU smoothers," *Journal of Computational and Applied Mathematics*, vol. 186, 2006, pp. 253 - 267.
- [26] C.H. Rohwer and D.P. Laurie, "The Discrete Pulse Transform," *SIAM Journal on Mathematical Analysis*, vol. 38, 2005, pp. 1-28.
- [27] M.D. Jankowitz, "Some Statistical Aspects of LULU smoothers," *Masters Thesis, University of Stellenbosch*, 2007.

- [28] R. Anguelov and I. Fabris-rotelli, "Properties of the Discrete Pulse Transform for Multi-Dimensional Arrays," *IEEE transaction on Image Processing*, 2010, pp. 1-5.
- [29] P.N. Heller and R.O. Wells, "The Spectral Theory of Multiresolution Operators and Applications," *Academic Press, San Diego*, 1994, pp. 13-31.
- [30] R. Anguelov and I. Fabris-rotelli, "LULU Operators and Discrete Pulse Transform for Multidimensional Arrays," *IEEE transaction on Image Processing*, vol. 19, 2010, pp. 3012-3023.
- [31] J. Pierre du Toit, "The Discrete Pulse Transform and Applications," *Masters Thesis, University of Stellenbosch*, 2007.
- [32] R. Anguelov and I. Fabris-rotelli, "Discrete Pulse Transform of Images," *Lecture Notes in Computer Science*, vol. 5099:1-9, 2008, pp. 1-9.
- [33] P. Maragos and R. W. Schafer, "Morphological Systems for Multidimensional Signal Processing," *Proceedings of the IEEE*, vol. 78, 1990, pp. 690-710.
- [34] B. Anguelov, "Discrete Pulse Transform of Images : Algorithm and Applications," *19th International Conference on Pattern Recognition (ICPR) 2008.*, 2008, pp. 1-4.
- [35] A. Chambolle and P. Lions, "Image Recovery via Total Variation Minimization and Related Problems," *Numerische Mathematik*, vol. 76, 1997, pp. 167-188.
- [36] L.I. Rudin, S. Osher, and E. Fatemi, "Nonlinear total variation based noise removal algorithms," *Physica*, vol. 60, 1992, pp. 259-268.
- [37] A. Morales, R. Acharya, and S.-J. Ko, "Morphological Pyramids with Alternating Sequential Filters," *IEEE transaction on Image Processing*, vol. 4, 1995, pp. 965 - 977.
- [38] S.-C. Pei and C.-L. Lai, "An Efficient Class of Alternating Sequential Filters in Morphology," *Graphical Models and Image Processing*, vol. 59, 1997, pp. 109-116.
- [39] S.T. Acton and D.P. Mukherjee, "Scale Space Classification Using Area Morphology," *IEEE transaction on Image Processing*, vol. 9, 2000, pp. 623-635.
- [40] I. Fabris-Rotelli and S.J.V.D. Walt, "The Discrete Pulse Transform in Two Dimensions," *Proceedings of the Twentieth Annual Symposium of the Pattern Recognition Association of South Africa-*, 2009.

- [41] T. de Wet and W. Conradie, "Smoothing Sequences of Data by Extreme Selectors," *Proceedings of ICOTS7 2006: The 7th International Conference on Teaching Statistics, Salvador, Bahia, Brazil, 2-7 July, 2006*.
- [42] J. Serra, "Connectivity on Complete Lattices," *Mathematical Morphology and Its Applications to Image and Signal Processing*, 1996, p. 81–96.
- [43] J. Serra, "A Lattice Approach to Image Segmentation," *Journal of Mathematical Imaging and Vision*, vol. 24, 2006, pp. 83-130.
- [44] H.-sung Han, D.-o Kim, and R.-hong Park, "Structural Information-Based Image Quality Assessment Using LU Factorization," *Digest of Technical Papers - IEEE International Conference on Consumer Electronics*, 2009.
- [45] D.-o Kim and R.-hong Park, "Image Quality Measure Using the Phase Quantization Code," *IEEE Transactions on Consumer Electronics*, vol. 56, 2010, pp. 937-945.
- [46] C. Li, X. Yang, B. Chu, W. Lu, and L. Pang, "A New Image Fusion Quality Assessment Method Based on Contourlet and SSIM," *Proceedings - 2010 3rd IEEE International Conference on Computer Science and Information Technology, ICCSIT 2010 5, art*, 2010, pp. 246-249.
- [47] A. Shnayderman, A. Gusev, and A.M. Eskicioglu, "An SVD-Based Gray-Scale Image Quality Measure for Local and Global Assessment," *Image Processing, IEEE Transactions on*, vol. 15, 2006, pp. 422-429.
- [48] Z. Wang, A.C. Bovik, H.R. Sheikh, and E. P. Simoncelli, "Image Quality Assessment : From Error Visibility to Structural Similarity," *IEEE transaction on Image Processing*, vol. 13, 2004, pp. 600-612.
- [49] A. Horé and D. Ziou, "Image quality metrics : PSNR vs . SSIM," *International Conference on Pattern Recognition*, 2010.
- [50] N. Kamel and S. Kafa, "Image SNR and Noise Variance Estimation Using Autoregressive Model," *Journal of Scanning Microscopes*, vol. 26, 2004, pp. 277-282.
- [51] "<http://en.wikipedia.org/wiki/PSNR>."
- [52] S.-o Shim, A.S. Malik, and T.-sun Choi, "Accurate Shape From Focus Based on Focus Adjustment in Optical Microscopy," *Microscopy Research and Technique*, vol. 370, 2009, pp. 362-370.
- [53] J. Khodjaev, Y. Park, and A.S. Malik, "Survey of NLOS identification and error mitigation problems in UWB-based positioning algorithms for dense environments," *Springer Annals of Telecommunications*, vol. 65, 2010, pp. 301-311.

- [54] A.S. Malik, "Simulation-based analysis of the resolution and SNR properties of partial k-space EPI," *Concepts in Magnetic Resonance Part B: Magnetic Resonance Engineering*, vol. 35B, 2009, p. 232–237.
- [55] A.S. Malik and T.-sun Choi, "Differentiating honeycombed images from normal HRCT lung images," *IEICE Transactions on Information & Systems*, vol. E92-D, 2009, pp. 1218-1221.
- [56] O. Kao, "Modification of the LULU Operators for Preservation of Critical Image Details," *International Conference on Imaging Science, Systems and Technology, Las Vegas, USA*, 2001.

APPENDIX A

In Table A.1, M is the median, I is the identity operator, C and F are, respectively, the ceiling (biased towards lower limits) and floor (biased towards upper limits) LULU operators.

Table A.1 Some of the properties of LULU operator

<i>Property</i>	<i>Comment</i>
$L \leq I \leq U$	I represents identity operator
$L^2 = L, U^2 = U$	Repetition of same operator would not affect the result
$L \leq M \leq U$	M denotes the median operator
$(LUL)^2 = LUL, (ULU)^2 = ULU$ [56]	Repetition of same operator would not affect the result
$LUL \leq ULU$ [56]	LUL due to applying L operator twice in different orders makes the result smaller than ULU which applies the U operator more
$(LU)^2 = LU, (UL)^2 = UL$ [32]	Repetition of same operator would not affect the result
$U_n(x) = L_n(x) = x$	“where x is a constant sequence and $x \in M_n$ ”
$L_n \leq U_n L_n \leq C_n \leq F_n \leq L_n U_n \leq U_n$ [26]	“The C_n and F_n operators (ceiling and floor) are given by: $C_0 = L_0 U_0 = I = U_0 L_0 = F_0$ $C_{n+1} = L_{n+1} U_{n+1} C_n$; $F_{n+1} = U_{n+1} L_{n+1} F_n$ ” [26]
$U_n U_k = U_m$ and $L_n L_k = L_m$ [26]	where $m = \max\{n, k\}$ [26]
$L_n U_n$ (and $U_n L_n$) are idempotent and co-idempotent [26]	“ A is idempotent if $A^2 = A$ and co-idempotent if $I - A$ is idempotent, therefore they are separators” [26]
$U_n L_n \leq M_n \leq L_n U_n$ [26]	M_n denote the median operator of order n [26] $(M_n x)_i = \text{median}\{x_{i-n}, \dots, x_i, \dots, x_{i+n}\}$

$L_n U_n$ (and $U_n L_n$) are syntone operators [26]	An operator S is syntone if $x > y \rightarrow S_x > S_y$ [26]
$L_n U_n$ (and $U_n L_n$) are ntp operators [26]	“An operator A is neighbor trend preserving (ntp) if for each sequence x , $x_i \geq x_{i+1} \rightarrow (Ax)_i \geq (Ax)_{i+1}$ $x_i \leq x_{i+1} \rightarrow (Ax)_i \leq (Ax)_{i+1}$ ” [26]
$L_n U_n$ (and $U_n L_n$) are ftp operators [26]	“An operator A is fully trend preserving (ftp) if A is ntp and, $ (Ax)_i - (Ax)_{i+1} \leq x_i - x_{i+1} $ ” [27]
U_n and L_n are variation preserving	A parameter expression that preserves orthonormality under variation up to n order
The operators L_n and U_n are duals in that $U_n(-x) = -L_n(x)$ [26]	Negation property [26]
$U_n(x+c) = U_n x+c$ (and $L_n(x+c) = L_n x+c$) for any constant sequence c [26]	Constant Shift property [26]
$U_n(\alpha x) = \alpha U_n(x)$ (and $L_n(\alpha x) = \alpha L_n(x)$) for any $\alpha > 0$ [27]	Constant Multiple property [26]
F_n and C_n are separators [26]	“A smoother A is a separator if it is both idempotent and co-idempotent” [26]

APPENDIX B

Simulated Cone: In this case the sequence is constructed from 97 different images with different focus values, with the resolution of 360×360 . Figure B.1, illustrates the simulated data of the cone. It has a dense texture [4].

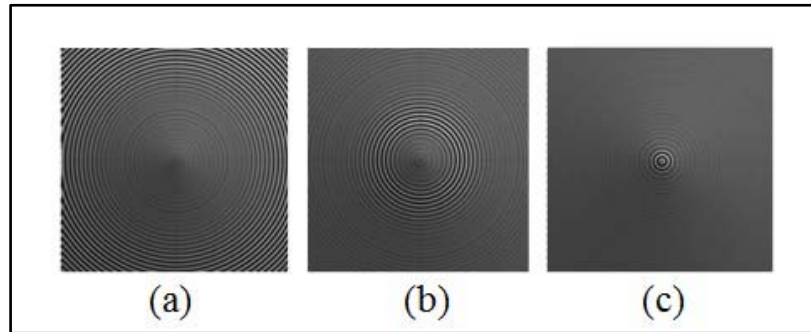


Figure B.1 Test object: simulated cone; (a) focused on the based section of the cone, (b) focused on the middle part of the cone and (c) focused on the apex part

Simulated Slope: This data consist of 60 frames with the resolution of 320×320 . Some of the frames are shown in Figure B.2.

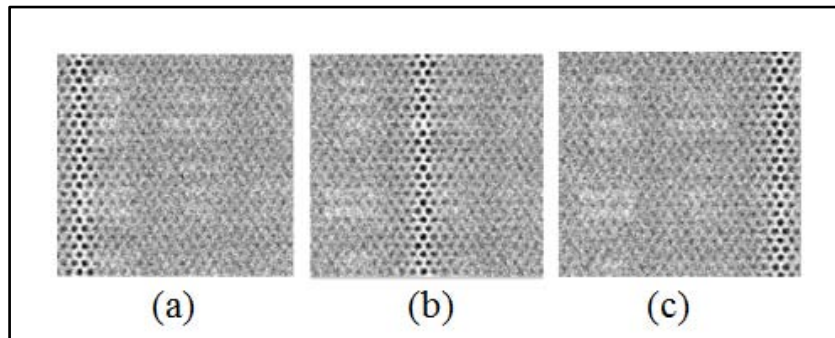


Figure B.2 Test object: simulated slope; (a) focused on a narrow column on the left side, (b) focused on a narrow column in the middle of the image and (c) focused on a narrow column on the right side

Simulated Cosine: Similar to slope and sine simulated data, simulated cosine also consists of 60 frames with the resolution of 320×320 . Some of the frames are shown in Figure B.3.

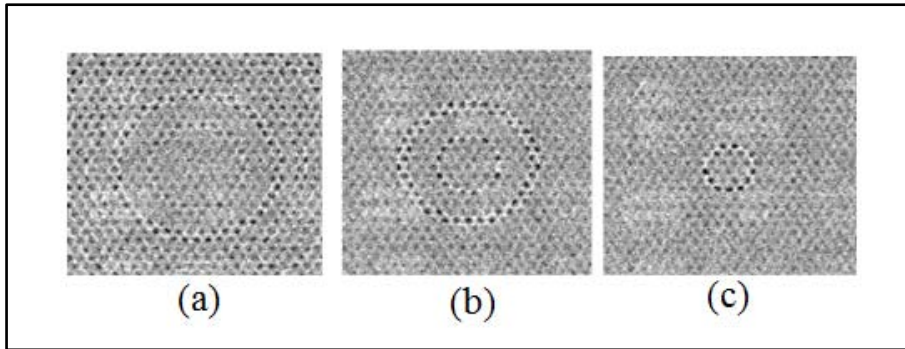


Figure B.3 Test object: simulated cosine; (a) focused on a large circular portion, (b) focused on a medium circular part and (c) focused on a small circular region in the middle

Real Cone: Real Cone object is the real data of the real cone. The resolution is 360×360 and the number of images in the sequence is 97. Some frames are shown in Figure B.4.

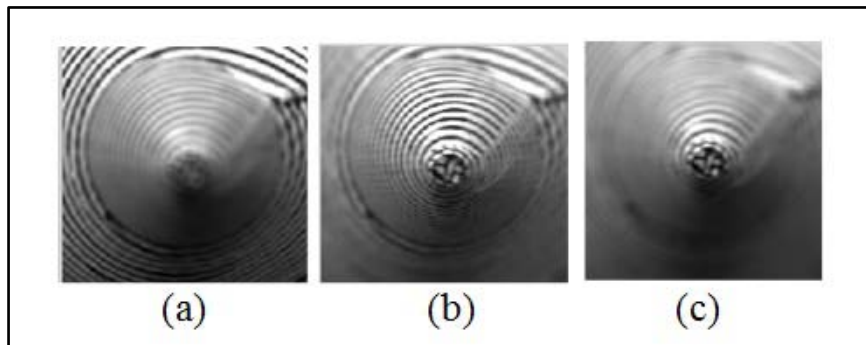


Figure B.4 Test object: real cone; (a) focused on the based section of the cone, (b) focused on the middle part of the cone and (c) focused on the apex part

Real Coin: This data has been collected from a microscopic object with 68 frames of 300×300 pixels. Figure B.5 shows different focused frames of this object. This object is the head of Lincoln on a one penny coin which is a good sample of a rough texture [4].

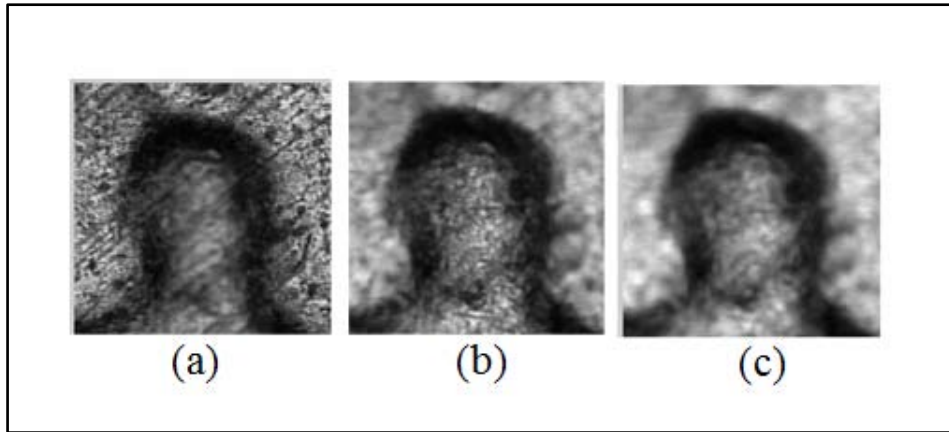


Figure B.5 Test object: real coin; (a) far section is focused, (b) focused on head section and (c) focused on the very far points

Real LCD: LCD is also another microscopic object which is a sequence of 60 real data. The resolution of the image is 300×300 . Figure B.6 shows three of the frames for Thin Film Transistor-Liquid Crystal Display (TFT-LCD).

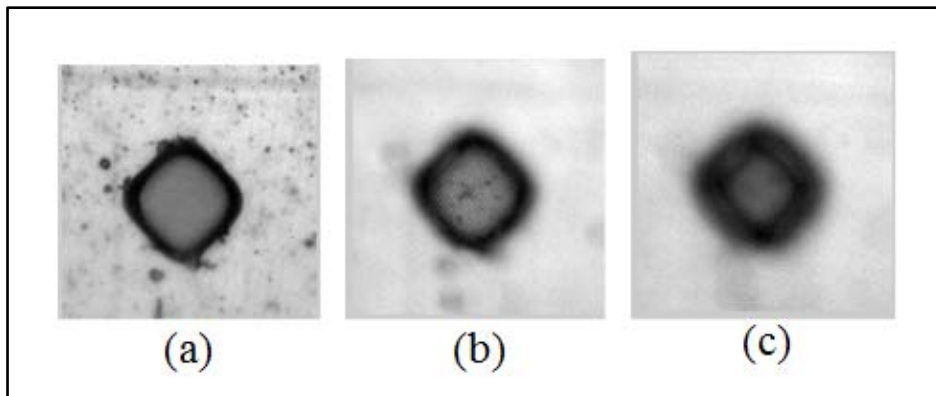


Figure B.6 Test object: real LCD; (a) focused on the back part, (b) focused on the middle part and (c) focused on the corner parts

Real Plane: Real Plane is the real data collected from a plane. Its SFF data consists of 87 frames at resolution of 200×200 pixels. This object is a good example of a poor texture and some of its different focused frames are illustrated in Figure B.7.

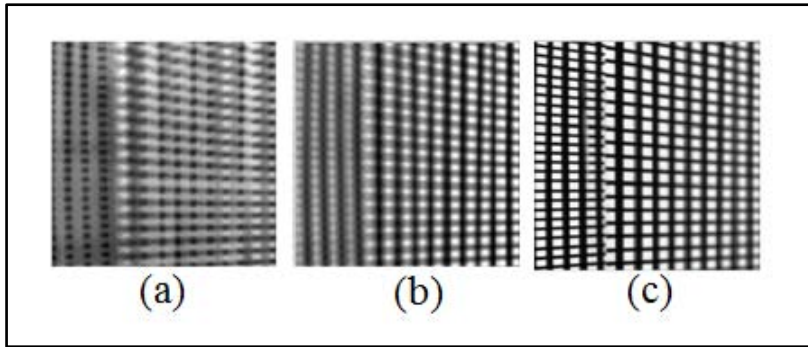


Figure B.7 Test object: real plane(a) far sectioned is focused, (b) focused on the middle section and (c) focused on the front points

APPENDIX C

This section shows the qualitative results of cascaded techniques in the presence of different noises for all the test images. Following figures show the result of impulse noise for various objects and different noise levels.

- Speckle noise with noise density of 0.005

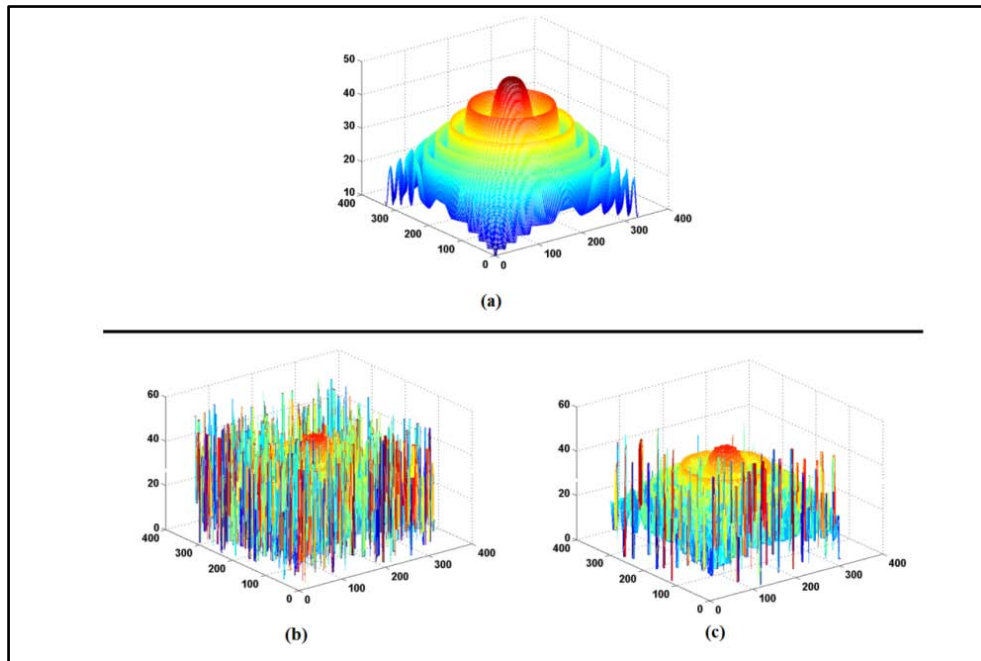


Figure C.1 Simulated cosine in the presence of speckle noise with noise density of 0.005; (a) Ground truth, (b) GLV focus measure and (d) MLULU+GLV focus measure

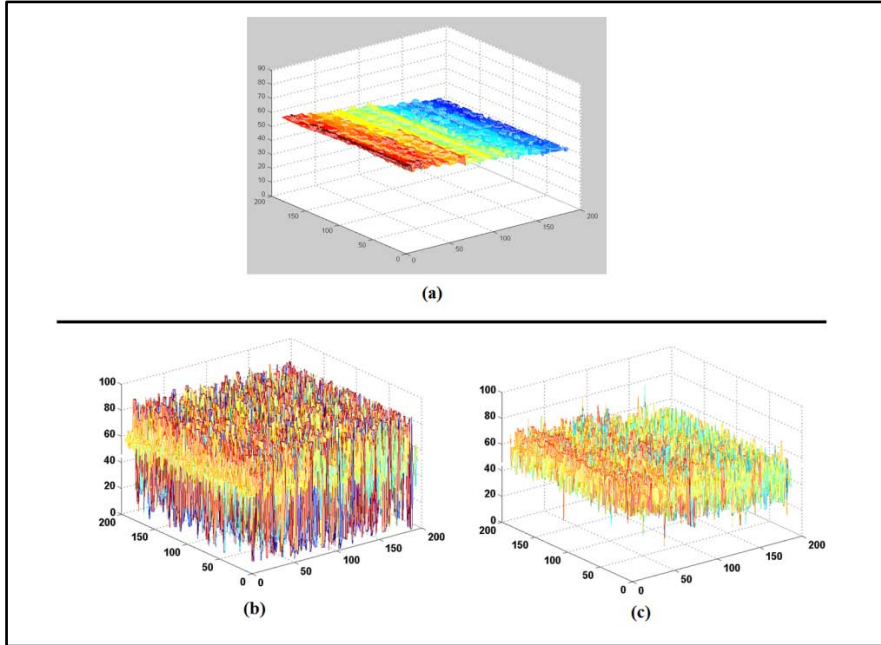


Figure C.2 Real plane in the presence of speckle noise with noise density of 0.005; (a) Ground truth, (b) SML focus measure and (d) MLULU+SML focus measure

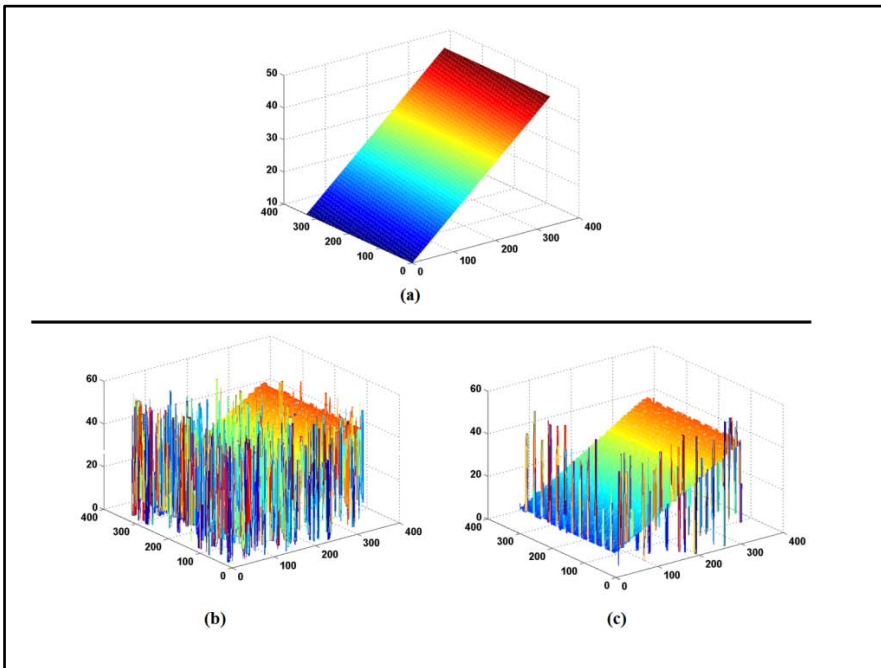


Figure C.3 Simulated slope in the presence of speckle noise with noise density of 0.005; (a) Ground truth, (b) TEN focus measure and (d) MLULU+TEN focus measure

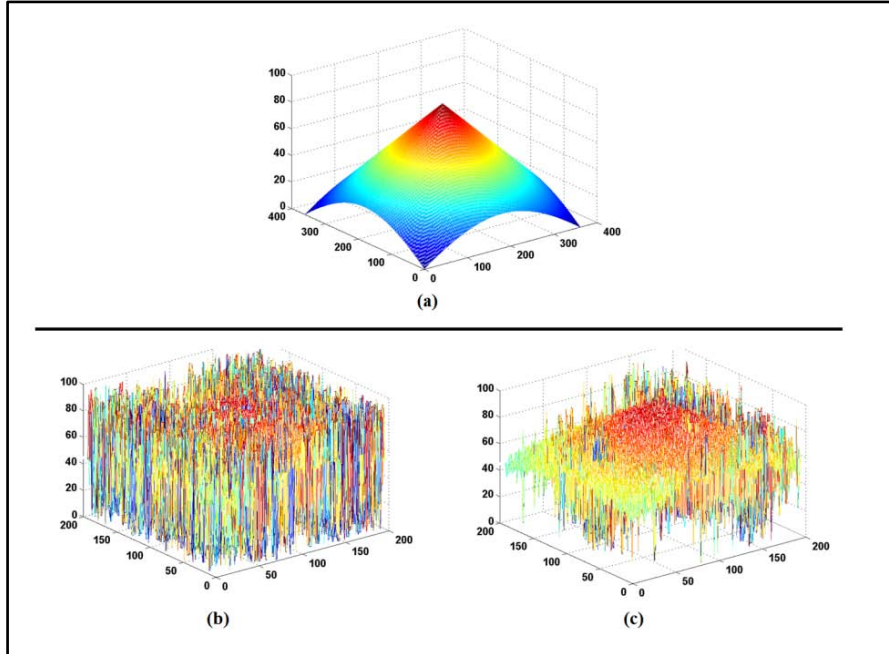


Figure C.4 Real cone in the presence of speckle noise with noise density of 0.005; (a) Ground truth, (b) SML focus measure and (d) MLULU+SML focus measure

- Speckle noise with noise density of 0.05

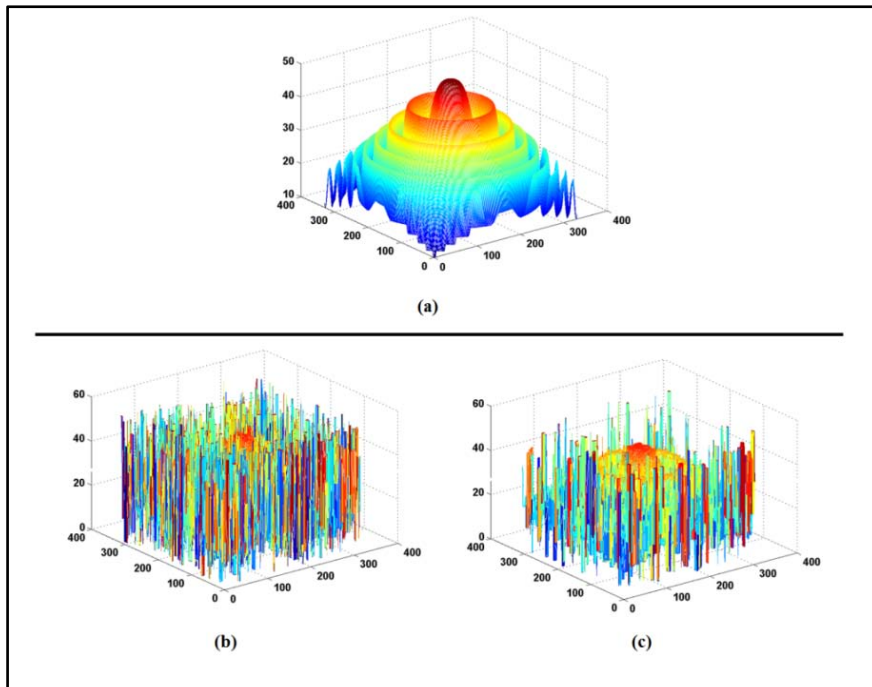


Figure C.5 Simulated cosine in the presence of speckle noise with noise density of 0.05; (a) Ground truth, (b) TEN focus measure and (d) MLULU+TEN focus measure

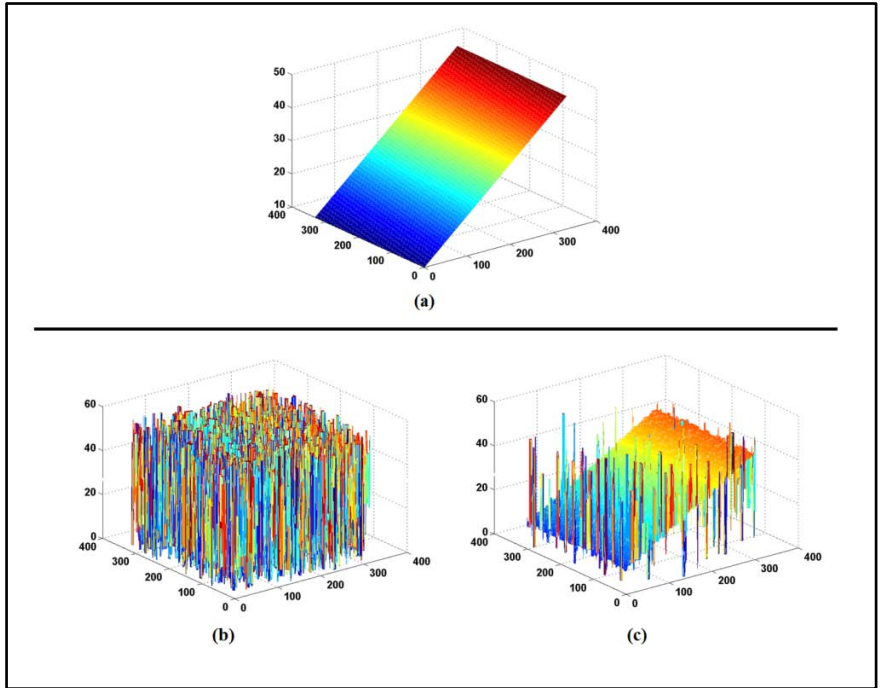


Figure C.6 Simulated slope in the presence of speckle noise with noise density of 0.05; (a) Ground truth, (b) GLV focus measure and (d) MLULU+GLV focus measure

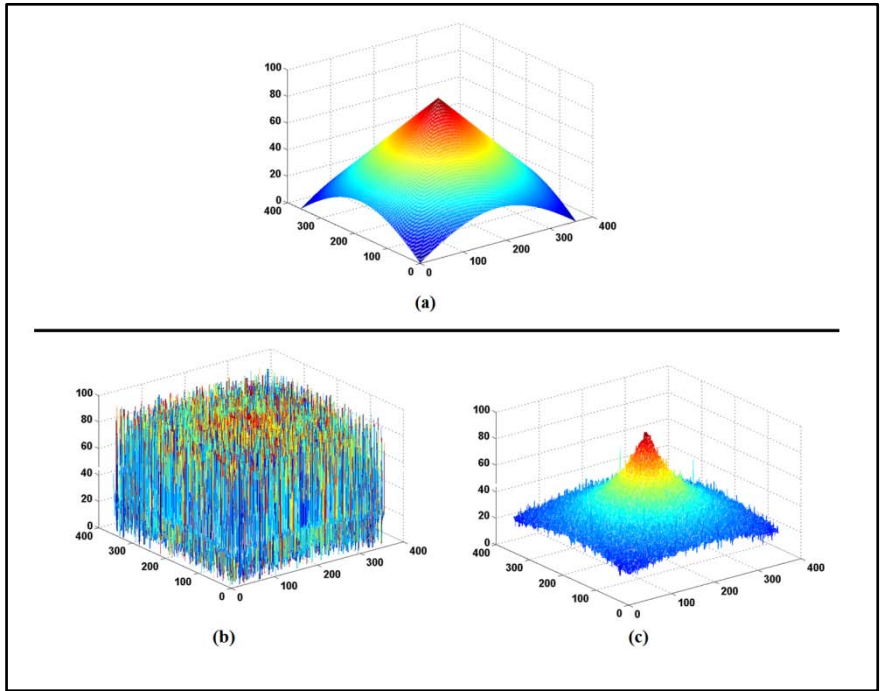


Figure C.7 Simulated Cone in the presence of speckle noise with noise density of 0.05; (a) Ground truth, (b) SML focus measure and (d) MLULU+SML focus measure

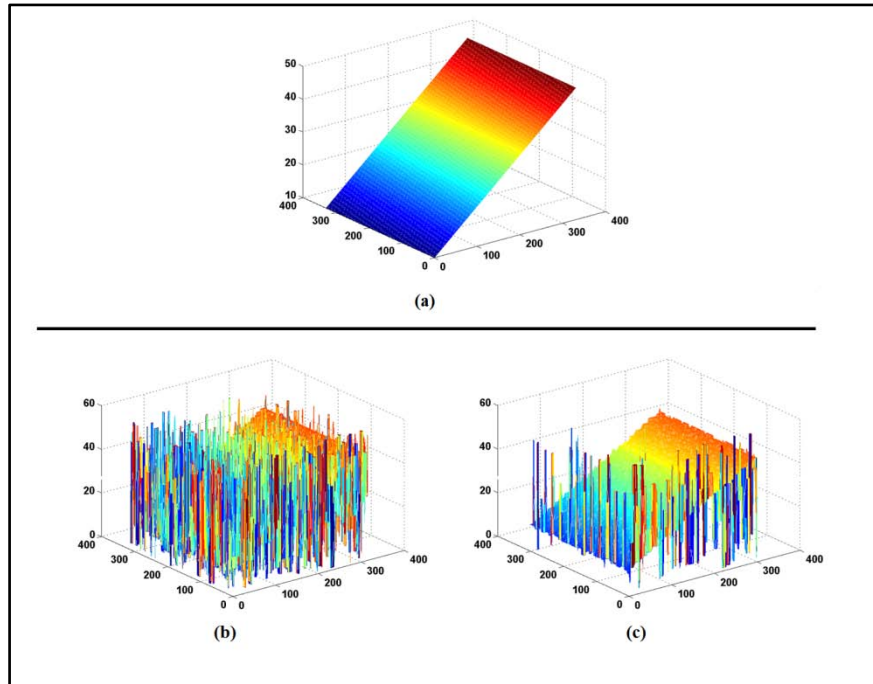


Figure C.8 Simulated slope in the presence of speckle noise with noise density of 0.05; (a) Ground truth, (b) TEN focus measure and (d) MLULU+TEN focus measure

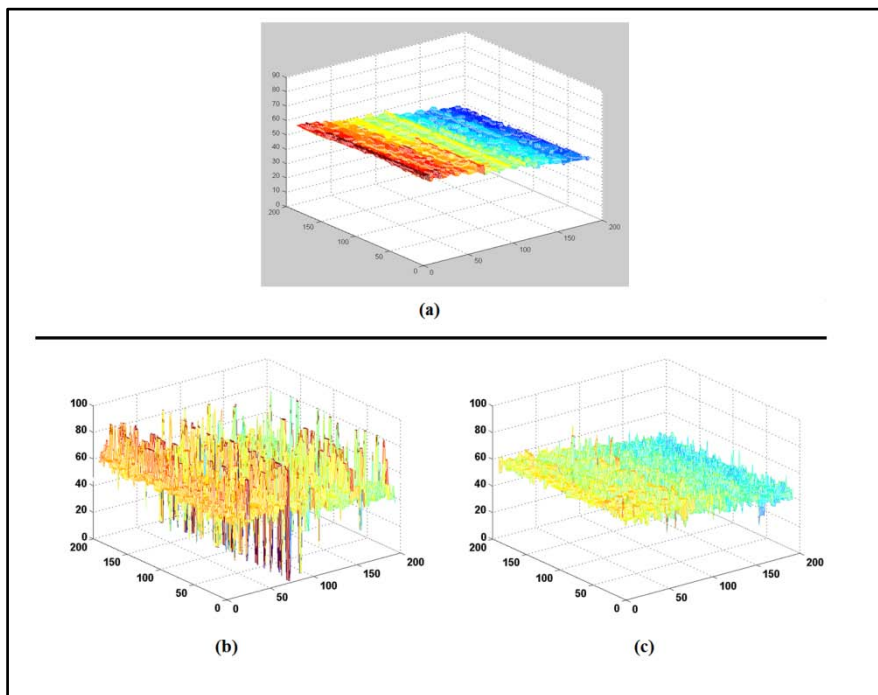


Figure C.9 Real Plane in the presence of speckle noise with noise density of 0.05; (a) Ground truth, (b) GLV focus measure and (d) MLULU+GLV focus measure

- Speckle noise with noise density of 0.5

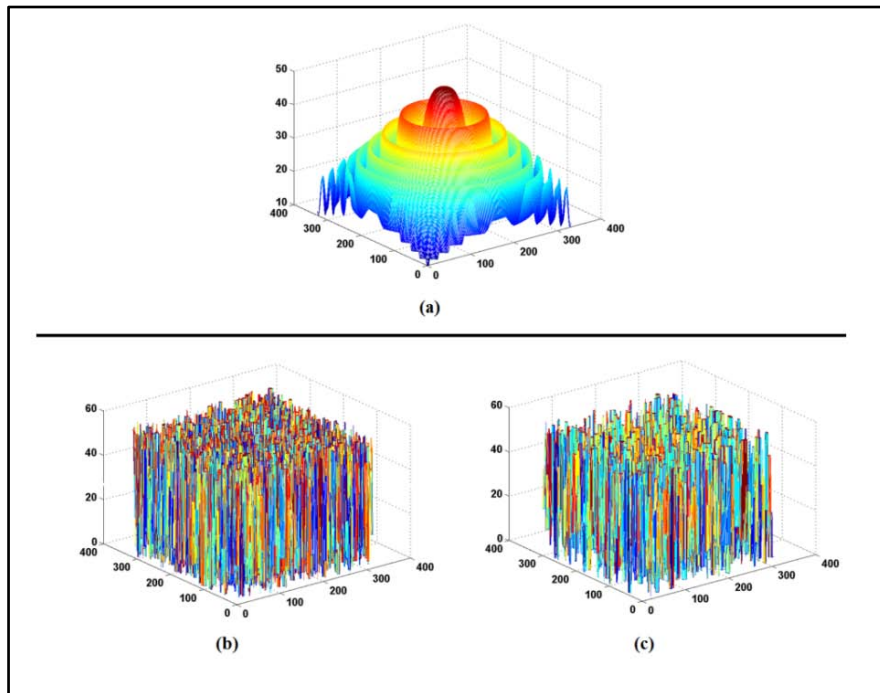


Figure C.10 Simulated cosine in the presence of speckle noise with noise density of 0.5; (a) Ground truth, (b) GLV focus measure and (d) MLULU+GLV focus measure

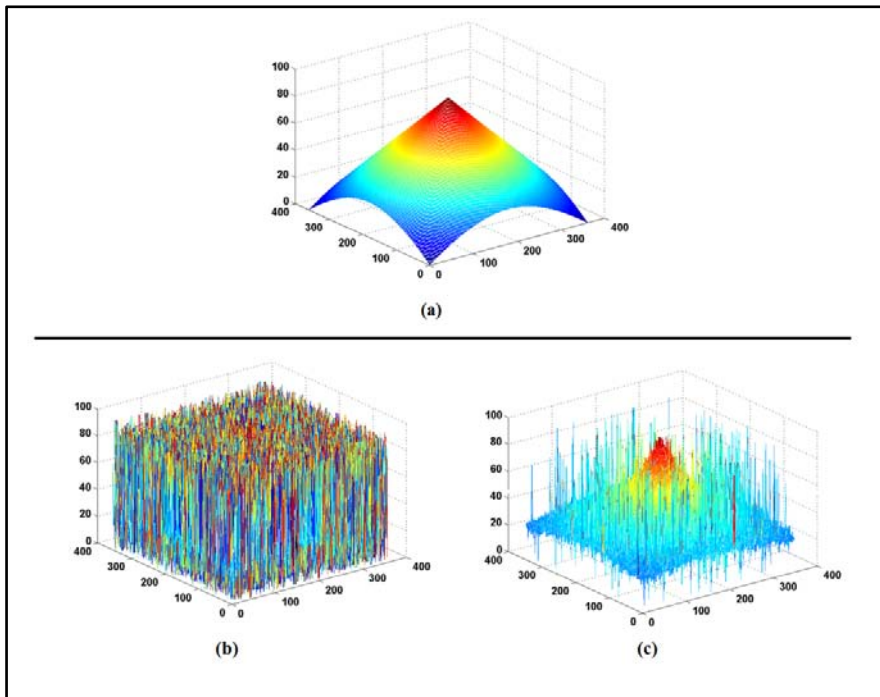


Figure C.11 Simulated cone in the presence of speckle noise with noise density of 0.5; (a) Ground truth, (b) SML focus measure and (d) MLULU+SML focus measure

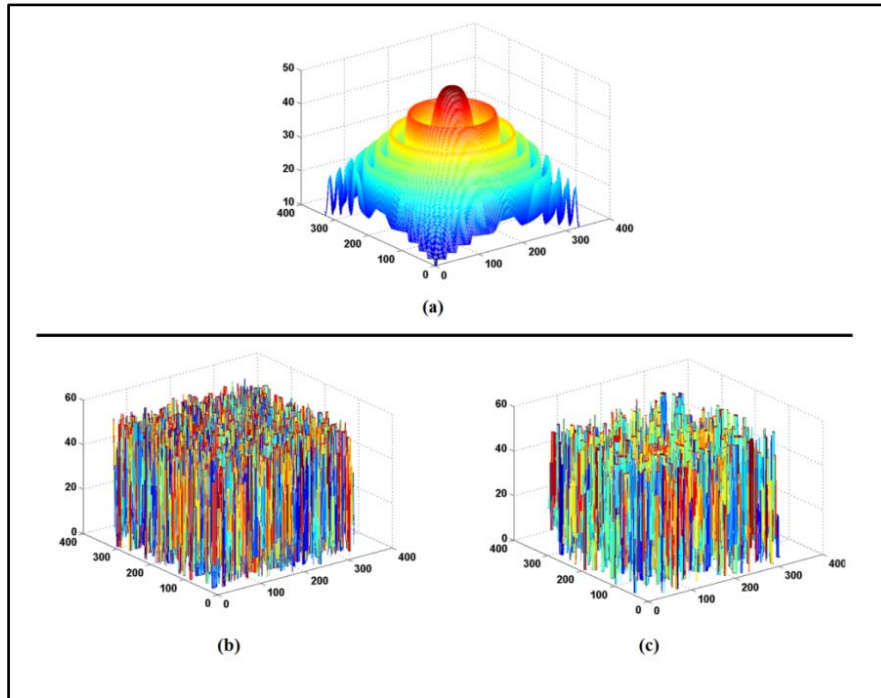


Figure C.12 Simulated cosine in the presence of speckle noise with noise density of 0.5; (a) Ground truth, (b) TEN focus measure and (d) MLULU+TEN focus measure

- Impulse noise with noise density of 0.005

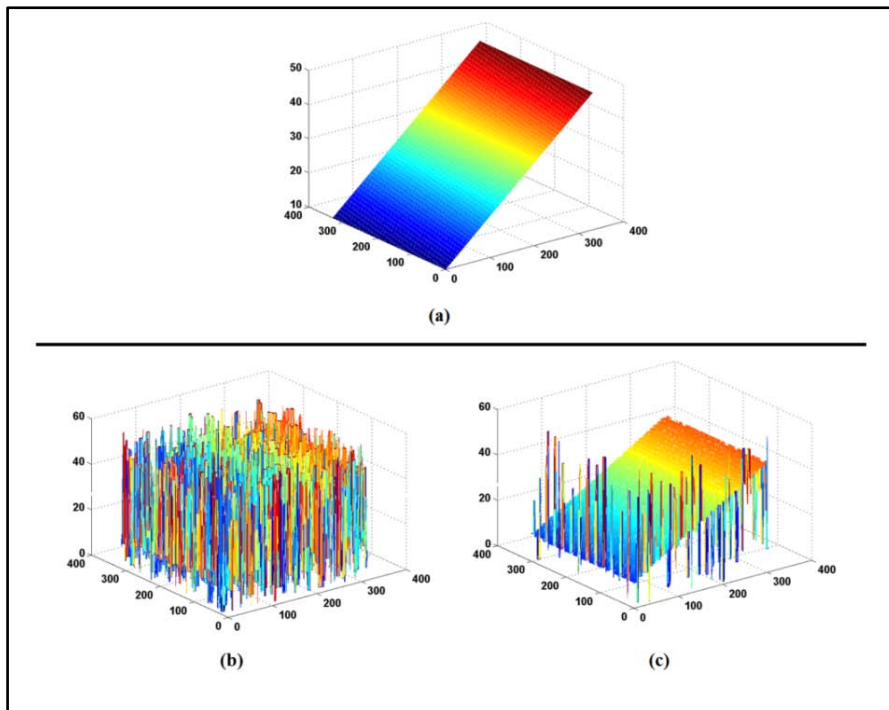


Figure C.13 Simulated slope in the presence of impulse noise with noise density of 0.005; (a) Ground truth, (b) GLV focus measure and (d) MLULU+GLV focus measure

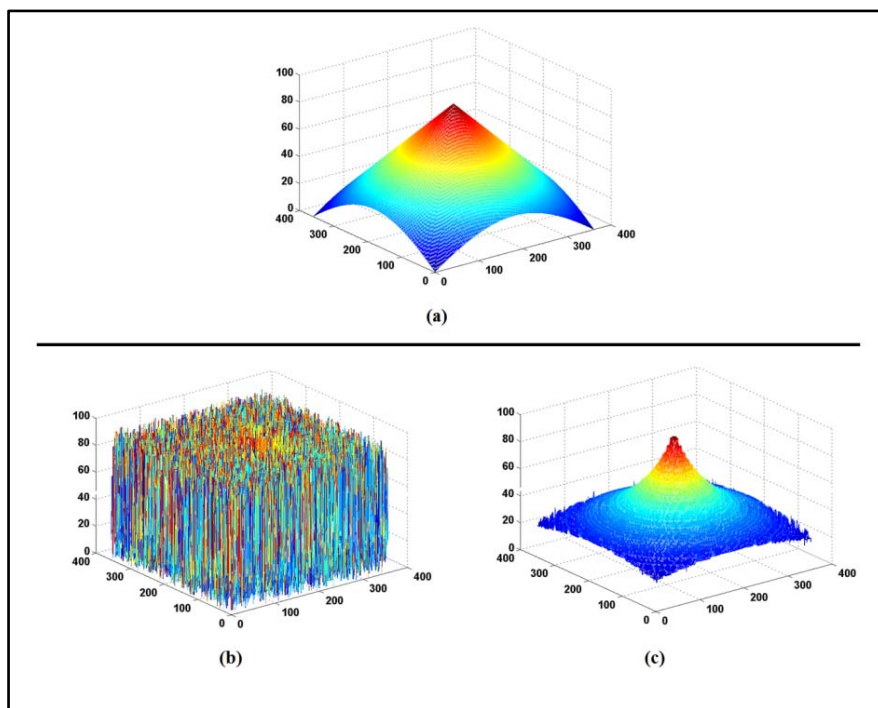


Figure C.14 Simulated cone in the presence of impulse noise with noise density of 0.005; (a) Ground truth, (b) SML focus measure and (d) MLULU+SML focus measure

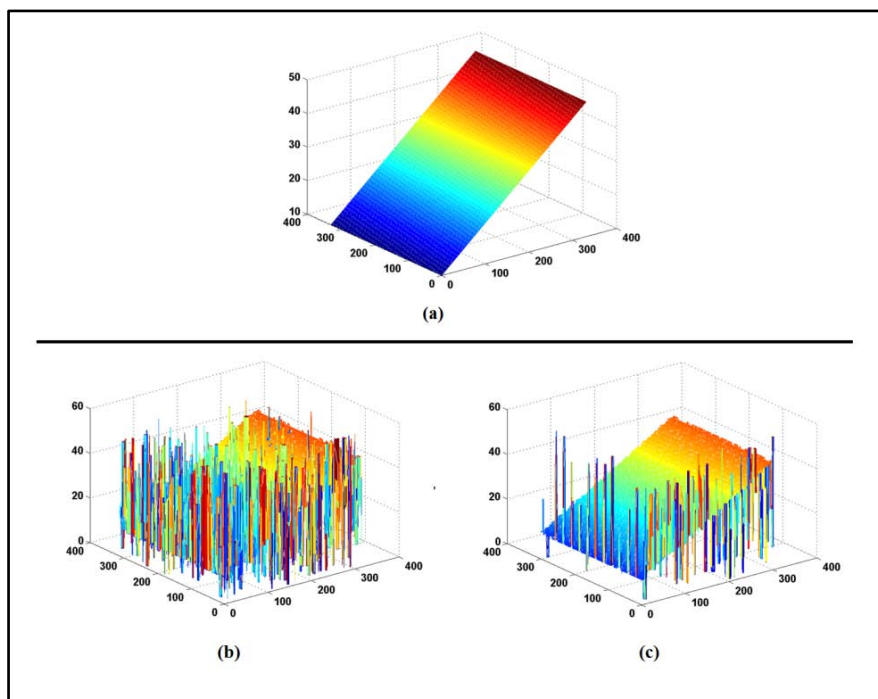


Figure C.15 Simulated slope in the presence of impulse noise with noise density of 0.005; (a) Ground truth, (b) TEN focus measure and (d) MLULU+TEN focus measure

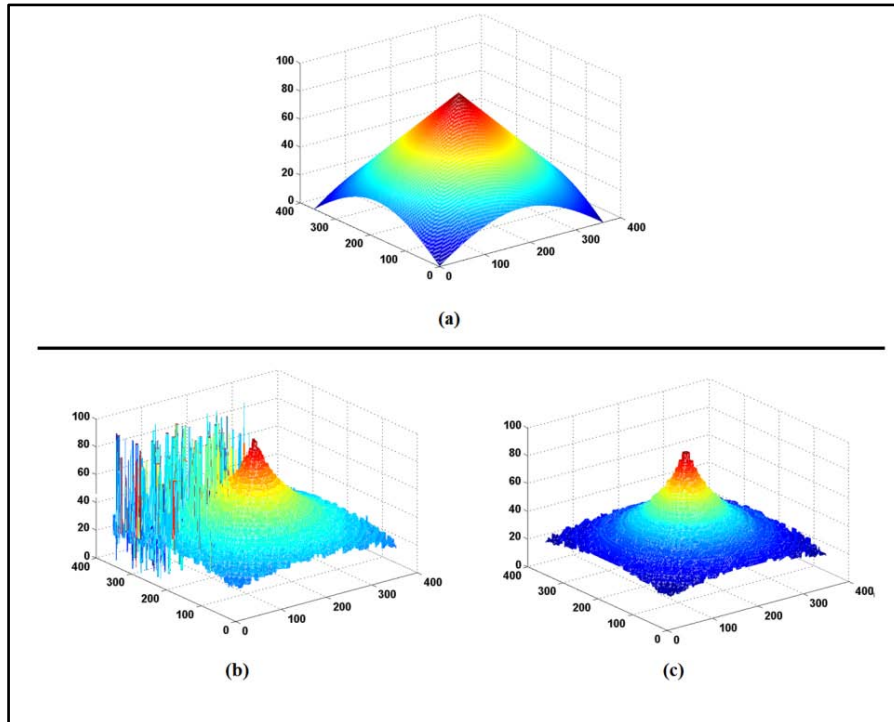


Figure C.16 Simulated cone in the presence of impulse noise with noise density of 0.005; (a) Ground truth, (b) GLV focus measure and (d) MLULU+GLV focus measure

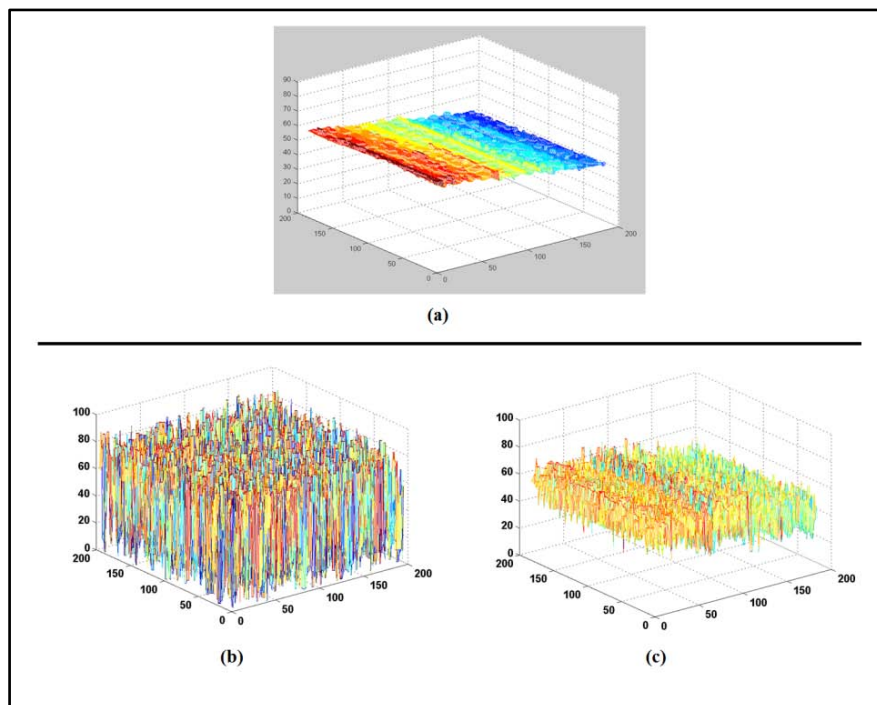


Figure C.17 Real plane in the presence of impulse noise with noise density of 0.005; (a) Ground truth, (b) SML focus measure and (d) MLULU+SML focus measure

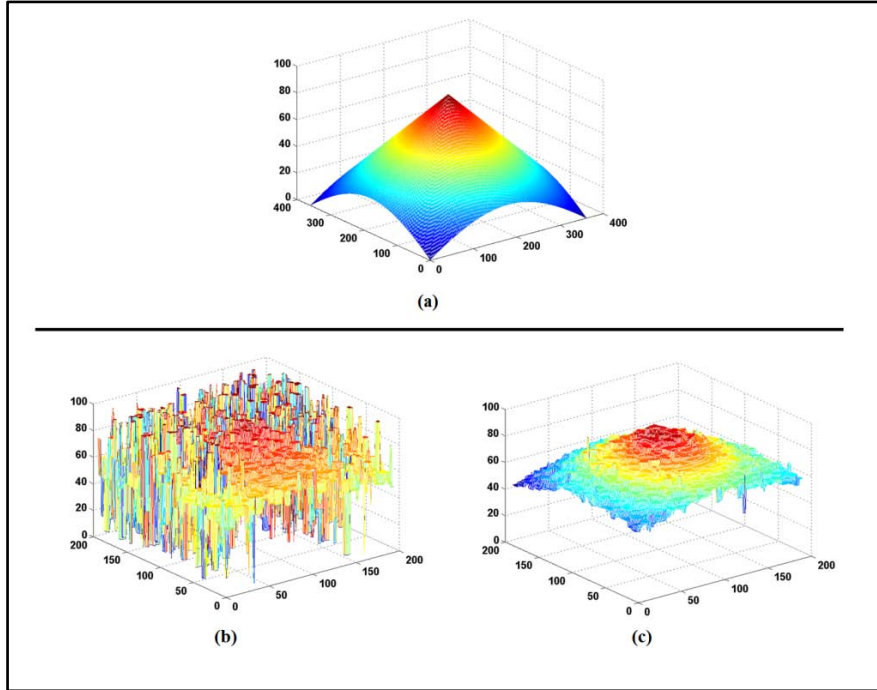


Figure C.18 Real cone in the presence of impulse noise with noise density of 0.005; (a) Ground truth, (b) GLV focus measure and (d) MLULU+GLV focus measure

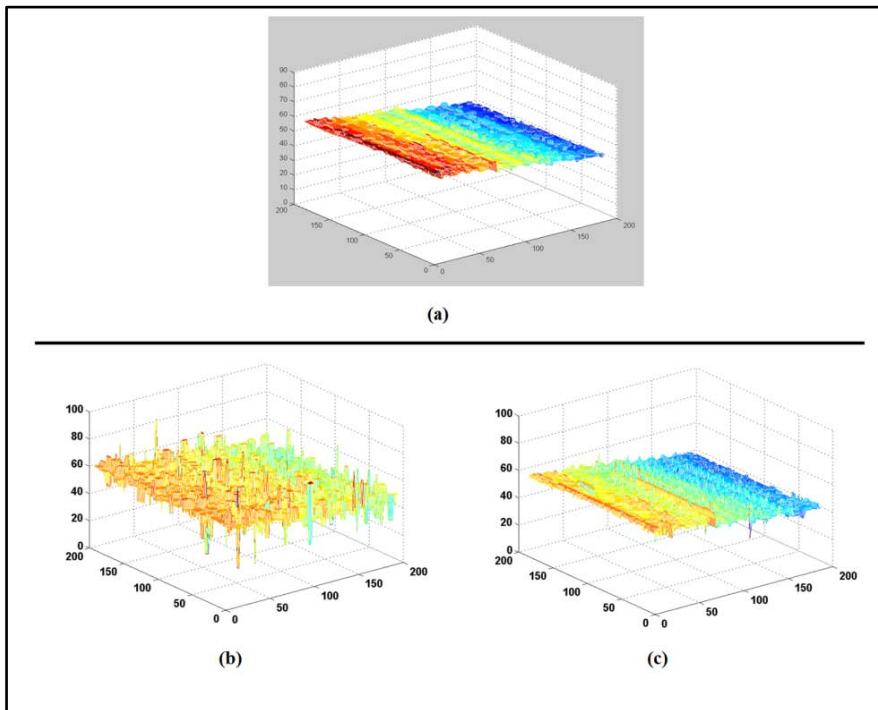


Figure C.19 Real plane in the presence of impulse noise with noise density of 0.005; (a) Ground truth, (b) GLV focus measure and (d) MLULU+GLV focus measure

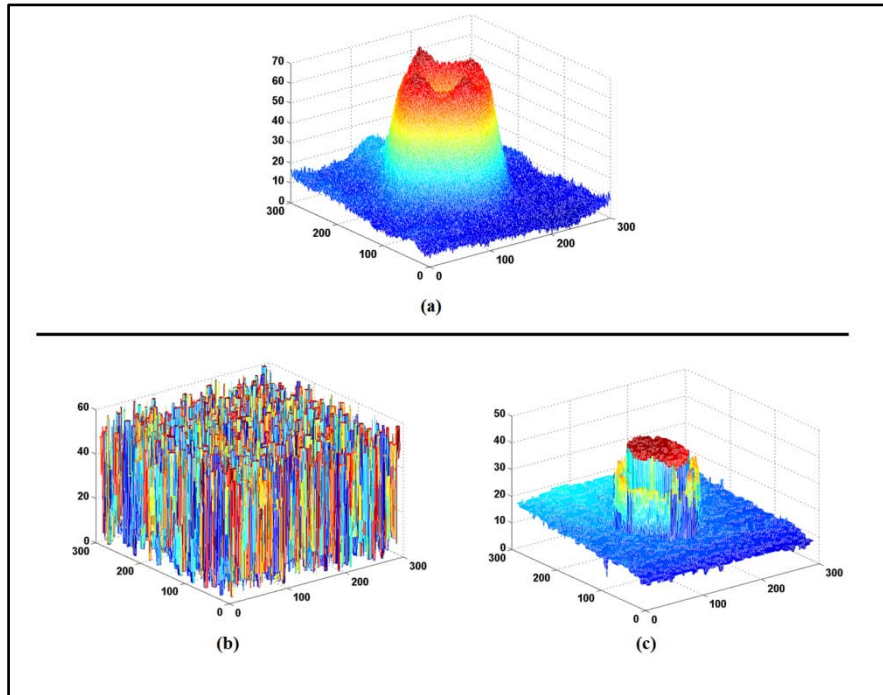


Figure C.20 Real LCD in the presence of impulse noise with noise density of 0.005; (a) Ground truth, (b) GLV focus measure and (d) MLULU+GLV focus measure

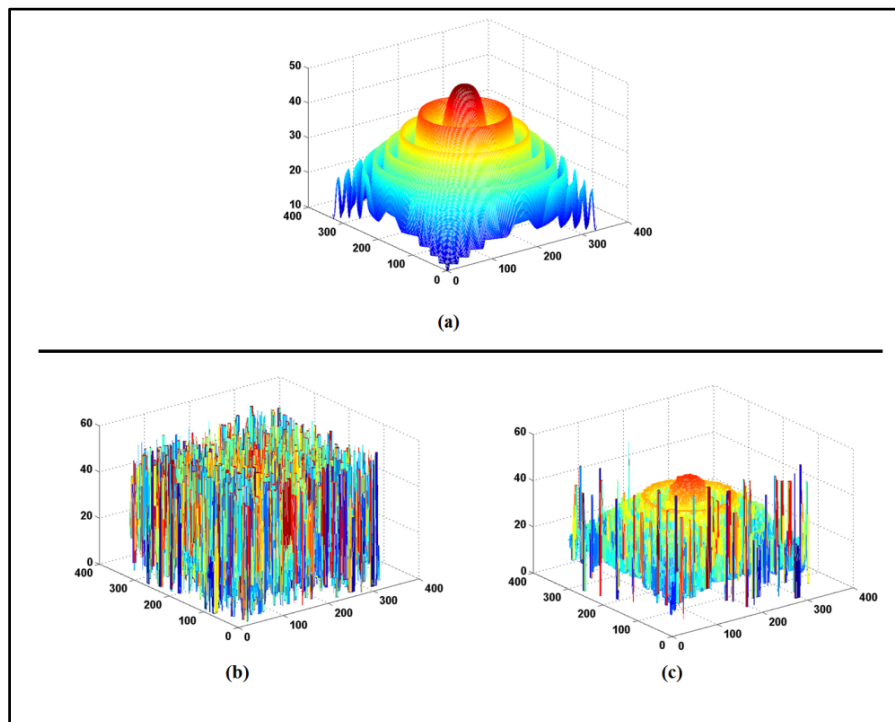


Figure C.21 Simulated cosine in the presence of impulse noise with noise density of 0.005; (a) Ground truth, (b) GLV focus measure and (d) MLULU+GLV focus measure

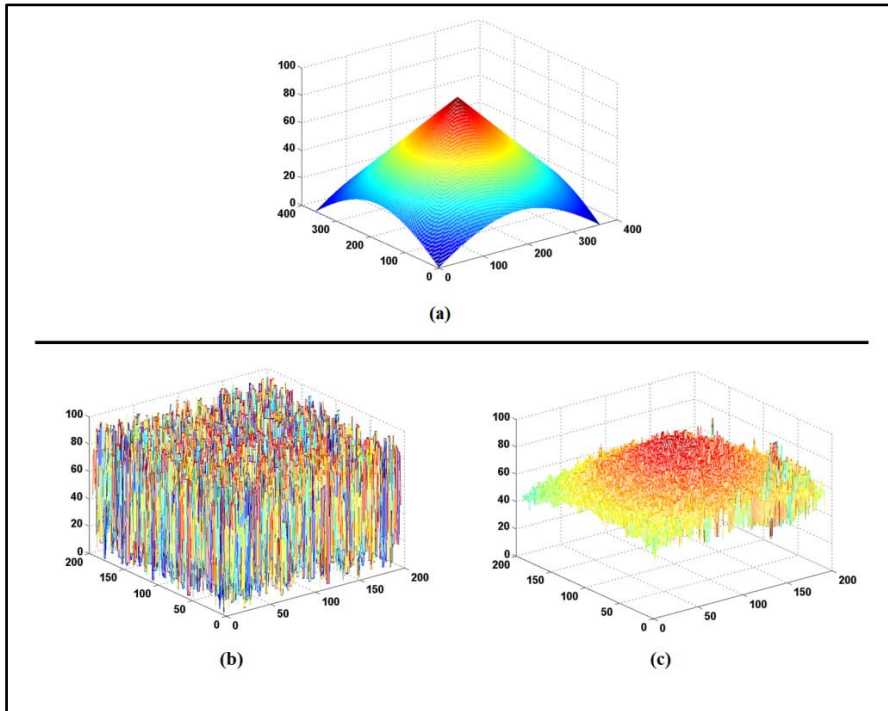


Figure C.22 Real cone in the presence of impulse noise with noise density of 0.005; (a) Ground truth, (b) SML focus measure and (d) MLULU+SML focus measure

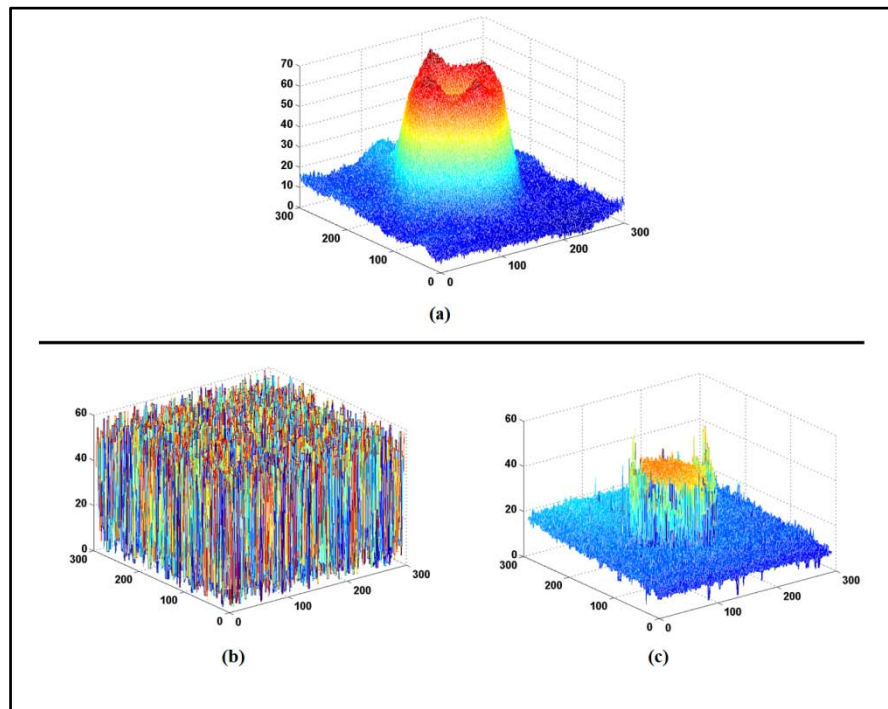


Figure C.23 Real LCD in the presence of impulse noise with noise density of 0.005; (a) Ground truth, (b) SML focus measure and (d) MLULU+SML focus measure

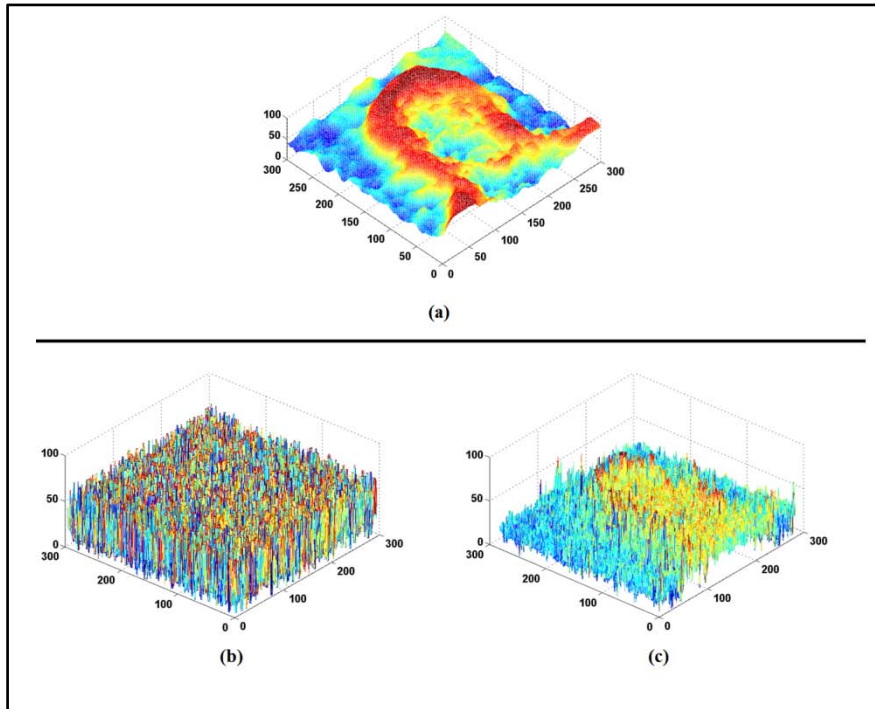


Figure C.24 Real coin in the presence of impulse noise with noise density of 0.005; (a) Ground truth, (b) SML focus measure and (d) MLULU+SML focus measure

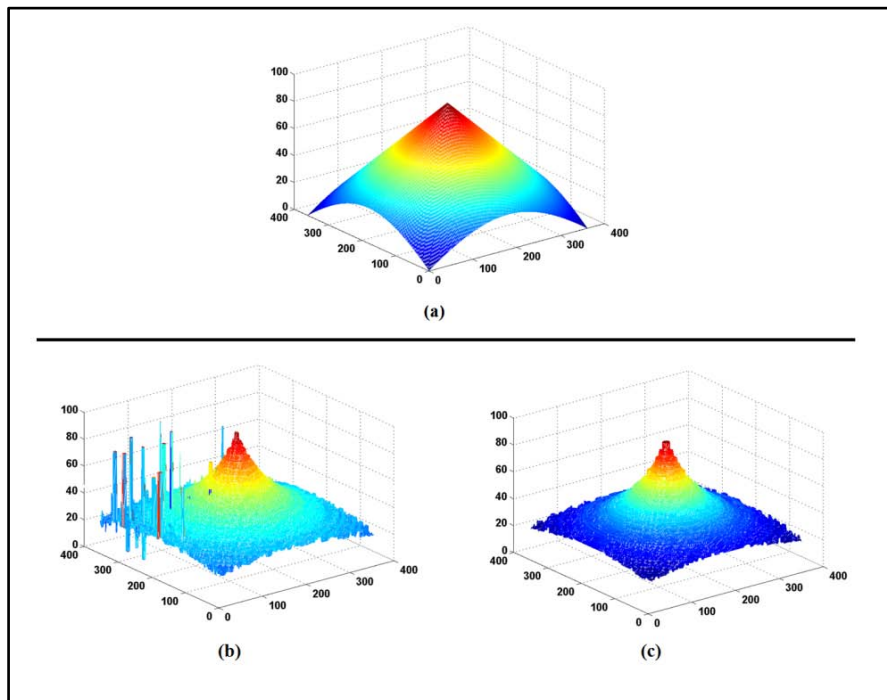


Figure C.25 Simulated cone in the presence of impulse noise with noise density of 0.005; (a) Ground truth, (b) TEN focus measure and (d) MLULU+TEN focus measure

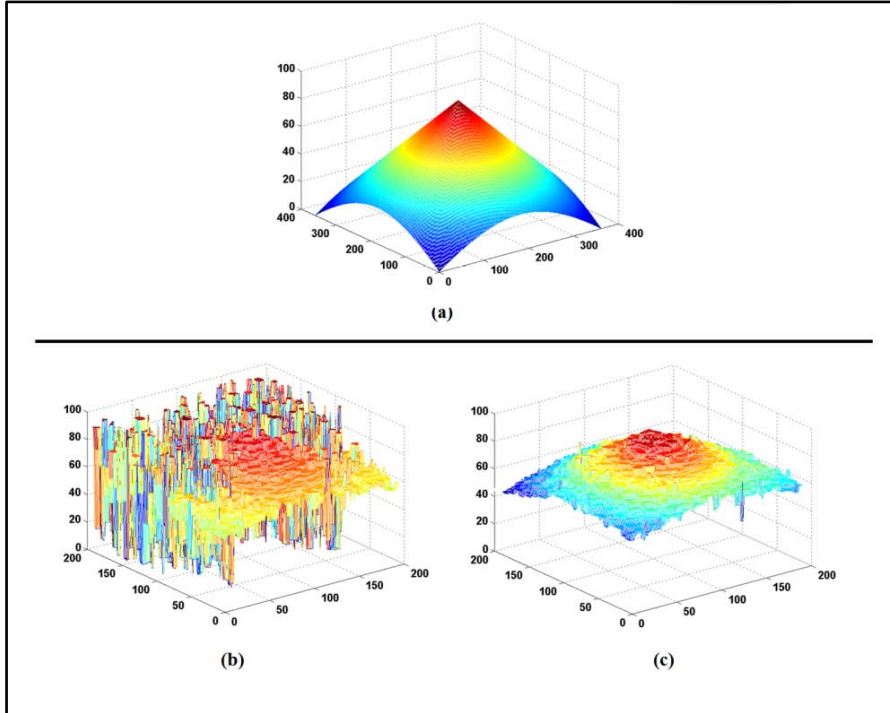


Figure C.26 Real cone in the presence of impulse noise with noise density of 0.005; (a) Ground truth, (b) TEN focus measure and (d) MLULU+TEN focus measure

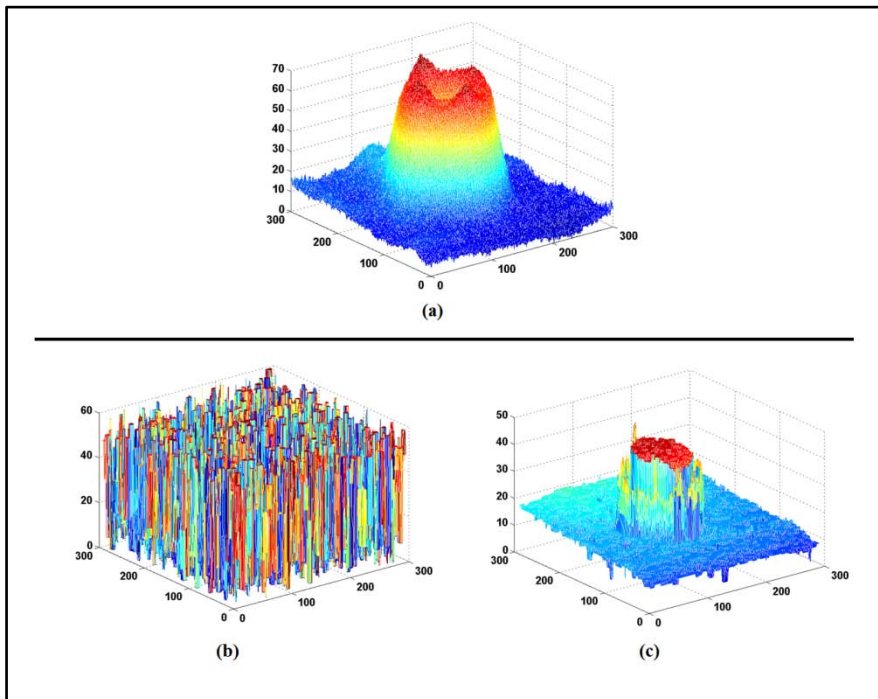


Figure C.27 Real LCD in the presence of impulse noise with noise density of 0.005; (a) Ground truth, (b) TEN focus measure and (d) MLULU+TEN focus measure

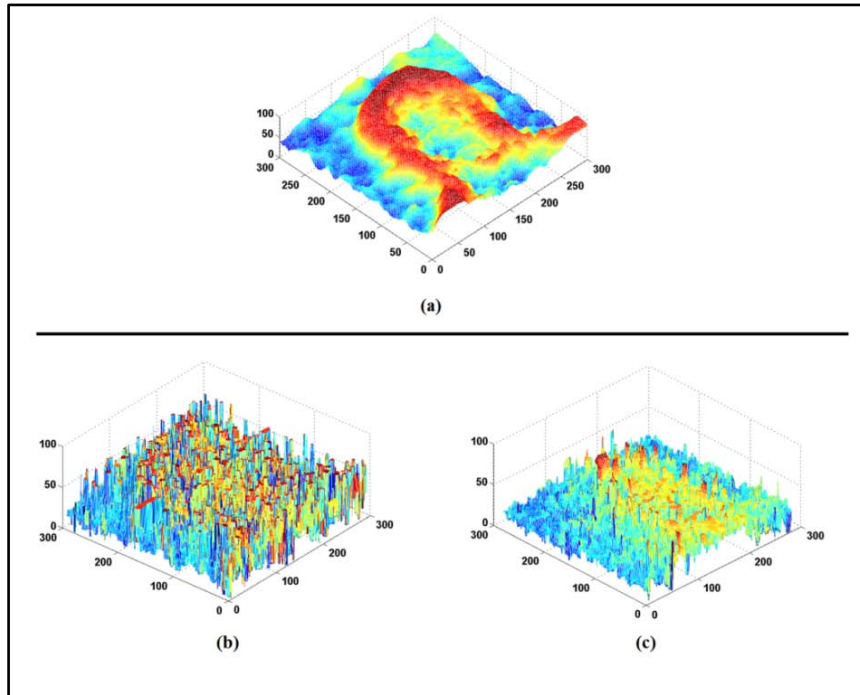


Figure C.28 Real coin in the presence of impulse noise with noise density of 0.005; (a) Ground truth, (b) TEN focus measure and (d) MLULU+TEN focus measure

- Impulse noise with noise density of 0.05

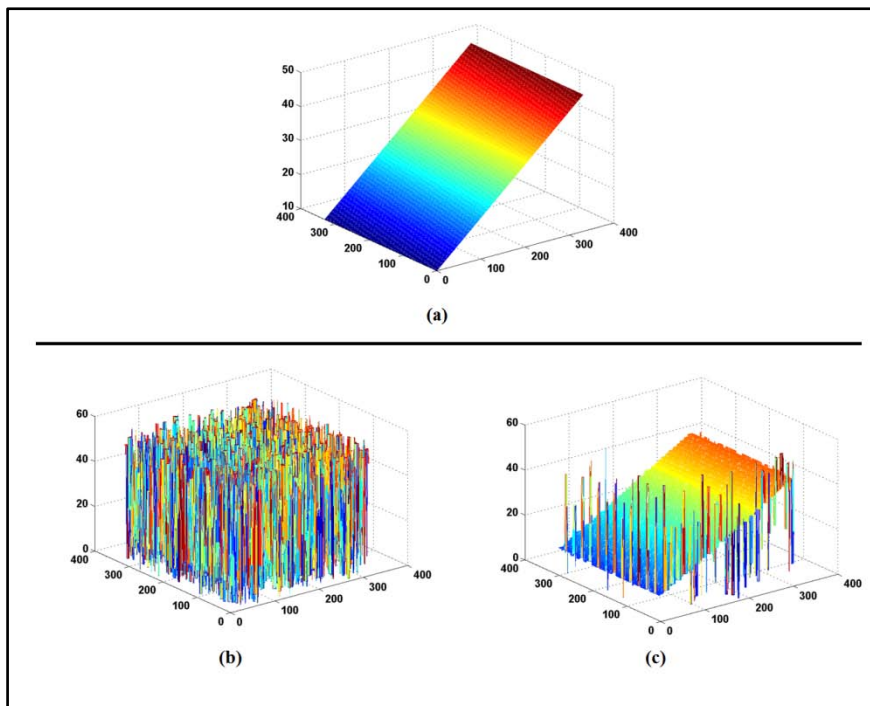


Figure C.29 Simulated slope in the presence of impulse noise with noise density of 0.05; (a) Ground truth, (b) GLV focus measure and (d) MLULU+GLV focus measure

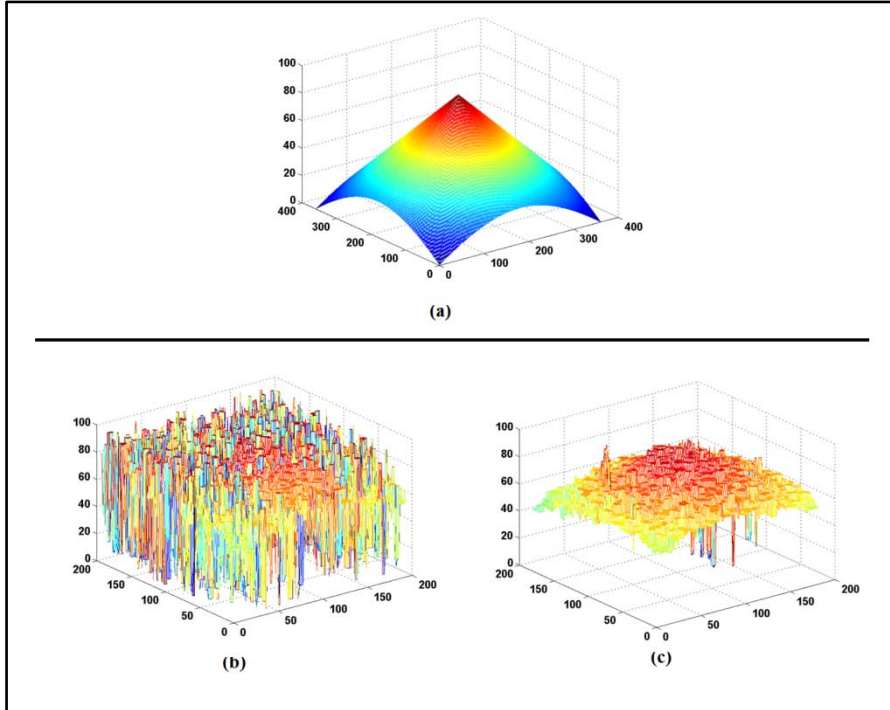


Figure C.30 Real cone in the presence of impulse noise with noise density of 0.05; (a) Ground truth, (b) GLV focus measure and (d) MLULU+GLV focus measure

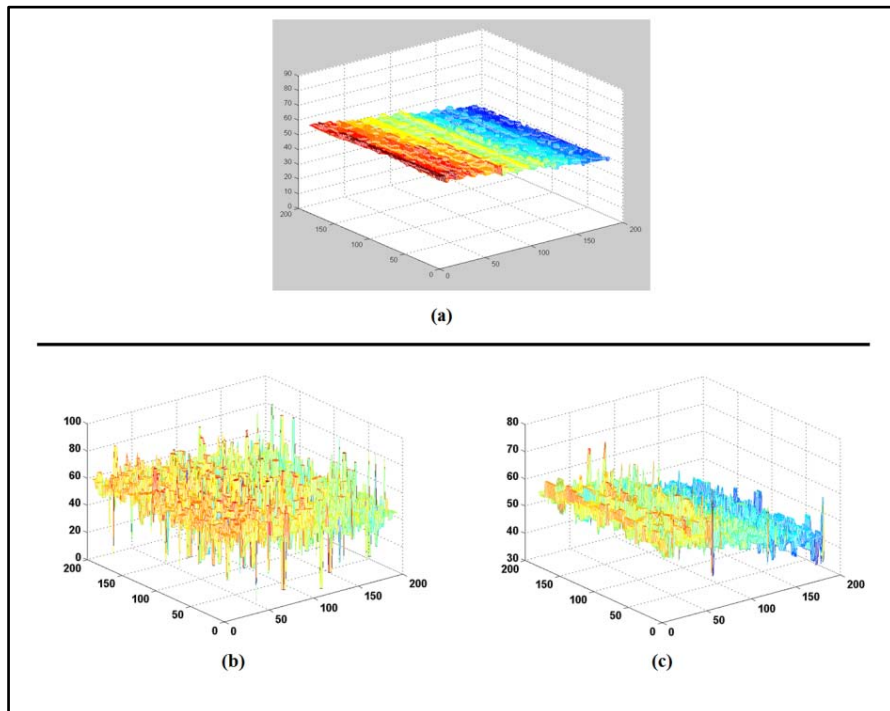


Figure C.31 Real plane in the presence of impulse noise with noise density of 0.05; (a) Ground truth, (b) GLV focus measure and (d) MLULU+GLV focus measure

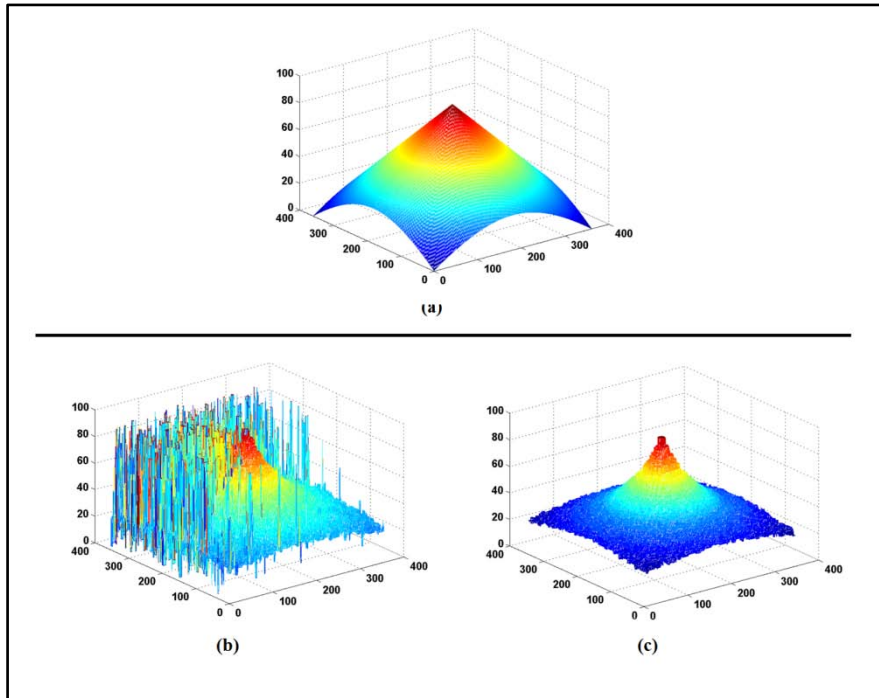


Figure C.32 Simulated cone in the presence of impulse noise with noise density of 0.05; (a) Ground truth, (b) GLV focus measure and (d) MLULU+GLV focus measure

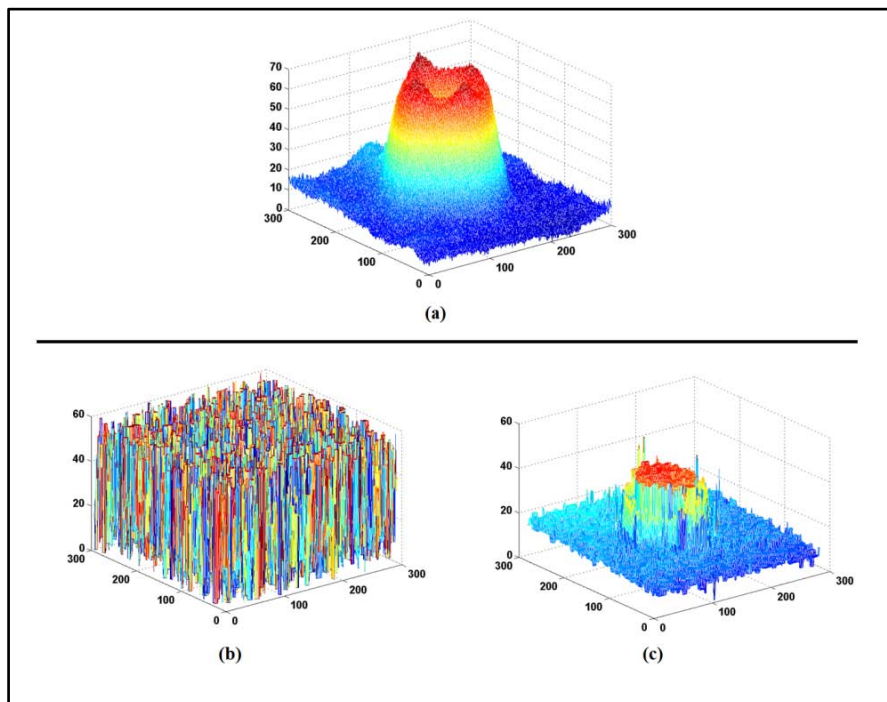


Figure C.33 Simulated slope in the presence of impulse noise with noise density of 0.05; (a) Ground truth, (b) GLV focus measure and (d) MLULU+GLV focus measure

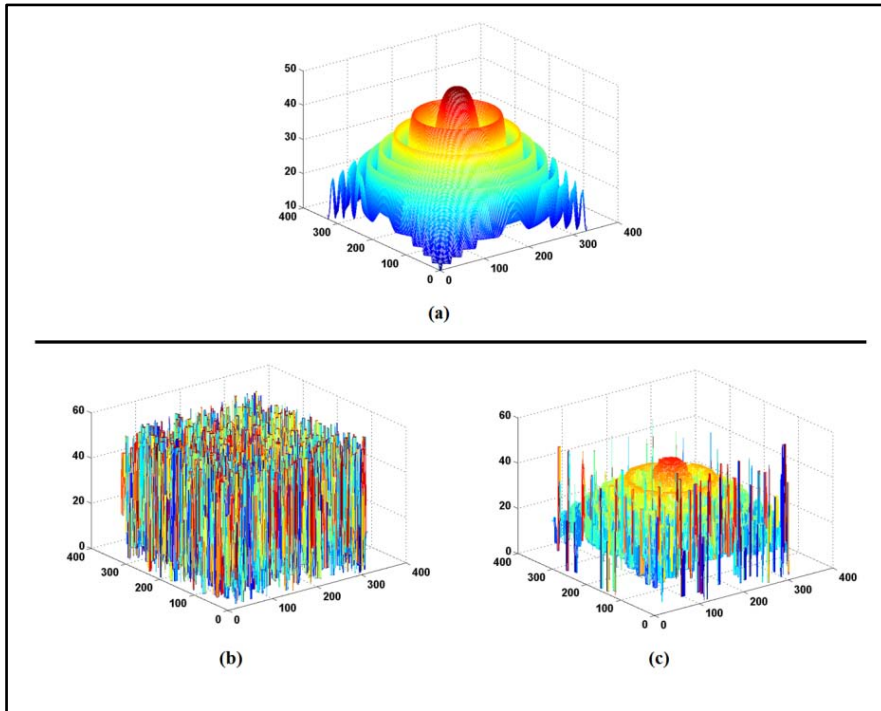


Figure C.34 Simulated cosine in the presence of impulse noise with noise density of 0.05; (a) Ground truth, (b) GLV focus measure and (d) MLULU+GLV focus measure

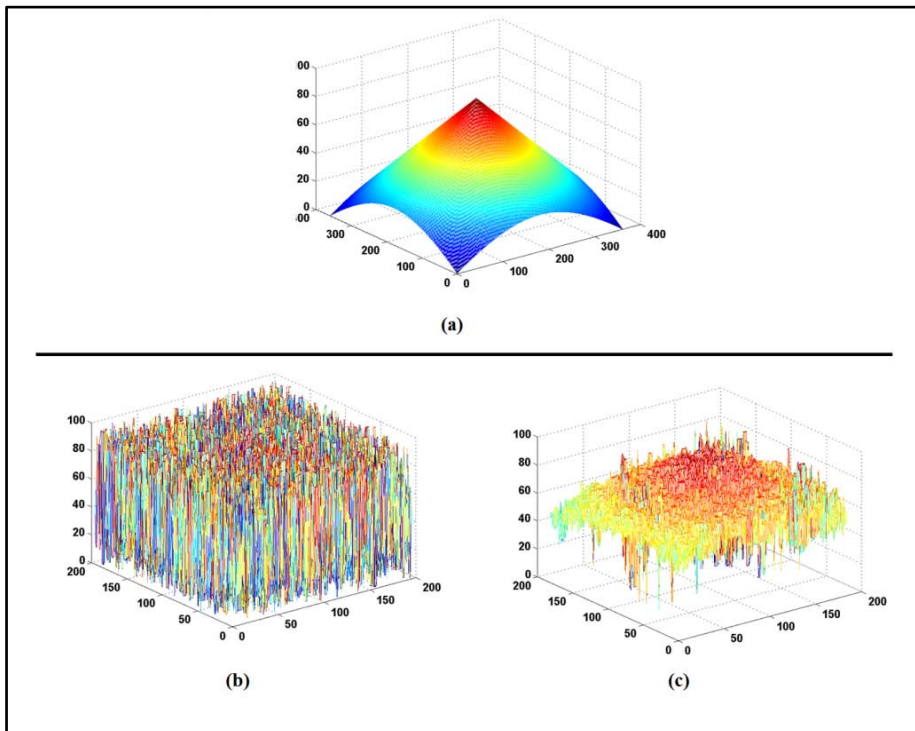


Figure C.35 Real cone in the presence of impulse noise with noise density of 0.05; (a) Ground truth, (b) SML focus measure and (d) MLULU+SML focus measure

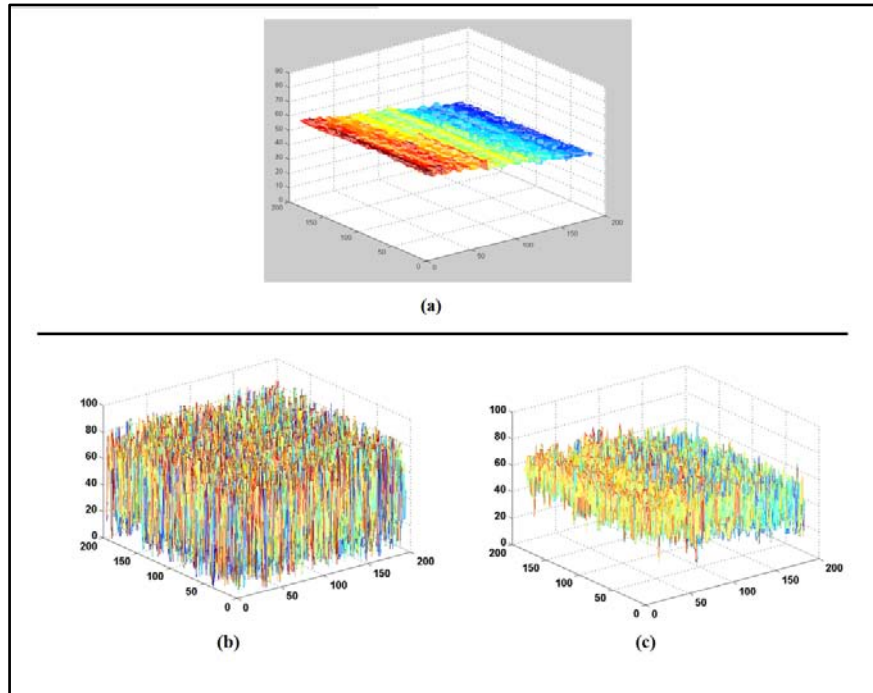


Figure C.36 Real plane in the presence of impulse noise with noise density of 0.05; (a) Ground truth, (b) SML focus measure and (d) MLULU+SML focus measure

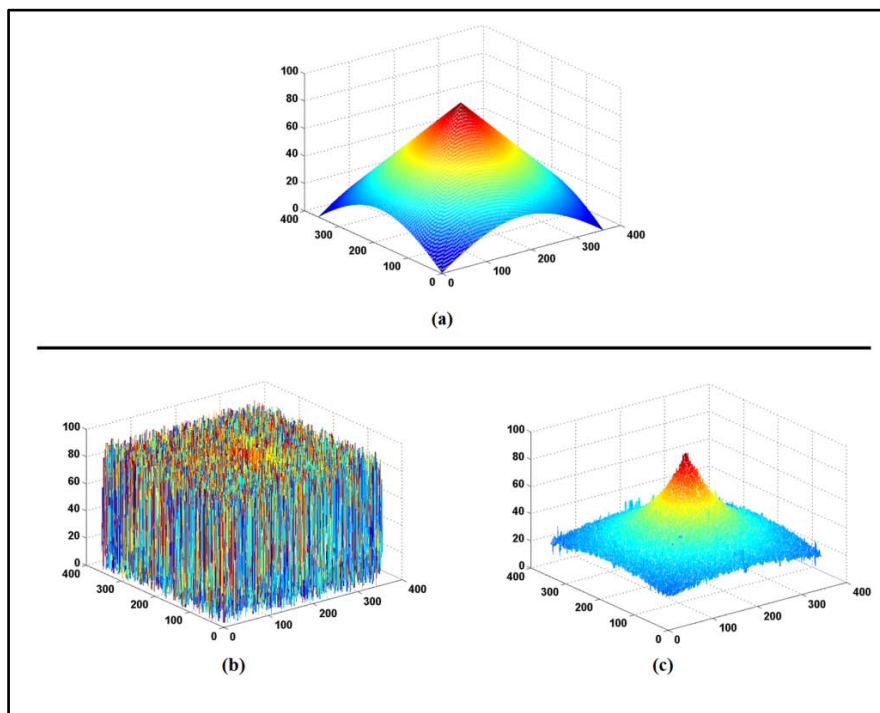


Figure C.37 Simulated cone in the presence of impulse noise with noise density of 0.05; (a) Ground truth, (b) SML focus measure and (d) MLULU+SML focus measure

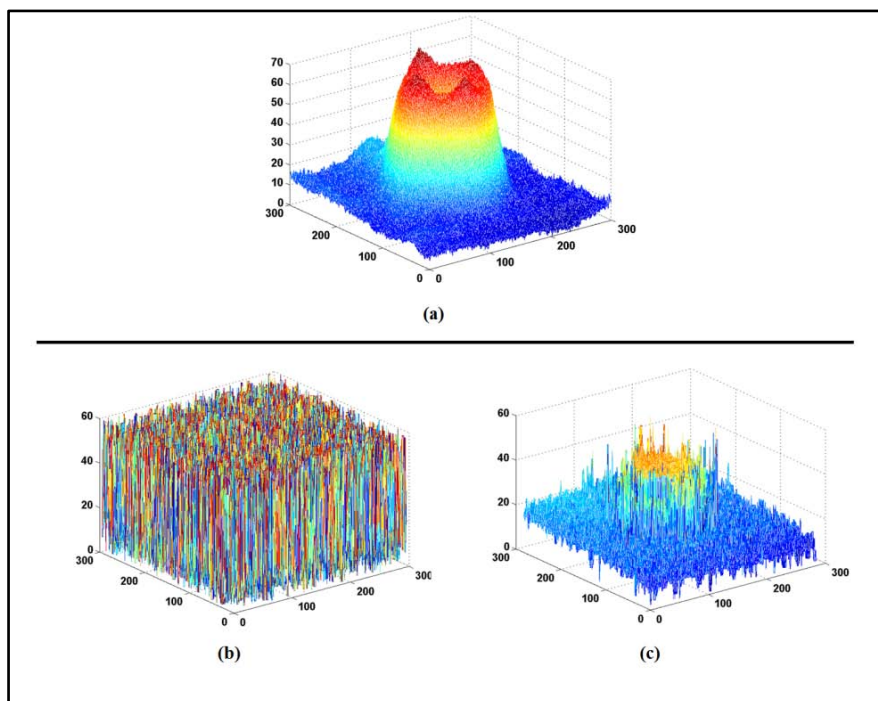


Figure C.38 Real LCD in the presence of impulse noise with noise density of 0.05; (a) Ground truth, (b) SML focus measure and (d) MLULU+SML focus measure

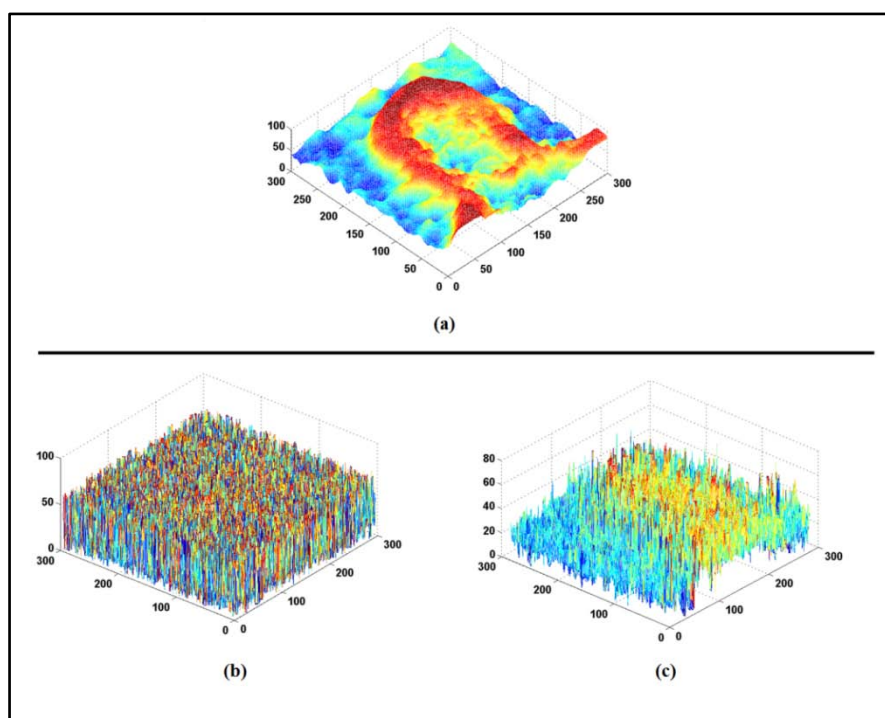


Figure C.39 Real coin in the presence of impulse noise with noise density of 0.05; (a) Ground truth, (b) SML focus measure and (d) MLULU+SML focus measure

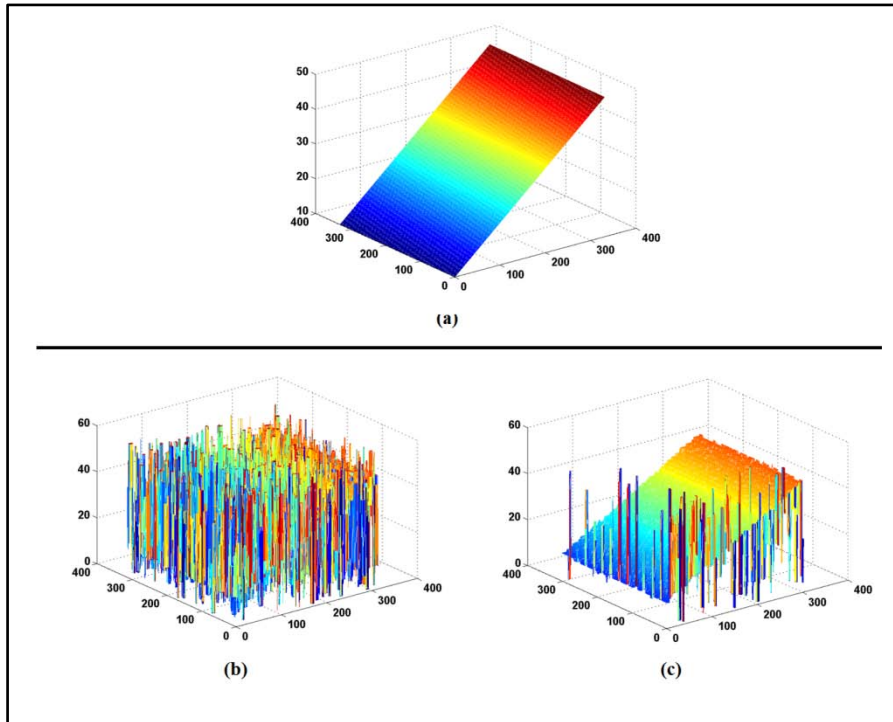


Figure C.40 Simulated slope in the presence of impulse noise with noise density of 0.05; (a) Ground truth, (b) TEN focus measure and (d) MLULU+TEN focus measure

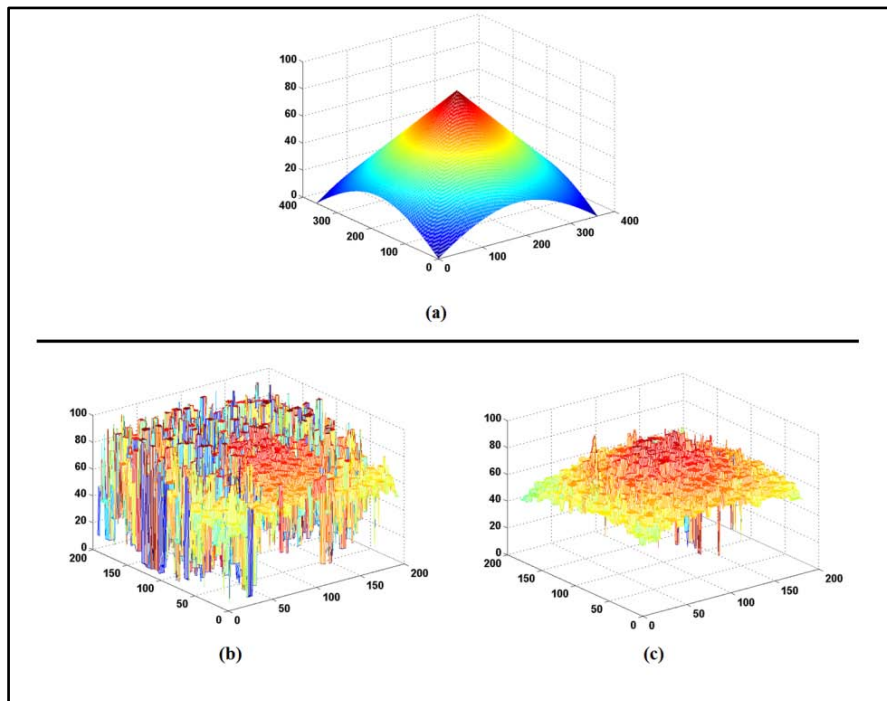


Figure C.41 Real cone in the presence of impulse noise with noise density of 0.05; (a) Ground truth, (b) TEN focus measure and (d) MLULU+TEN focus measure

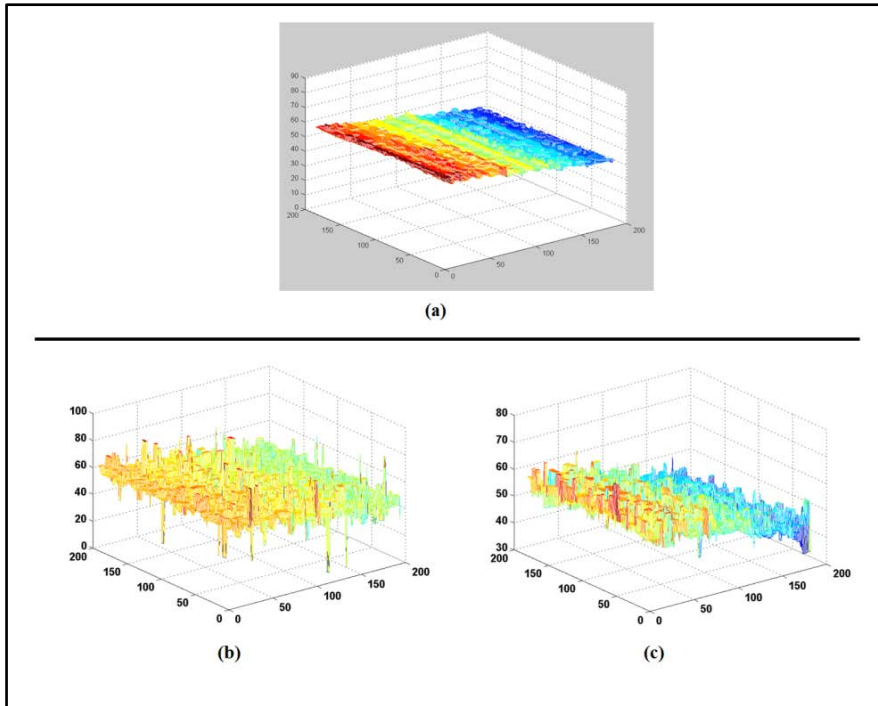


Figure C.42 Real plane in the presence of impulse noise with noise density of 0.05; (a) Ground truth, (b) TEN focus measure and (d) MLULU+TEN focus measure

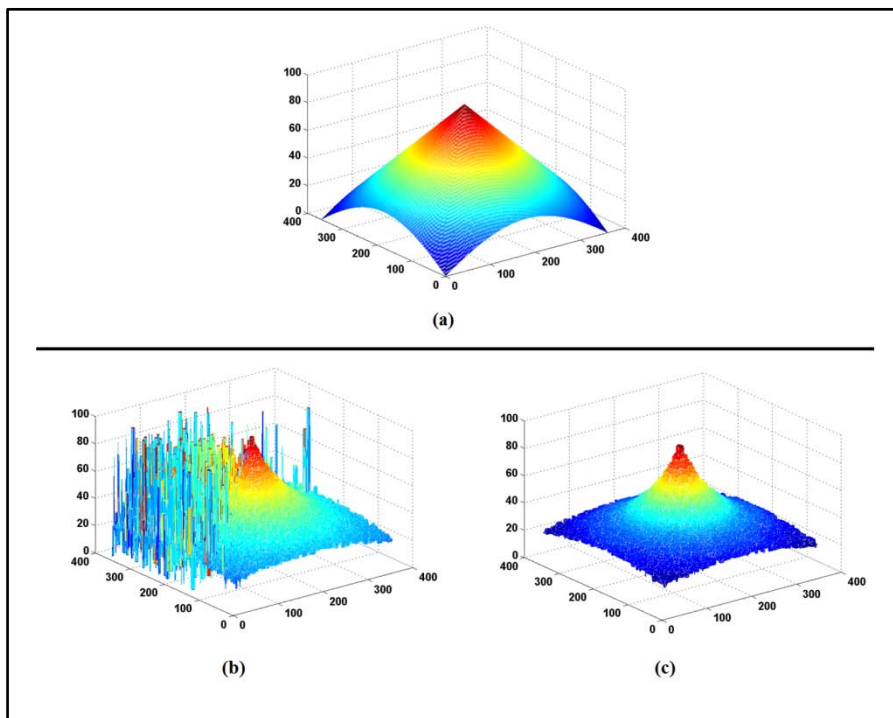


Figure C.43 Simulated cone in the presence of impulse noise with noise density of 0.05; (a) Ground truth, (b) TEN focus measure and (d) MLULU+TEN focus measure

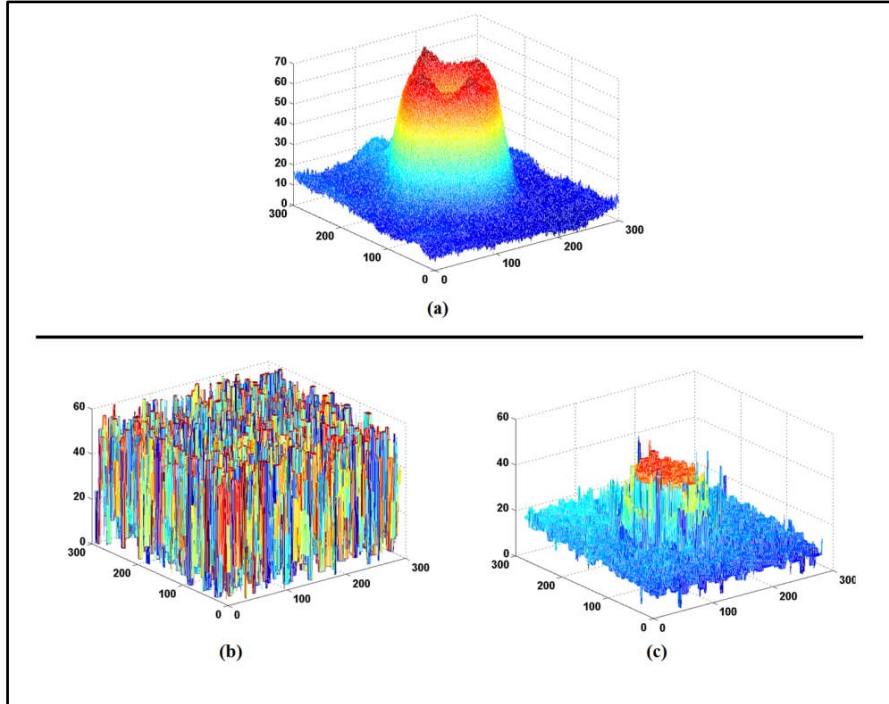


Figure C.44 Real LCD in the presence of impulse noise with noise density of 0.05; (a) Ground truth, (b) TEN focus measure and (d) MLULU+TEN focus measure

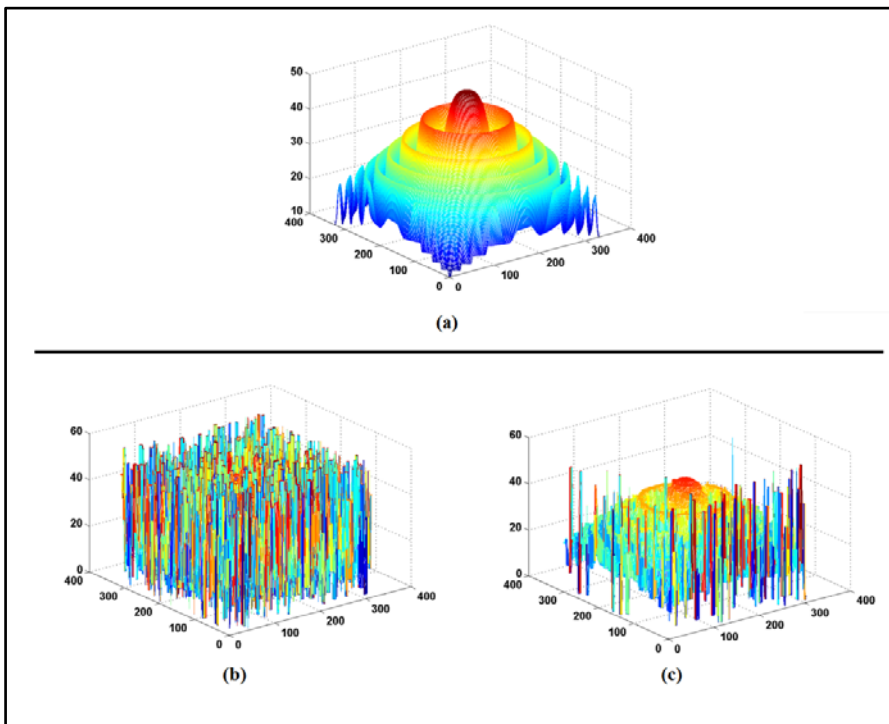


Figure C.45 Simulated cosine in the presence of impulse noise with noise density of 0.05; (a) Ground truth, (b) TEN focus measure and (d) MLULU+TEN focus measure

- Impulse noise with noise density of 0.5

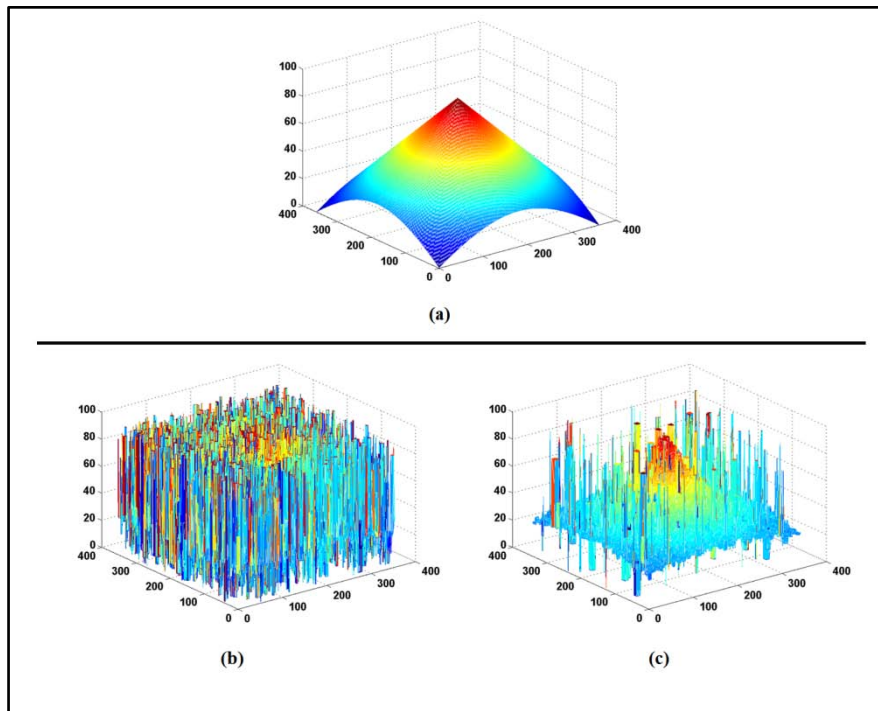


Figure C.46 Simulated cone in the presence of impulse noise with noise density of 0.5; (a) Ground truth, (b) TEN focus measure and (d) MLULU+TEN focus measure

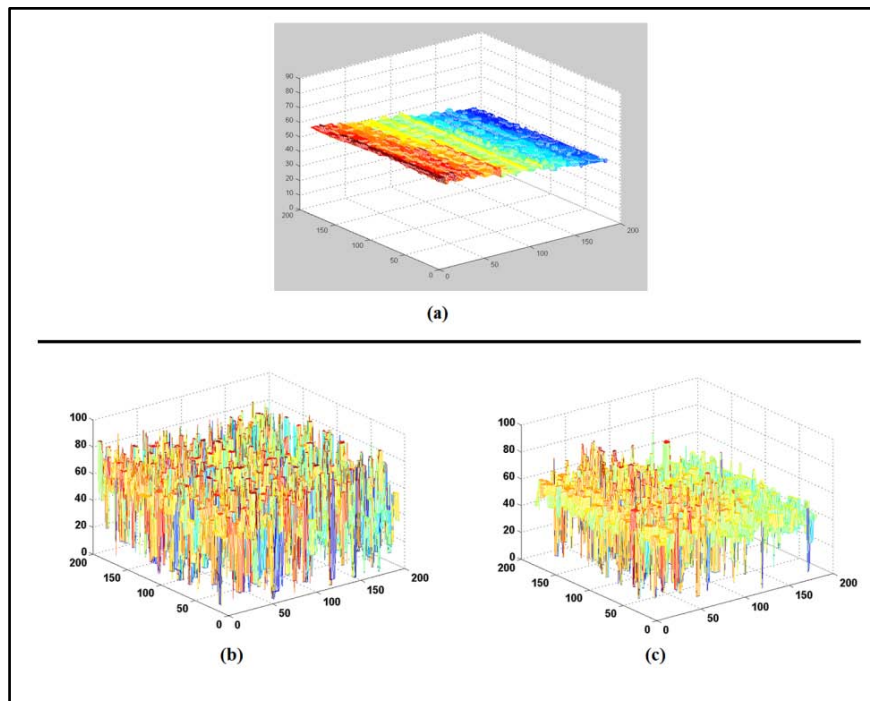


Figure C.47 Real plane in the presence of impulse noise with noise density of 0.5; (a) Ground truth, (b) TEN focus measure and (d) MLULU+TEN focus measure

- Gaussian noise with noise density of 0.005

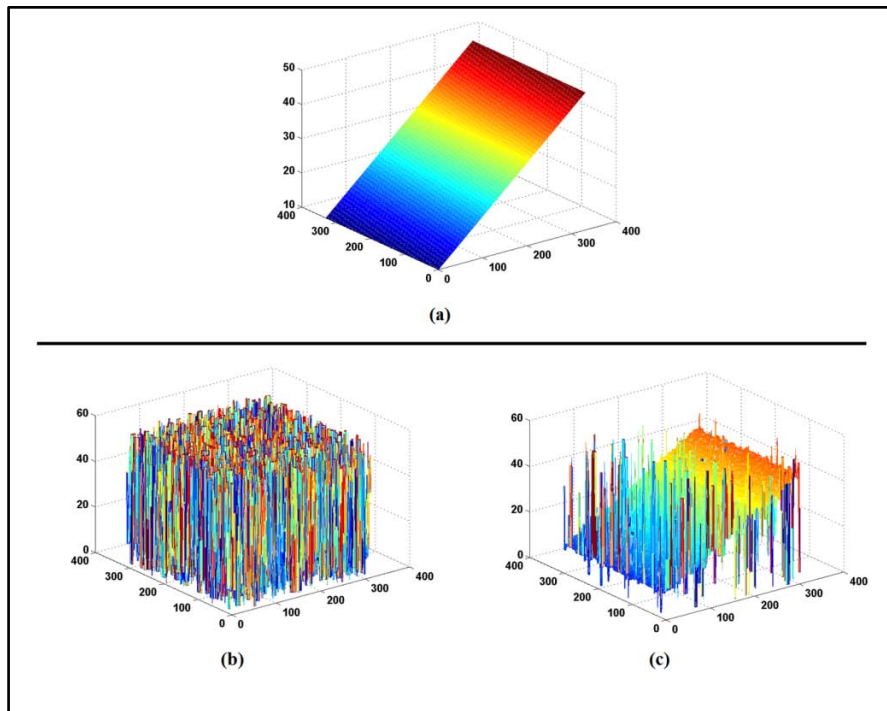


Figure C.48 Simulated slope in the presence of Gaussian noise with noise density of 0.005; (a) Ground truth, (b) GLV focus measure and (d) MLULU+GLV focus measure

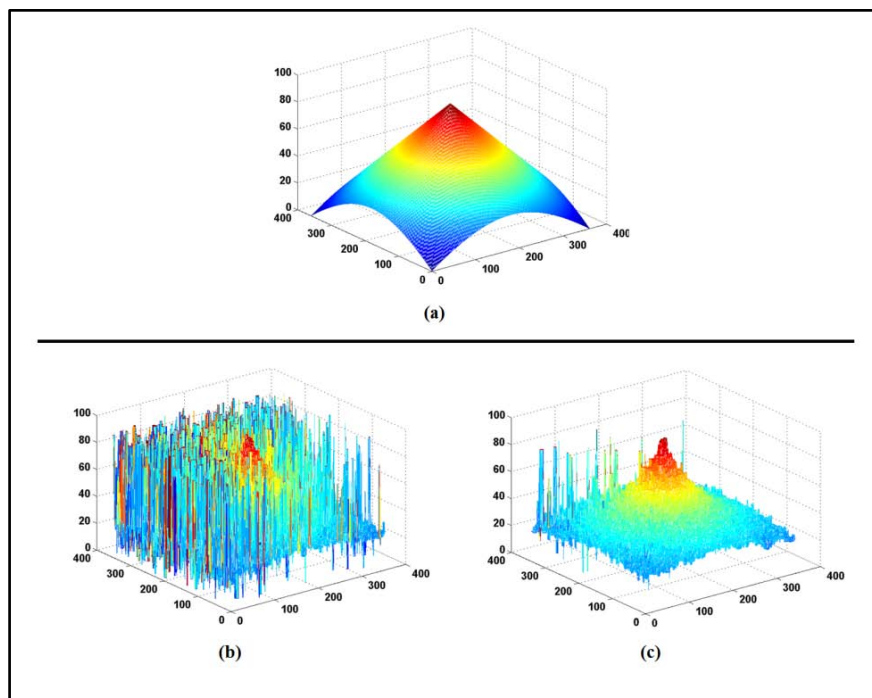


Figure C.49 Simulated cone in the presence of Gaussian noise with noise density of 0.005; (a) Ground truth, (b) GLV focus measure and (d) MLULU+GLV focus measure

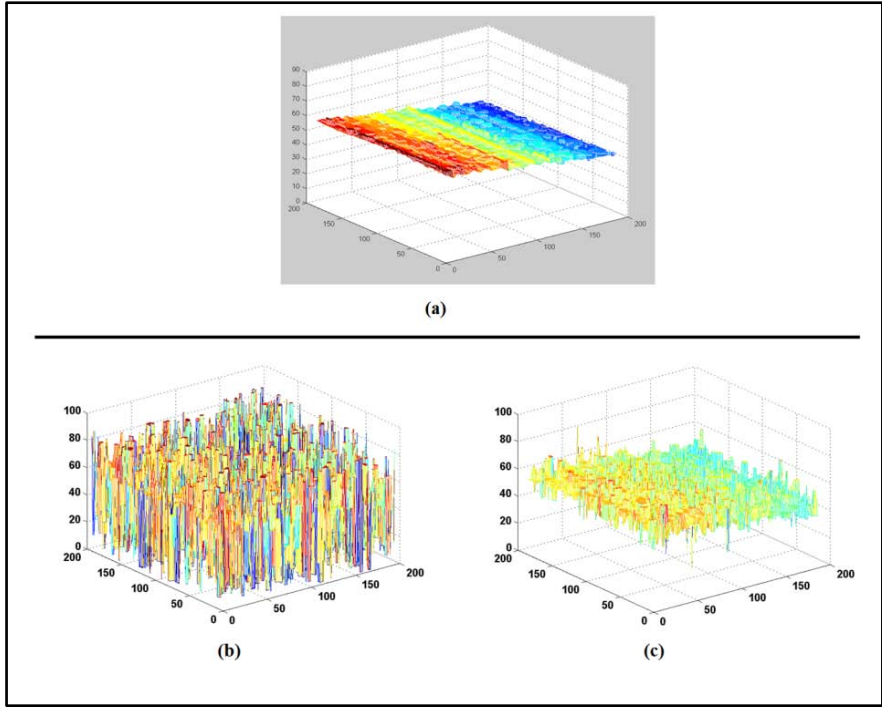


Figure C.50 Real plane in the presence of Gaussian noise with noise density of 0.005; (a) Ground truth, (b) GLV focus measure and (d) MLULU+GLV focus measure

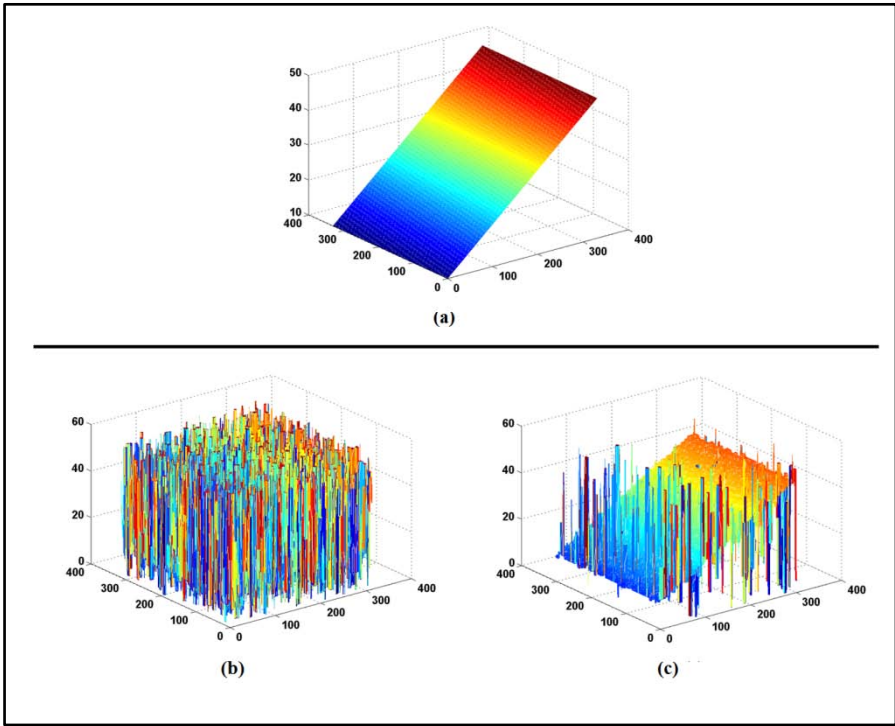


Figure C.51 Simulated slope in the presence of Gaussian noise with noise density of 0.005; (a) Ground truth, (b) TEN focus measure and (d) MLULU+TEN focus measure

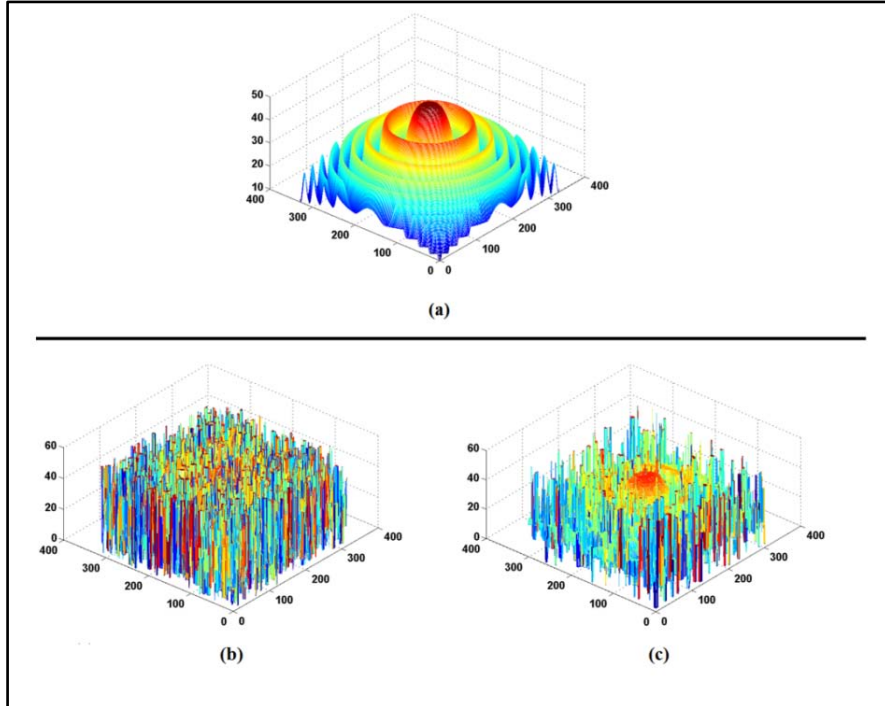


Figure C.52 Simulated cosine in the presence of Gaussian noise with noise density of 0.005; (a) Ground truth, (b) TEN focus measure and (d) MLULU+TEN focus measure

- Gaussian noise with noise density of 0.05

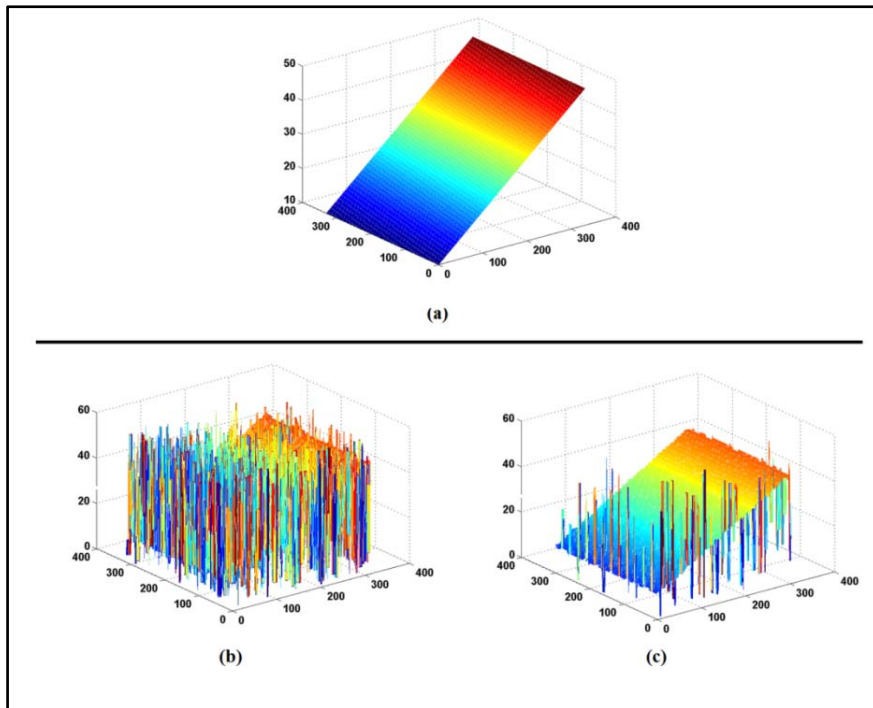


Figure C.53 Simulated slope in the presence of Gaussian noise with noise density of 0.05; (a) Ground truth, (b) GLV focus measure and (d) MLULU+GLV focus measure

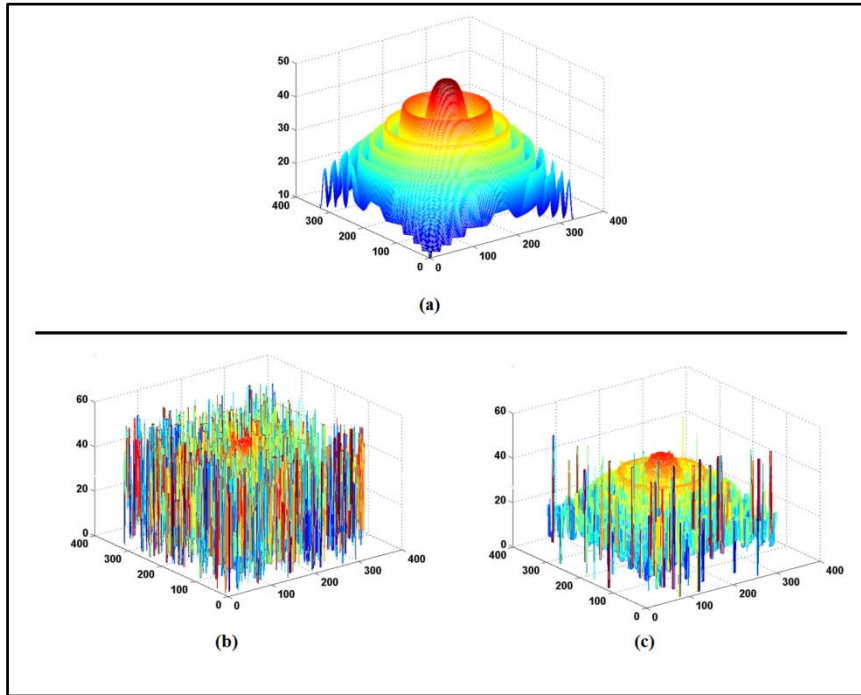


Figure C.54 Simulated cosine in the presence of Gaussian noise with noise density of 0.05; (a) Ground truth, (b) GLV focus measure and (d) MLULU+GLV focus measure

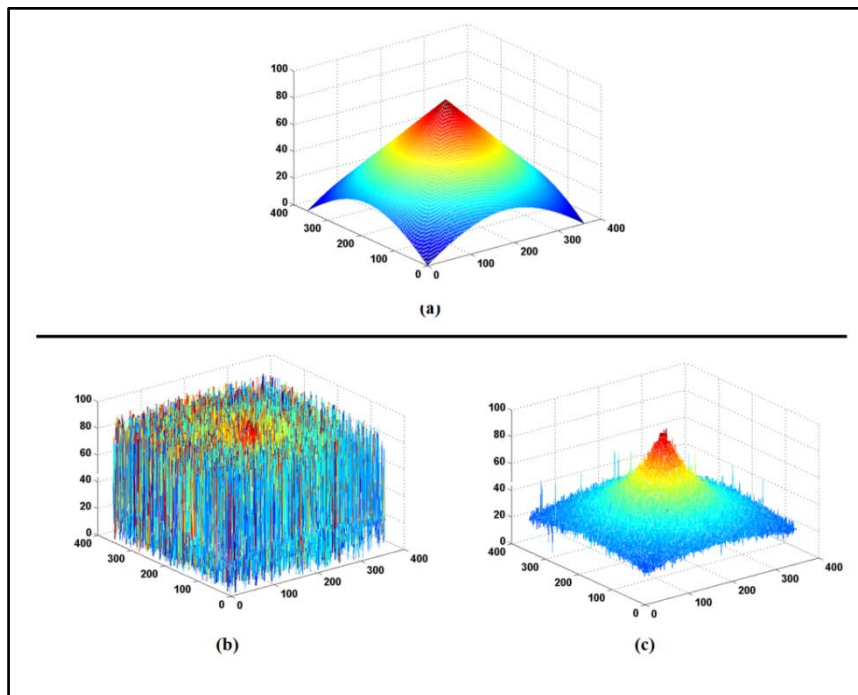


Figure C.55 Simulated cone in the presence of Gaussian noise with noise density of 0.05; (a) Ground truth, (b) SML focus measure and (d) MLULU+SML focus measure

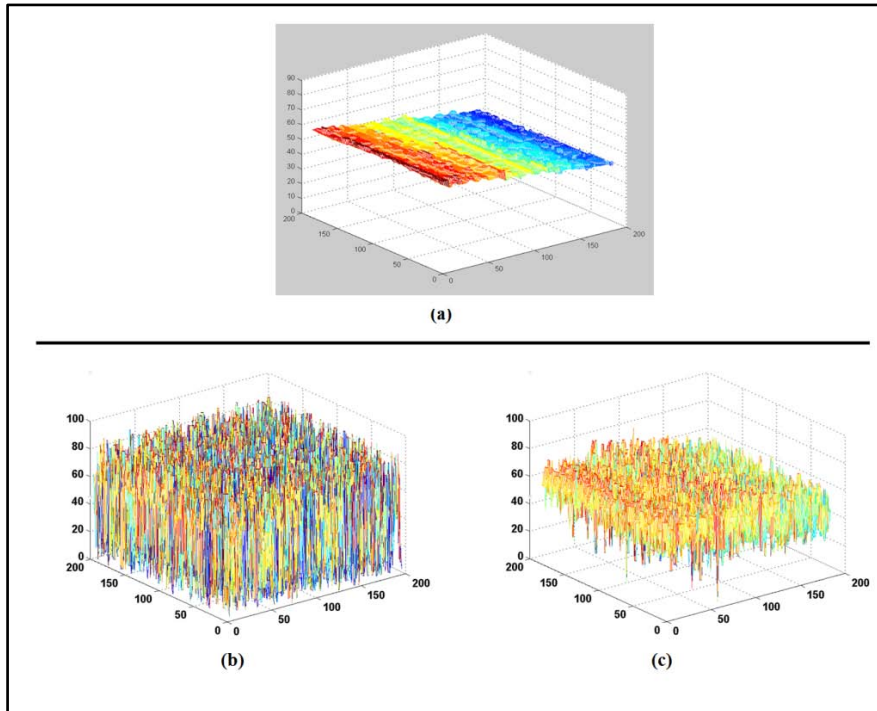


Figure C.56 Real plane in the presence of Gaussian noise with noise density of 0.05; (a) Ground truth, (b) SML focus measure and (d) MLULU+SML focus measure

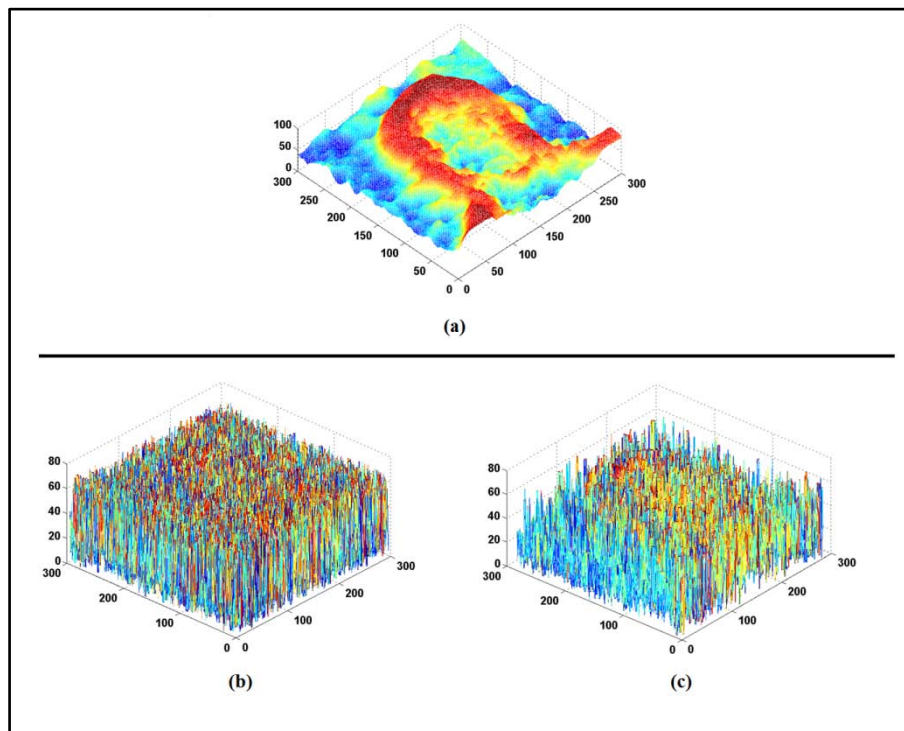


Figure C.57 Real coin in the presence of Gaussian noise with noise density of 0.05; (a) Ground truth, (b) SML focus measure and (d) MLULU+SML focus measure

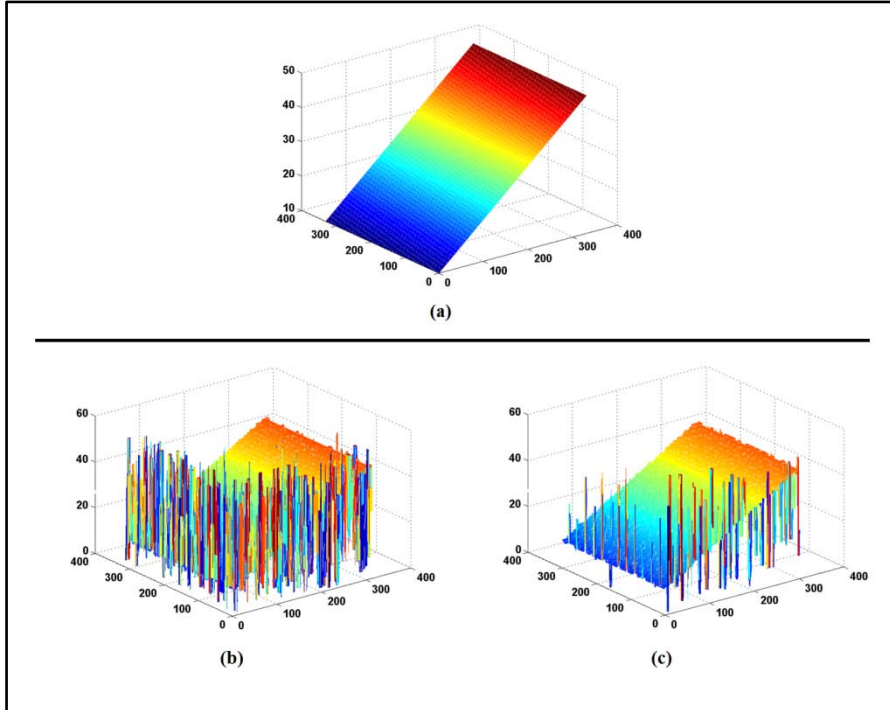


Figure C.58 Simulated slope in the presence of Gaussian noise with noise density of 0.05; (a) Ground truth, (b) TEN focus measure and (d) MLULU+TEN focus measure

PUBLICATIONS

- Roushanak Rahmat, Aaamir Saeed Malik, Ibrahima Faye and Nidal S. Kamel, “*An Overview of LULU Operators and Discrete Pulse Transform for Image Analysis*”, *Imaging Science Journal*, vol:59, no:5, 2011.
- Roushanak Rahmat, Aaamir Saeed Malik, and Nidal S. Kamel, “*3-D Content Generation using Optical Passive Reflective Techniques*”, *The 15th IEEE International Symposium on Consumer Electronics, Singapore on 14-17 June 2011*.
- Roushanak Rahmat, Aaamir Saeed Malik, and Nidal S. Kamel, “*Comparison of LULU and Median Filter for Image Denoising*”, *3rd Conference on Signal Acquisition and Processing (ICSAP2011), Singapore on 26th-28th February 2011*.
- Roushanak Rahmat, Aaamir Saeed Malik, and Nidal S. Kamel, “*Comparison of LULU and Median Filter for Image Denoising*”, Accepted in *Procedia Engineering*.